Solar-Terrestrial Centre of Excellence

Annual Report 2021

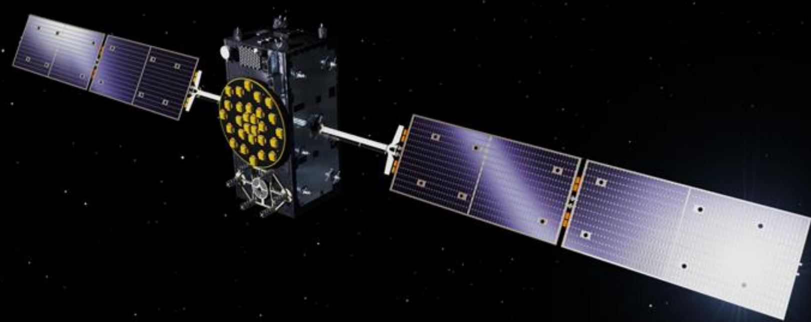

Belgian Science Policy Office
belspo

Royal Observatory of Belgium

RMI

BIRA-IASB

.be

STCE

Solar-**T**errestrial **C**entre of **E**xcellence

https://stce.be/

Ringlaan 3

B-1180 Brussels

Tel.: +32 2 373 0211

Fax: + 32 2 374 9822

Front page: *artist's composition of a Galileo satellite transmitting data to a ground GNSS receiving antenna mounted on top of the telescope dome at the Royal Observatory of Belgium (ROB). Galileo is the European Global Navigation Satellite System (GNSS), a system similar to the American GPS and the Russian GLONASS systems. The ROB/GNSS research group (http://gnss.be/), in close collaboration with the RMI, BIRA-IASB, and international partners, uses GNSS signals for various applications such as the monitoring of ground deformations, the transfer of time and frequency, and the monitoring of the Earth's atmosphere. In 2021, a special 41-cm wide radome was installed over the antenna to reduce the satellite tracking degradations caused by rain, snow and birds. The dome can be seen just above the square supporting plate.*

Table of Contents

A word from the STCE coordinator

Dear Readers,

Once again we present to you the annual report of the STCE. Besides listing our major achievements and activities performed during 2021, it also gives you a peek behind the curtains, illustrating real life at the STCE.

Following the year of confinement due to COVID, 2021 became the year of new beginnings. We were gradually allowed to come back to work in our offices and could once again strengthen the ties with colleagues and between teams. This shift in work regime is clearly reflected by the rising number of presentations and posters at conferences. The period of confinement seemed to have allowed our researchers to focus on writing publications: the surge in peer-reviewed publications that started in 2020 continued throughout 2021.

The Sun itself also continued its rise towards the next solar cycle maximum, as illustrated by the increased activity observed in 2021. We saw the first 2 X-class flares from solar cycle 25, as well as the first Ground Level Enhancement.

Scientifically speaking, 2021 was a year of new projects and new directions. New instruments and labs were installed. News methods were developed and tested. New concepts were introduced and applied. The Belgian Radiometric Characterization Laboratory was founded, a novel K-index was developed, FAIR principles were introduced, the SVO became operational, and an outreach play premiered.

The return to in-person contact this year once again proved the worth of one of the key-values of the STCE: fostering collaborations between the three institutes, thus allowing once more to boost the scientific output to more than the sum of the separate parts.

Happy reading.

Ronald Van der Linden
General Coordinator of the Solar-Terrestrial Centre of Excellence
Director General of the Royal Observatory of Belgium

Structure of the STCE

The Solar-Terrestrial Centre of Excellence is a project of scientific collaboration that focuses on the Sun, through interplanetary space, up to the Earth and its atmosphere.

The solid base of the STCE is the expertise that exists in the 3 Federal Scientific Institutes of the Brussels Space Pole: the Royal Observatory of Belgium, the Royal Meteorological Institute and the Royal Belgian Institute for Space Aeronomy. The STCE supports fundamental solar, terrestrial and atmospheric physics research, is involved in earth-based observations and space missions, offers a broad variety of services (mainly linked to space weather and space climate) and operates a fully established space weather application centre. The scientists act at different levels within the frame of local, national and international collaborations of scientific and industrial partners.

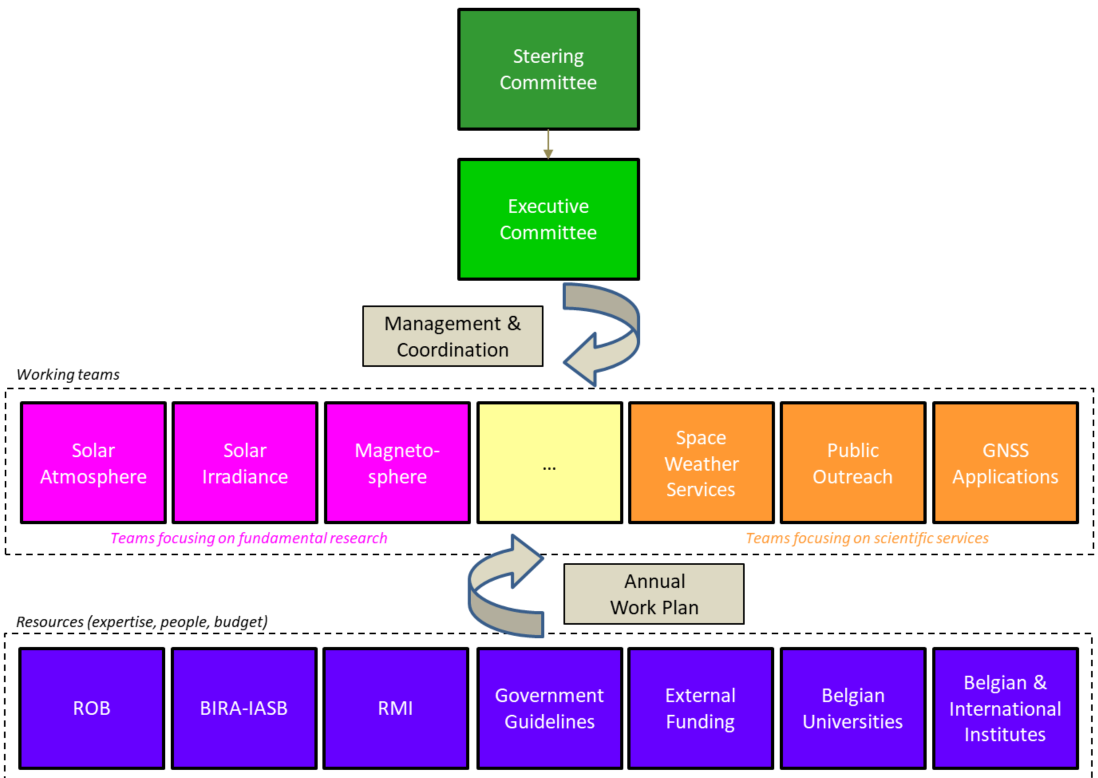

Figure 1: The STCE management structure

The STCE's strengths are based on sharing know-how, manpower, and infrastructure.

In order to optimize the coordination between the various working groups and institutions, as well as the available resources such as ICT, personnel and budget, a management structure for the STCE was put into place, consisting of a steering committee and an executive committee.

The ***steering committee*** takes all the final decisions on critical matters with regard to the STCE. It assures the integration of the STCE into the 3 institutions and the execution of the strategic plans. It is composed of:

- BELSPO Director General "Research Programmes and Applications"

  Dr. Frank Monteny (BELSPO)

- Director General of each of the 3 institutions at the Space Pole

  Dr. Ronald Van der Linden (ROB)
  Dr. Daniel Gellens (RMI)
  Dr. Martine De Mazière (BIRA-IASB)

The ***executive committee*** assures the global coordination between the working groups and the correct use of the budgetary means for the various projects. It also identifies new opportunities and is the advisory body to the Steering Committee. It is composed of:

- STCE Coordinator

  Dr. Ronald Van der Linden

- Representatives of the research teams in the 3 institutes

  Dr. David Berghmans (ROB)
  Dr. Carine Bruyninx (ROB)
  Dr. Johan De Keyser (BIRA-IASB)
  Dr. Norma Crosby (BIRA-IASB)
  Dr. Stanimir Stankov (RMI)
  Dr. Stijn Nevens (RMI)
  Dr. Hugo De Backer (RMI)

A promotional movie giving a flavor of the STCE's tasks, interactions and various research programmes can be found via the STCE website (in English, and subtitled in French and Dutch).

Early 2021, most were still teleworking due to the continuing COVID-19 pandemic. Only a few ventured to the premises of the Space Pole, thus enjoying a fairy winter landscape. Credits: Sergei Shestov.

Monitoring space weather: solar-terrestrial highlights in 2021

The official annual sunspot number (S_N) for 2021, as determined by the WDC-SILSO (World Data Center - Sunspot Index and Long-term Solar Observations), was 29.6. This is an increase compared to 2020 (8.8). Sunspot numbers of the last few months of 2021 were somewhat higher than predicted which - IF this trend continues - may be indicative that SC25 maximum can be a bit higher and/or earlier than the original prediction by the SC25 panel of 115+/-10 in July 2025 +/- 8 months .

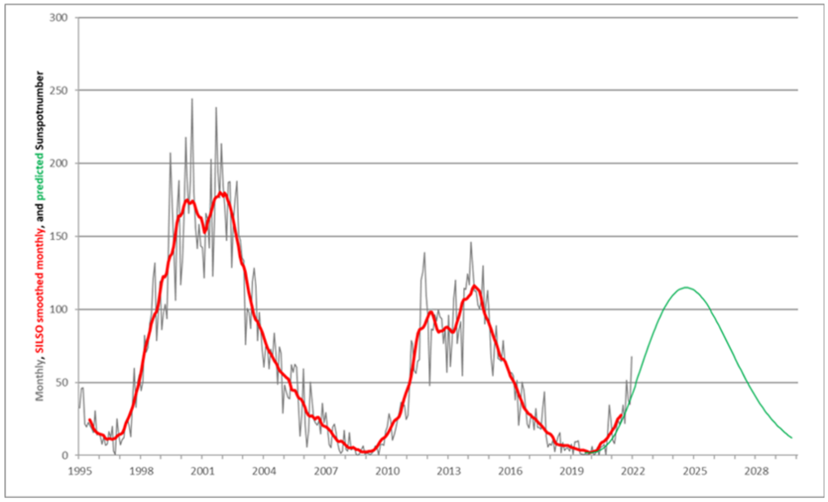

*Figure 2: The evolution of the monthly and SILSO smoothed monthly S_N (1995-2020 ; **SILSO formula**). The monthly sunspot numbers late 2021 were somewhat higher than the expected values (depicted in green, with the predicted maximum advanced and occurring in August 2024).*

SILSO's Spotless Days page indicated there were still 50 spotless days, with about half of them generated during the first 2 months of 2021, and still 3 in December. The evolution of SC25 for various space weather (SWx) parameters can be followed on the STCE's SC25 Tracking page.

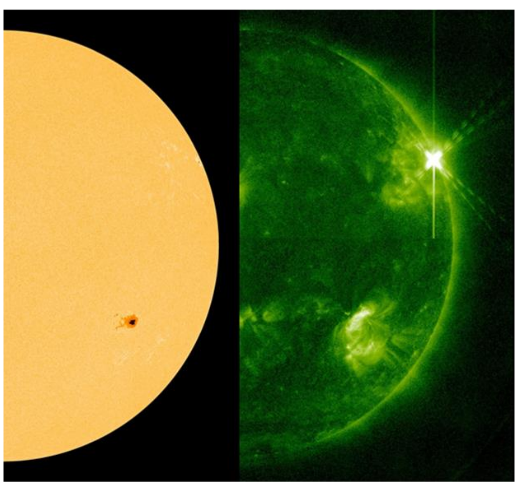

*Figure 3: The Sun's visible western hemisphere at the time of the peak of the X1.5 flare. On the right is the view in extreme ultraviolet (EUV), on the left in white light (Credits: **SDO**). The X-class event originated in NOAA 2838, a tiny sunspot region near the northwest solar limb. The big spot is NOAA 2835, the largest sunspot group of 2021 and reported visible by the (protected) naked eye on 30 June, 1 and 2 July.*

Sunspot numbers increased through the year, with the daily S_N reaching 100 or more around 9 September, late October and again during the second half of December. The highest S_N was recorded on 22 December (150), when also the 10.7cm radio flux (Penticton) reached its highest daily value for the entire year (140.4 sfu, with 1 sfu = 10^{-22} W m^{-2} Hz^{-1}). The largest sunspot groups were NOAA 2835 in July and NOAA 2866 in September, which reached maximum areas of about respectively 4 and 3 times the total surface area of the Earth. Both groups were reported visible by the (protected) naked eye.

The year 2021 also saw the first 2 X-class flares of the new solar cycle. The first one was produced on 3 July by NOAA 2838, a small but quickly developing sunspot region near the Sun's northwest limb. This was the first X-class flare since the X8 event on 10 September 2017, thus ending a stretch of 1391 days without X-class eruptions. The coronal mass ejection (CME) associated with this X1.5 flare was not directed to Earth.

The 2nd X-class flare took place on 28 October and was produced by NOAA 2887, which was also not an impressive sunspot region. This eruption was associated with a minor proton event (the 2nd of 2021 after the 29 May event), but also the greater than 100 MeV reached its alert threshold (1 pfu; 1 pfu = 1 particle $cm^{-2}\,s^{-1}\,sr^{-1}$). As a result, a small Ground Level Enhancement (GLE) was recorded by ground-based neutron monitors. GLE73 was the first GLE since September 2017. The bulk of the CME was directed south of the Earth, and only a minor geomagnetic storm was recorded on 31 October.

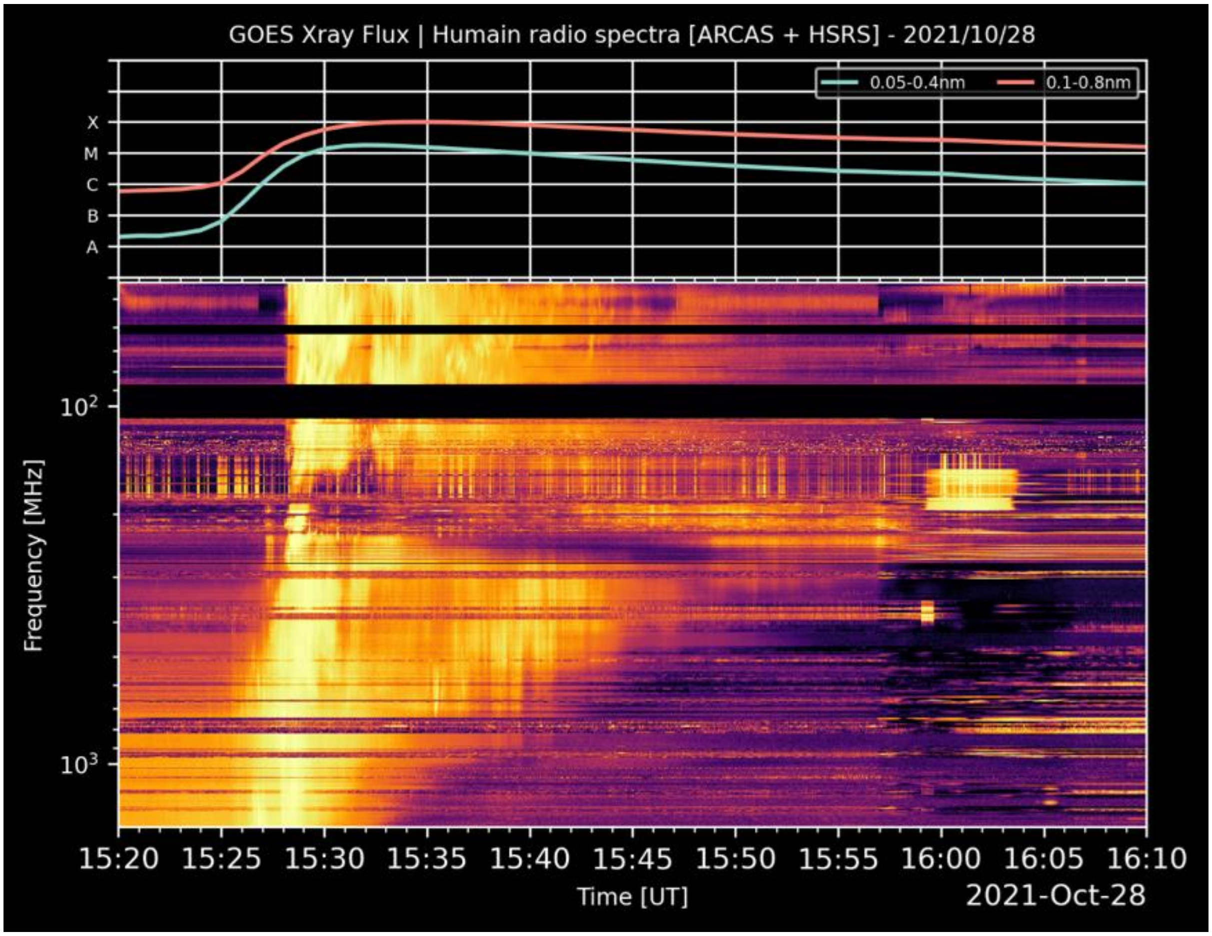

*Figure 4: The Humain Radioastronomy Station recorded the radio emission associated with the 28 October X-class event. Type II and Type IV radio bursts can be seen. The STCE's **SWx classification page** has more info on the different types of radio bursts. The top portion of the graph shows the evolution of the x-ray flux as measured by GOES.*

Aside the 2 X-class flares, there were also 28 M-class ("medium") events of which about two thirds were produced during 4 relatively short burst periods: 22-23 May , 3-4 July, 26 October-2 November, and 17-28 December. Some of the source regions of these flares were already active while still behind the east limb, or continued their eruptive activity while having rounded the west limb. As a result, several farside CMEs were observed throughout the year. In particular on 13 and 15 July two whopping halo CMEs were observed by coronagraphs on board the SOHO and STEREO-A spacecraft. Despite their farside location, the eruptions were so energetic they managed to enhance the proton fluxes recorded by spacecraft located near the first Lagrange point (L1), just 1.5 million km upstream from the Earth.

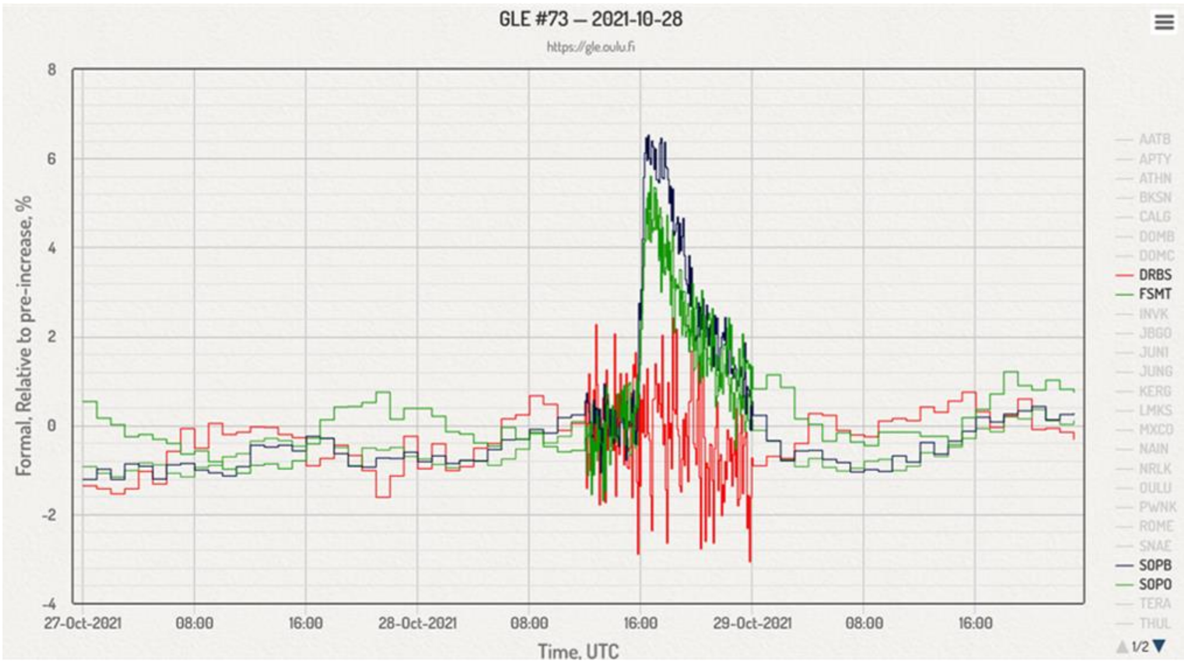

*Figure 5: The chart above was created on the **Oulu webpage** and provides a view on the GLE associated with the X-class flare of 28 October. The 5-7% enhancement above background neutron counts was not observed in **Dourbes** (DRBS - red curve), but in the more (sub)polar stations such as Fort Smith (FSMT) and neutron monitors operated near the South Pole (SOPO, SOPB). During strong GLEs, the enhancements can reach several 10s to 100s % above background levels.*

Another episode of important CME activity took place early November. Following eruptions in NOAA 2887 on 1 November and in NOAA 2891 early on 2 November, the fast earth-directed CME associated with the latter caught up with the much slower CMEs related to the NOAA 2887 activity. The resulting type of CME is called a "cannibal CME" as it overtakes the slower CMEs in front of it, thus creating more complex and enhanced magnetic fields which may result in stronger geomagnetic storms than one would expect.

The interplanetary CME (ICME) arrived at 19:24UT on 3 November when a shock was observed in the solar wind. Solar wind speed reached values over 750 km/s (DSCOVR), the highest of the year. It was accompanied by some periods of significant and sustained southward magnetic field orientation, with Bz getting as low as -18 nT. This resulted in the strongest geomagnetic storm of 2021 (K_p=8-) with the Dst index reaching -105 nT and as such descending for the first time this solar cycle under -100 nT (Kyoto World Data Center).

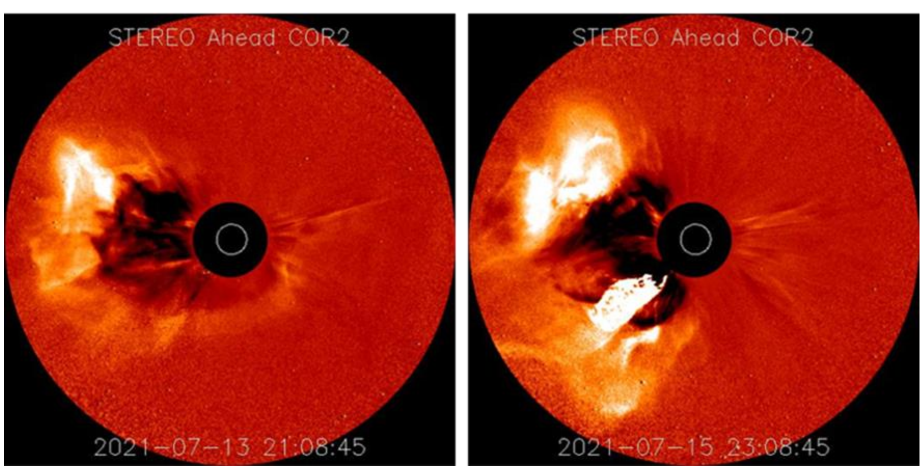

Figure 6: Coronagraph images by the STEREO-A/COR2 instrument of the impressive farside CMEs observed on 13 and 15 July. STEREO-A was trailing the Earth by about 46 degrees at that time, so the Earth is to the right in both images.

Aurorae were photographed as far south as California and New Mexico. The magnetic shielding provided by this strong ICME resulted in a significant decrease in the harmful cosmic rays, as recorded by neutron monitors around the world (a so-called "Forbush decrease"). The neutron monitor in Oulu, Finland showed a brief but sharp decrease of 11% in the 1-hour count rates compared to undisturbed levels.

In terms of Dst, some other weaker geomagnetic storms occurred on 12 May, 27 August, 17 September and 12 October, with minimum Dst values ranging from -61 to -82 nT. They were all associated with ICME impacts, which in turn had their origin in flaring activity or filament eruptions.

High-speed streams from coronal holes (CHs) regularly disturbed the earth environment, but they were less prominent and had a smaller SWx impact than in 2020. High speed wind streams (HSS) related to these CHs drove the maximum solar wind speeds to around 650 km/s for a few days during the February-April and November-December timeframe, with Bz briefly dipping to -19 nT. The passage of these HSS generated elevated levels of energetic (energies of more than 2 MeV) electrons in the Earth's outer radiation belt, as measured by the GOES satellites. Daily maxima occasionally rose above the alert threshold of 1000 pfu (particle flux units; 1 pfu = 1 electron / cm^2 s sr). A maximum flux of nearly 20,000 pfu was reached on 23 April, and the daily electron fluence was at high levels from 21-23 April, the only days of the year. High levels of these electrons can lead to electrostatic discharges (ESD) resulting in malfunctions of a satellite and occasionally even in the satellite failure. After the solar wind speed has decreased to nominal values, high levels of energetic electrons can still persist for several days.

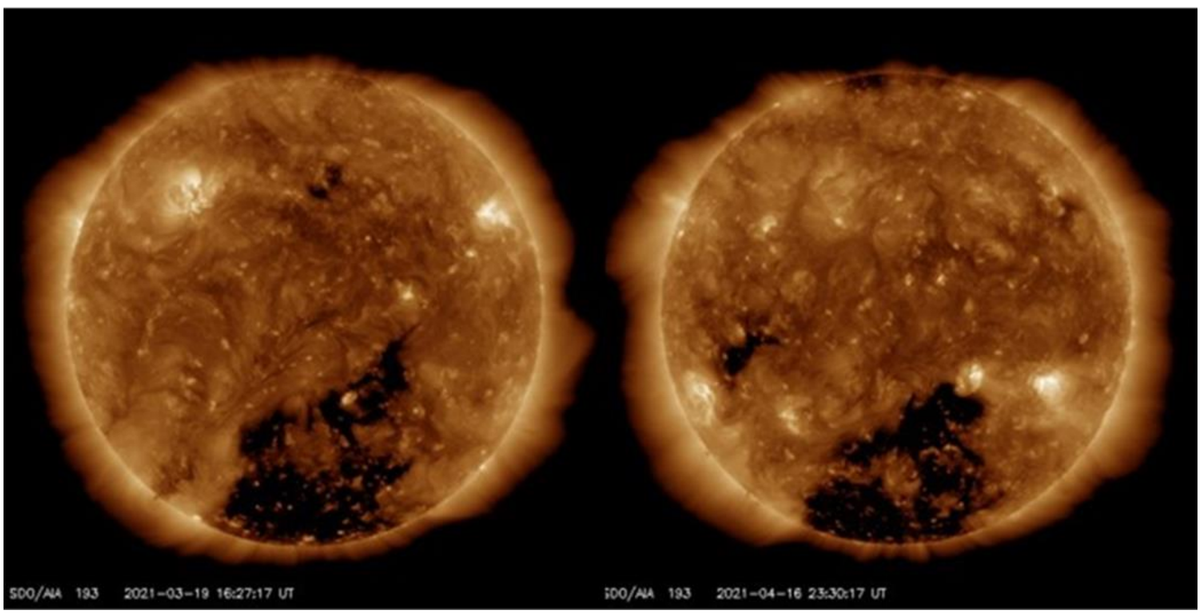

Figure 7: The extension of the southern polar CH responsible for elevated solar wind conditions near the earth environment around 20 March and 20 April.

Public outreach meets Science

Panic in the space weather room

In 2021, the STCE communicators launched a new activity to introduce the general public to the world of space weather: a play called "Panic in the space weather room!".

Figure 8: A view of the "Panic in the space weather room" stand during the WISENIGHT event.

This play starts with a guided tour of the space weather room, where two forecasters are on duty, keeping an eye on the screens with data, movies and dashboards. The tour guide discusses solar activity, data and observations and the duties of the forecasters. Suddenly, an alarm rings! A major solar eruption is seen on the displays. The forecasters jump into action to analyse the event and prepare an alert message, while the guide explains to the public what has happened and what action needs to be taken.

This play is an excellent format to show the daily life of the forecasters and to highlight our most recent bulletins for the PECASUS consortium, focusing specifically on the impacts of space weather on aviation. The active format also engages the public and invites questions and interaction.

Our space weather play premiered during the WISENIGHT event at the Planetarium on 24 and 25 September and was performed 4 times each day, alternating between Dutch and French versions. In the future, we plan to bring "Panic in the space weather room!" to science fairs and the Space Pole Open Days.

MOMSTER: MObile Meteor STation for Education & outReach

What is MOMSTER? - The BRAMS (Belgian Radio Meteor Stations) team, the communication cell at the Royal Belgian Institute for Space Aeronomy (BIRA-IASB), the KU Leuven and the Planetarium Brussels have developed MOMSTER (MObile Meteor STation for Education & outReach), a Meteor Education Kit, as a resource for STEAM (Science, Technology, Engineering, Arts, Mathematics) teachers in secondary schools. This kit includes a mobile radio meteor station and an educational package to learn all about meteors and their impact on the atmosphere and the planet as a whole, while at the same time conveying a fascination for the ephemeral beauty and complexity of these natural light shows. The project goals are stimulating STEAM (ultimately resulting in nudging future career choices towards science or engineering career paths)

Figure 9: A view on a MOMSTER box (top), and the radio meteor station consisting of a short dipole antenna (lower left) and a receiving box (lower right).

and the use of citizen science (especially the Radio Meteor Zoo initiative) at schools, and reaching the general public.

The development of educational resources builds upon preliminary experience we gained from our participation in an Erasmus+ project called BRITEC (Bringing Research into ThE Classroom), in which teachers and pupils took part in the Radio Meteor Zoo activity. In 2021, three MOMSTER boxes were developed. Each of them includes a mobile, easy-to-use radio meteor station consisting of a short dipole antenna and a receiving box, a PC with the program to visualize the stream of data recorded by the system, as well as educational material. In a pilot phase, three Belgian schools (two Dutch speaking and one French speaking) tested the mobile radio meteor station and the educational resources, and gave their feedback. The educational material will continue to grow with and thanks to teachers' experiences in the classroom.

What makes MOMSTER innovative? - Space and atmospheric science are STEM disciplines par excellence, involving various science fields (physics, mathematics, chemistry, biology, geography, engineering, ...). The "study of shooting stars and meteor showers" is a subject triggering the imagination. It has the potential to raise interest in STEM disciplines and increase science information retention by linking with Art (i.e., "STEAM-education") and citizen science, both in formal and informal education. We foster collaborations with teachers from secondary schools to boost interest in the science behind these phenomena.

The project BRITEC was unique in its kind by bringing citizen science into the classroom. The MOMSTER project goes even one step further by physically bringing the measuring devices to the schools. This approach will likely increase levels of ownership (the school "takes care" of the device) and will facilitate interactions between pupils of all ages. It creates extra possibilities to involve art students and others who are otherwise less likely to get in touch with STEM-content.

MOMSTER was supported by the 2020 round of the Europlanet Public Engagement Funding Scheme.

Figure 10: A radio expert from BIRA-IASB explaining to a group of school children how to use the PC that contains the program to visualize the stream of data recorded by the radio meteor station.

In September 2021, the STCE sent its dream team (Elke, Sabrina, Shreya, Yana and Petra) to the WISENIGHT event for the premiere of "Panic in the space weather room!".

Fundamental research

The discovery of "campfires" on the Sun

The "Extreme Ultraviolet Imager" (EUI) is a combination of 3 telescopes on board Solar Orbiter. In particular, the HRIEUV telescope ("High Resolution Imager in the EUV") has an outstanding performance taking images of the solar corona at extreme resolution. Depending on the distance to the Sun, a footprint of a HRIEUV pixel can be as small as 100 km on the solar surface, and the imaging cadence can be as fast as 2 seconds. Such a performance in the solar corona has only been reached by one earlier instrument that operated only for a few minutes, as it was mounted on a sounding rocket. HRIEUV is therefore one of the success stories on Solar Orbiter, which started its nominal mission phase on 27 November 2021 for an expected duration of about 10 years.

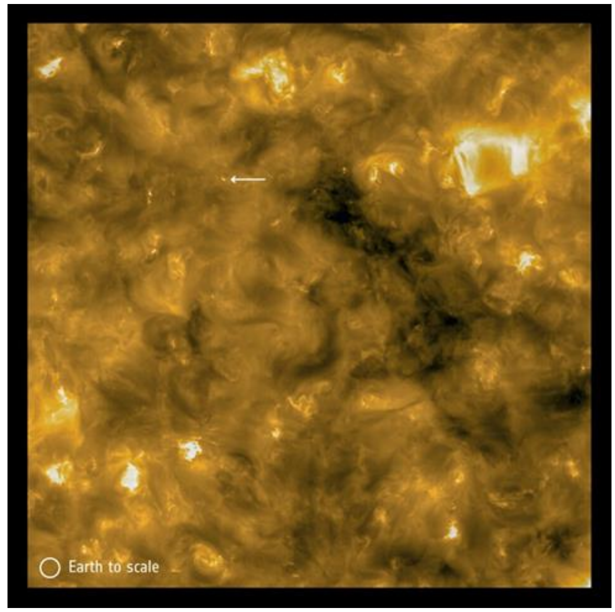

Figure 11: Snapshot from an ESA press release covering the campfires seen as tiny bright specs in the EUI images.

Before the start of the nominal mission phase however, HRIEUV already took many series of test images. In one of the early sequences (30 May 2020), short-lived brightenings were discovered (Berghmans et al. 2021) which were jokingly called "campfires" to illustrate their very small size (Figure 11). In reality, these small brightenings are still between 400 and 4000 km large, but as compared to the big solar flares, they are tiny. Tiny flares have been observed before and are of particular interest as they might collectively contribute more to the heating of the solar corona than their bigger cousins that can even influence the space weather around the Earth.

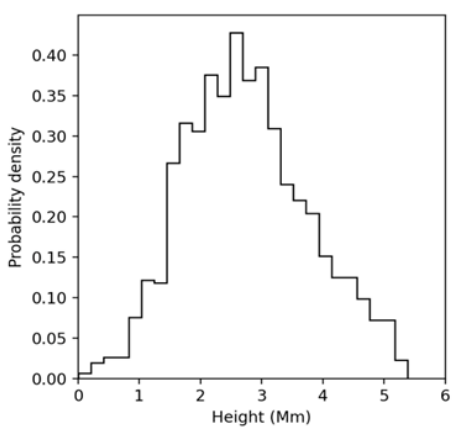

Figure 12: The height of campfires above the solar surface (reproduced from Zhukov et al. 2021). Note 1 Mm = 1000 km.

Nevertheless, campfires turned out to be special. Never were flare-like brightenings observed so sharply at such small scales. The next best telescope (SDO/AIA) could confirm most of the campfires, but only sees fuzzy patches, whereas HRIEUV can clearly see tiny loop-like structures interacting. Moreover, triangulation between HRIEUV and AIA revealed that campfires live at the lower boundary of the corona, barely sticking out of the cooler chromosphere (Figure 12, Zhukov et al. 2021).

Follow-up observations were made with another high-resolution instrument on board Solar Orbiter, the "Polarimetric and Helioseismic Imager" (PHI). PHI can make magnetic maps of the solar surface (see Figure 13) and these showed that most of the campfires coincide with magnetic

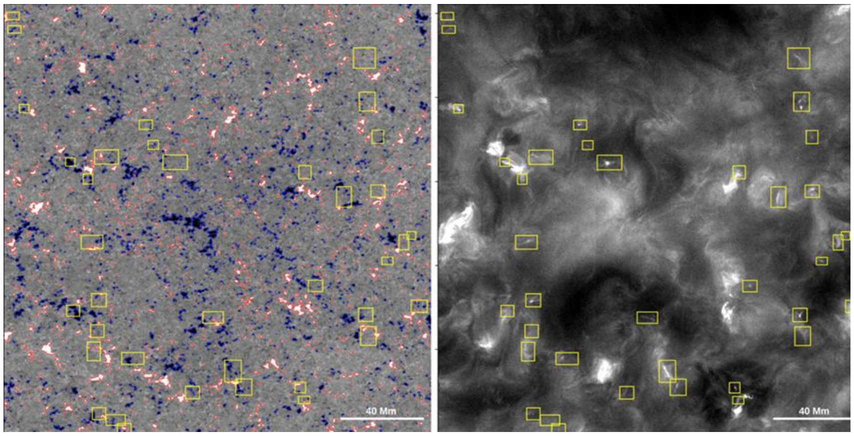

Figure 13: Distribution of campfires (yellow boxes) as seen in PHI magnetograms (left) and EUI/HRIEUV images (right). Blue and red contours on the left correspond to negative and positive magnetic flux. The scale indicator (40 Mm) corresponds to the Earth circumference (reproduced from Kahil et al. 2022).

cancellation events in which magnetic flux disappears from the solar surface (Kahil et al. 2022). With the help of 3D simulations of the solar corona, it was shown that magnetic energy can indeed be converted and released, resulting in brightenings in the EUV emission that we see as campfires (Chen et al. 2021). Several other publications studied the dynamics in campfires, sometimes seen as tiny jets.

Finally, the relevance of campfires for the coronal heating mystery is being addressed by studying statistically if a large number of campfires can collectively make a significant contribution to the heating of the million degrees solar corona.

The $F_{10.7}$ radio flux revisited

The solar radio flux at a wavelength of 10.7 cm ($F_{10.7}$) is a long-term reference index of solar activity that represents the background radio flux when there are no flares. Its source is mostly thermal radio emission (i.e. the emitting particles are in local thermodynamic equilibrium) from the lower corona. It is a good standard long-term proxy of the solar ultraviolet (UV) irradiance going back to 1947. It is closely related to the Sunspot Number S_N, which is available since 1700, and the $F_{10.7}/S_N$ proxy relation allows backward reconstructions of UV irradiance over multiple centuries.

However, over the years, a confusing picture arose as to the exact relation between $F_{10.7}$ and S_N, with about a dozen of publications providing 18 different formulae that mostly disagree (Figure 14), and for which no error bars had been determined. Since the Sunspot Number was re-evaluated in 2015 (S_N version 2.0; Clette & Lefèvre, 2016), it seemed time to re-evaluate the relationship between this new S_N and $F_{10.7}$.

Thus, in 2021, Frédéric Clette developed a new 4th degree polynomial with errors, and of which the equation can be found in the research paper published in the open access Journal of Space Weather and Space Climate (Clette, 2021).

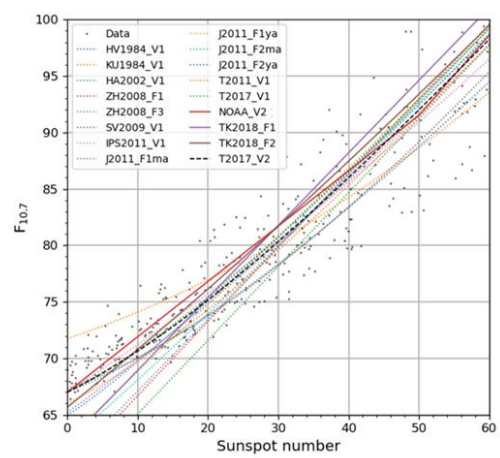

Figure 14: Different relationships between S_N and $F_{10.7}$

Frédéric also discovered a very interesting fact, unbeknownst to everyone until now: this relationship is not stable over time and there is an abrupt change of more than 10% in 1980 (Figure 15 left), with the relation being stable before and after this jump (Figure 15 right).

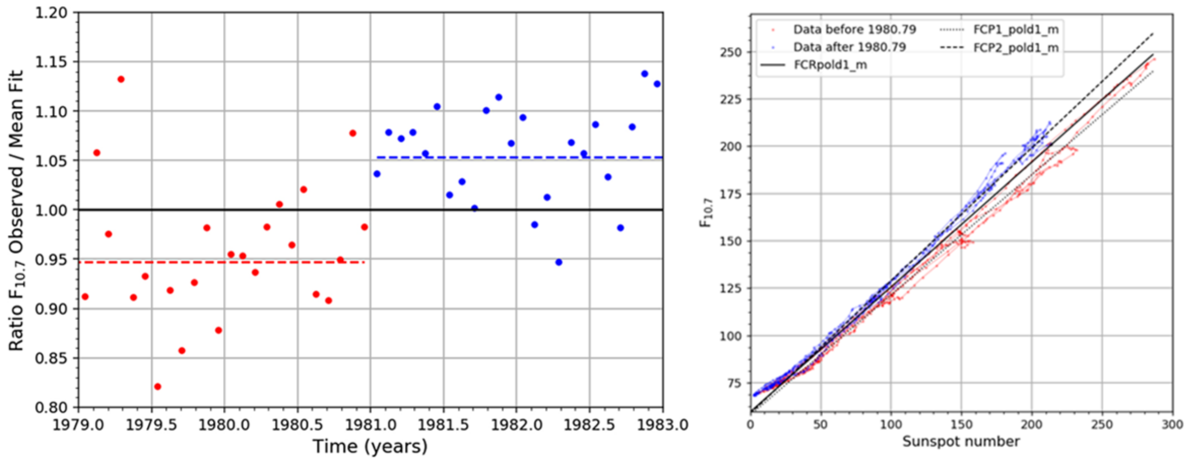

Figure 15: (left) Monthly ratios between the observed monthly mean $F_{10.7}$ flux and the proxy value derived from the linear fit over the entire interval 1947-2015. The dashed lines correspond to the global fits on the entire half-series before and after 1980. (right) Relationship between S_N and $F_{10.7}$ before (red) and after 1980 (blue).

Although the timing is suspiciously close to the time when the sunspot number S_N was transferred from Zürich to Brussels in 1981, there is no evidence that this jump occurs in S_N, so it points towards an undocumented change in the $F_{10.7}$ radio flux. The exact reason is still being investigated.

The main conclusions advanced in the paper are that the base $F_{10.7}/S_N$ relation is fully linear except for the 0 point, and that the non-linearity is entirely due to the temporal smoothing. Thus, the optimal proxy is a 4^{th} order polynomial based on monthly means. The mean quiet-Sun $F_{10.7}$ flux varies with the number of spotless days with an invariable base flux of 67 sfu (solar flux units). A 10.5% upward jump in the $F_{10.7}/S_N$ relation occurring in 1980-1981 seems not to be due to the revised S_N.

Results from the VAL-U-SUN project

World Data Center for Sunspot Index - The Sunspot Number (S_N) is the longest scientific experiment still ongoing and a crucial benchmark to study solar activity, space weather and climate change. The Royal Observatory of Belgium (ROB) plays a central role in the continuation of this experiment, as it hosts the Sunspot Index and Long-term Solar Observations World Data Center (WDC SILSO). This World Data Center aims at collecting solar data, as well as producing and distributing the International Sunspot Number, which is used in about two hundred scientific publications on an annual basis.

The BRAIN-be project Val-U-Sun (2017-2021) aimed at valorizing the long-term solar observations from the ROB. In collaboration with UCLouvain and PhD student Sophie Mathieu, we conducted a comprehensive statistical analysis of the WDC SILSO sunspot numbers collection and laid the ground for a future monitoring of all active stations in near real time. We summarize here the main results of Sophie Mathieu's PhD thesis.

Uncertainty quantification in sunspot numbers - To be able to alert observers when they start deviating from the network, one must first study the errors in the S_N, in other words, to develop an uncertainty model. We consider the period 1947-2013, and a dataset of 21 stations with records of the number of spots Ns, the number of groups Ng, and the composite Nc = Ns + 10Ng based on the original formula by Rudolf Wolf in 1849. Our uncertainty model is valid for Ns, Ng, and Nc and contains three types of errors (Mathieu et al. 2019):

- A short-term, rapidly evolving, error that describes the counting error and variable seeing conditions at station i and time t.
- A station-specific long-term error that accounts for systematic biases. We are interested in estimating its mean and see if it experiences sudden jumps or drifts on longer time scale.
- A third and final error term that captures what happens during minima of solar activity when there are few or no sunspots during extended periods.

An observer typically makes larger errors when the Sun is more active and produces more sunspots, which means that both the short- and long-term error terms should be multiplicative errors. Thus, having devised a procedure for estimating s(t), which is a latent (unobserved) variable representing the "true" solar signal, we get access to the observed values of errors. Those exhibit an excess of zeros, i.e. an unusual local peak in the density at zero due to solar minima periods, as well as several modes. To account for these characteristics, we use zero-altered mixture of Probability Density Functions (PDF) to fit those values. The Interquartile Range (IQR) is an appropriate measure of the dispersion in these PDF. Figure 16 represents a scatter plot of the long-term versus short-term empirical IQR of the number of spots Ns for several stations. Basically, it provides us with a view on the stability of stations outside periods of solar minima. Typically, we see that teams of observers (in red) experience more short-term variability than individual observers (in black), but show a better long-term stability.

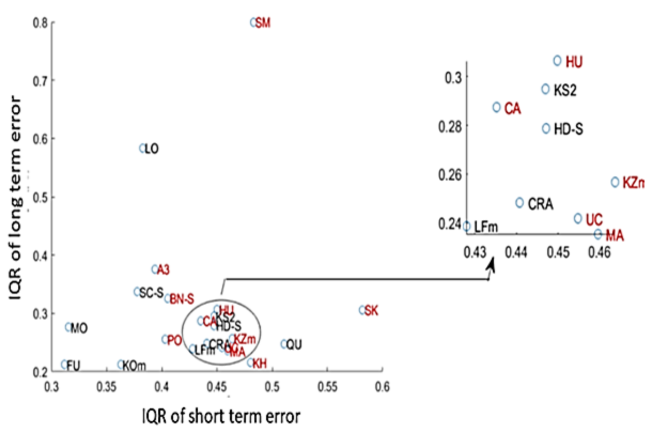

Figure 16: Scatter plot of long- versus short-term error IQR for the number of spots Ns. Red stations are teams of observers, black are individual observers. Teams usually have larger short-term errors. MO (Mochizuki, Japan), FU (Fujimori, Japan), and KOm (Koyama, Japan) correspond to long-time observers with stable observation practices, and have low variability both on short- and long-term. UC (Uccle, Belgium) shows a large variability in the short-term, due to many observers, but has an interesting long-term variability.

Monitoring the sunspot number observations by stations - Now that we've determined an uncertainty model, we need to monitor the stations. The so-called "Cumulative sum" (CUSUM) Control chart is a sequential analysis technique used for monitoring change detection. It was first devised for normally distributed errors, and in the presence of In-Control (non-deviating) observations. We saw that the time series of the S_N composite Nc exhibit strong noise, a complex autocorrelation structure, non-normality, and missing values. Hence, in Mathieu et al. (2022), we devised a monitoring strategy tailored to Nc. We first selected a group of In-Control stations and use them to standardize all the stations. Second, the standardized data were monitored by a CUSUM chart adapted to time series. This control scheme was applied on past observations to study the deviations of the sunspot numbers, as seen in Figure 17.

The VAL-U-SUN project, thanks to Sophie Mathieu's work, has given the WDC SILSO the means to use the most advanced statistical methods to monitor its network and compute the International Sunspot Number in near real time.

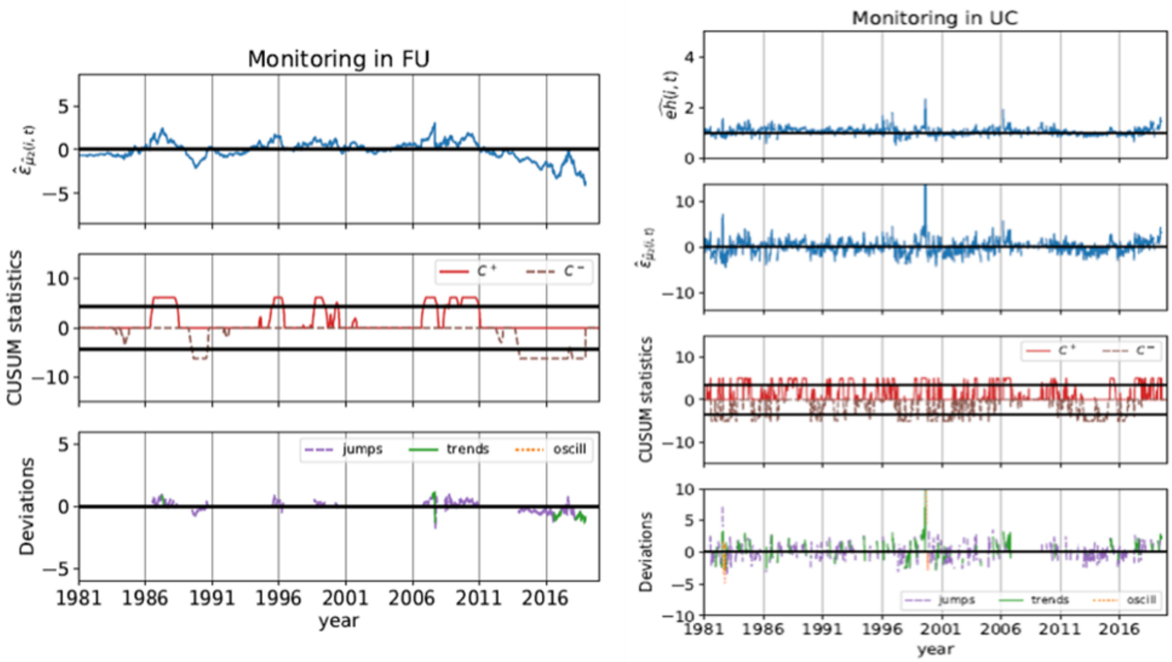

Figure 17: (left) Control scheme for Nc (smoothed over 365 days) of the FU (Fujimori) station, which is composed of a single dedicated observer in Japan who observed without interruption since 1968 until today. Although the series was remarkably stable for decades, it suffers from recent deviation, see e.g. the downward trend beginning in 2011 which might be associated with the health condition of the observer. (right) Control scheme for Nc (smoothed over 27 days) for the UC (Uccle, Belgium) station. ROB's station is stable over time but suffers from a large jump in 1999, due to the intense participation of a particular observer that did not count with the same precision as the other members of the team. He was recruited at a time where there was a lack of observers, but eventually stopped observing.

Electron heat flux instabilities in the inner heliosphere

The solar wind is a stream of electrons and ions blown away by the Sun in all directions. It is known to be populated by different types of plasma waves affecting its properties: bulk speed, temperature, velocity distributions of particles, etc. Some of these waves can be directly caused by the Sun and its atmosphere (for instance, Alfvén waves), others are generated by plasma instabilities in situ in the solar wind. In particular, electron heat flux events (EHFs) -events with a strong flux of suprathermal electrons (i.e. electrons with energies of about 60 - 1000 eV) streaming along the interplanetary magnetic field (see an example sketch in Figure 18)- provide a free energy source for the excitation of waves.

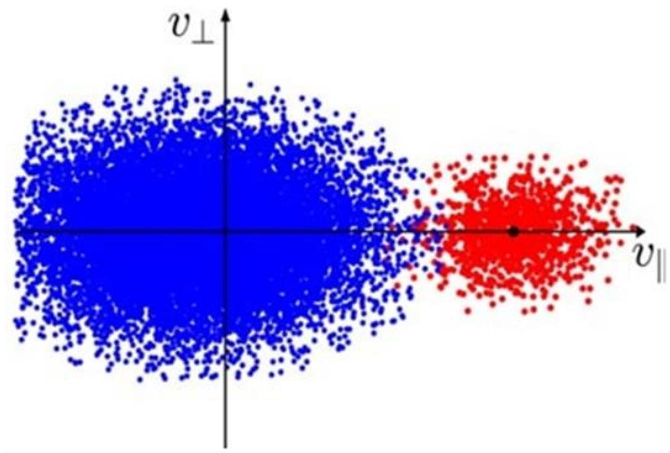

Figure 18: Example of the electron velocity distribution in the solar wind. The plot shows the velocity components parallel and perpendicular to the local interplanetary magnetic field. In addition to the main thermal electron population (blue dots) there is a suprathermal electron beam (red dots) carrying the heat flux along the interplanetary magnetic field. In this particular example the thermal spread of the electron velocities $v_{||}$ parallel to the magnetic field is larger than the spread of the perpendicular velocities $v_{\perp}$.

As EHF events are widespread in the solar wind, the instabilities and waves they create are of high importance for the solar wind dynamics. In collaboration with Chinese colleagues, we investigated from a theoretical perspective a number of specific plasma instabilities driven by EHFs. We found that the relatively fast EHFs generate electron-acoustic waves, reminiscent of acoustic waves in our atmosphere. However, anisotropic velocity distributions, like that shown in Figure 18, preferentially generate oblique whistler waves, which are similar to the whistlers (VLF radio waves) generated in the terrestrial magnetosphere by lightning. These waves can be generated by fast EHFs anywhere in the solar wind between the Sun and the Earth.

Close to the solar wind base, at heliocentric distances of 10-30 solar radii, we predicted that several other instabilities can dominate. Among them, the strongest are the parallel whistler EHF instability at distances of around 10 solar radii, and the highly oblique lower-hybrid EHF instability at distances around 30 solar radii. The lower-hybrid waves are electrostatic oscillations with frequencies near the lower-hybrid frequency, which is close to the geometrical mean of the electron-cyclotron and proton-cyclotron frequencies $(\Omega_{ce}\Omega_{cp})^{1/2}$. These instabilities are much less restricted by the EHF speed and can be driven by 2-3 times slower electron beams than the electron-acoustic and oblique whistler EHF instabilities. Our predictions for lower-hybrid waves generated by the EHFs at distances of 30 solar radii are illustrated in Figure 19 (Sun et al. 2021). The fastest growing lower-hybrid waves are expected to possess a dimensionless wavenumber $\lambda_e k \sim 0.17$ and propagate almost perpendicular to the magnetic field (at an angle $\theta \sim 87°$). The wave amplitudes grow fast, with a characteristic growth time of ~1 s.

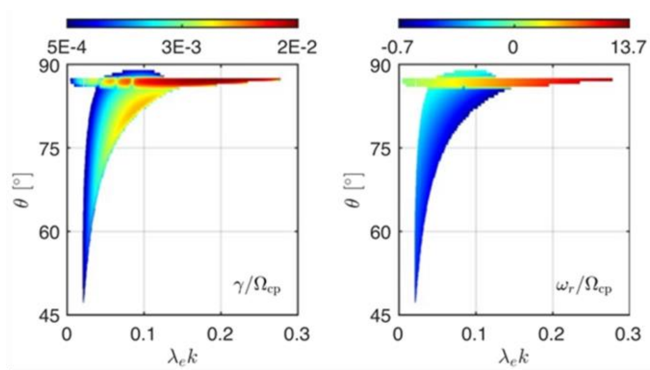

Figure 19: Distribution of the dimensionless growth rate γ/Ω_{cp} and frequency ω/Ω_{cp} (Ω_{cp} is the proton cyclotron frequency) of the unstable lower-hybrid waves in the wavenumber space $\lambda_e k$-ϑ (k is the wavenumber, λ_e is the electron inertial length, and ϑ is the inclination angle between the wave vector k and the background magnetic field B). Such waves are expected to be generated by the electron heat flux in the solar corona at heliocentric distances of 10-30 solar radii.

In conclusion, theory suggests that lower-hybrid waves are generated efficiently by the relatively slow EHFs at heliocentric distances of 10-30 solar radii. After the launch of the Parker Solar Probe mission, direct in situ observations of plasma particles and waves at such heliocentric distances became possible and can be used to verify our theoretical predictions. This study is now ongoing.

Study of the Earth's radiation belts

The Solar Wind group in the Space Physics division of the Royal Belgian Institute for Space Aeronomy (BIRA-IASB) conducts research of the near-Earth space radiation environment, and of the radiation belts in particular. This region beyond our atmosphere contains very energetic particles, mainly electrons and ions, trapped in the Earth's magnetic field in the so-called Van Allen belts. BIRA-IASB has contributed to the development of a detector, the Energetic Particle Telescope (EPT), that was launched in May 2013 on board the satellite PROBA-V into a high-inclination Low Earth Orbit at an altitude of 820 km (see Figure 20).

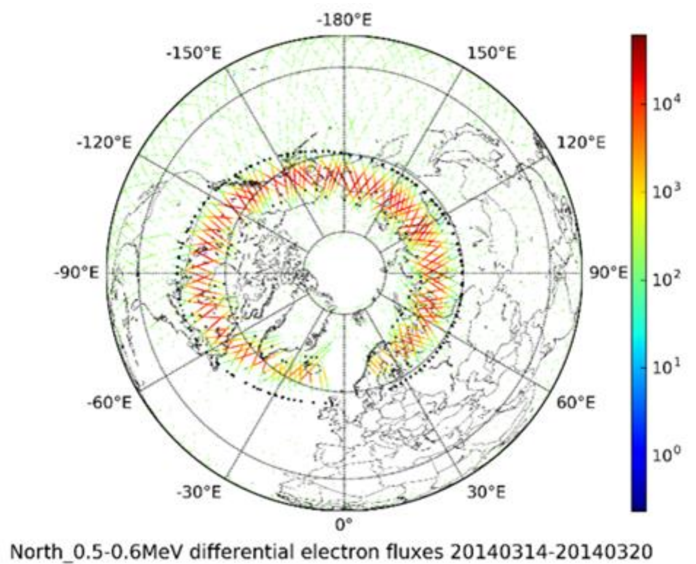

Figure 20: EPT observations at an altitude of 820 km in the Northern hemisphere of 500-600 keV electron fluxes from 14 to 20 March 2014. The black circles with increasing radius correspond to constant latitudes of 80°, 60° and 30°. (Pierrard et al. 2021c)

This instrument, presently still active, gives exceptional observations simultaneous to the measurements of NASA's Van Allen Probes. These in situ observations of the energetic particles have allowed us to determine the dynamics of the electron fluxes during geomagnetic storms, characterized by dropouts, flux enhancements and slower decays after the events.

Using kinetic simulations, we identified the physical mechanisms leading to the losses of the electrons during dropouts and slower decays (Pierrard et al. 2021b). We established also the links of the radiation belts boundaries with other regions of the magnetosphere, and especially with the auroral oval, the plasmapause position and the ionospheric trough (Pierrard et al. 2021c). Low-energy particles forming the plasmasphere, i.e. the "cold" plasma rotating with the Earth, interact with the belts via electromagnetic waves. Using measurements of Van Allen Probes in the plasmasphere and the 3D dynamic plasmasphere model that we have developed (Pierrard et al. 2008) we were able to calculate the diffusion coefficients contributing to the loss of energetic electrons (Pierrard et al. 2021b).

Solar wind studies

The perturbations in the radiation belts and the plasmasphere are due to solar wind variations. Solar wind has been investigated using the recent observations by the Parker Solar Probe approaching the Sun as never done before (Maksimovic et al. 2021). This allowed us to explore the effects of the presence of solar wind suprathermal electrons in the acceleration process of the solar wind (Pierrard et al. 2021d). This work was part of a publication about kappa distributions (see Figure 21). The effects of heat flux instabilities on the radial evolution of the particle velocity distribution functions have been studied using kinetic simulations (Sun et al. [2021](#)). On the occasion of these exceptional new results, reviews concerning the solar wind have been published (Rouillard et al. [2021](#)).

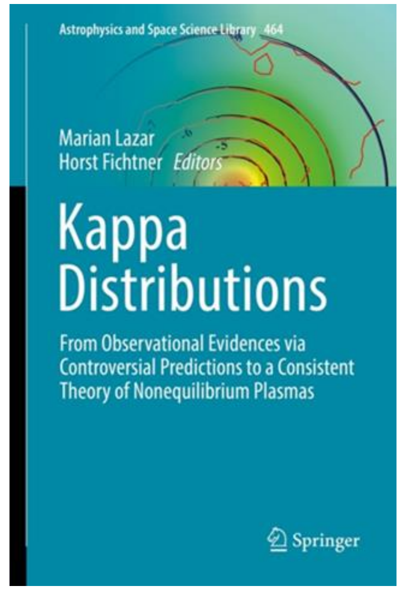

Figure 21: Kappa Distributions: From Observational Evidences via Controversial Predictions to a Consistent Theory of Nonequilibrium Plasmas, published by Springer.

Reconstructing meteoroid trajectories using data from the BRAMS network

When meteoroids hit Earth's upper atmosphere atoms and molecules, they leave a trail of plasma (charged particles) behind. This region, composed of free electrons and positively charged ions, is capable of reflecting radio signals emitted from the ground. The reflection on the plasma trails is essentially specular, which means that the radio wave is reflected mostly at a given point along the meteoroid trajectory.

This specular point is the point which minimizes the total distance travelled by the radio signal, from the transmitter to the receiver, after reflection on the trail. For forward scatter systems (where both the transmitter and the receiver are at different locations), the position of this specular point depends only on the meteoroid trajectory and on the positions of both the transmitter and the receiver. Using multiple receivers in different locations, one obtains several specular reflection points along the trajectory. Therefore, the receivers will detect a reflected signal (usually called a meteor echo) at slightly different time instants for a given meteoroid. This is illustrated in Figure 22.

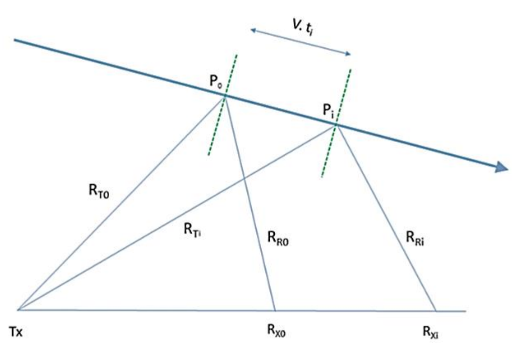

Figure 22: Geometry of the problem (Tx = transmitter, Rx = receiver, P = specular point).

We have implemented and tested a method that aims at reconstructing the meteoroid's trajectory and speed from the data of a forward scatter radio system using only the time delays measured between meteor echoes recorded at several receiving stations. If meteor motion at constant speed is assumed, there are 6 unknowns: the coordinates of one specular reflection point and the three coordinates of the speed. They are computed through an iterative procedure, which involves a system of at least 6 equations with the time differences measured at the receivers as the only inputs.

This method has been applied to actual radio observations from the [BRAMS](#) (Belgian RAdio Meteor Stations) network. The latter consists of a dedicated transmitter and of 42 receiving stations located in and nearby Belgium. The BRAMS network also includes an interferometer in the radio astronomy site of Humain (south of Belgium). Unlike the other receiving stations, the interferometer allows to determine the direction of arrival of the meteor echo. This additional information strongly simplifies the trajectory determination process but can only be applied to a limited number of meteoroid trajectories, namely those that have been detected by the interferometer and at least 3 additional BRAMS receiving stations.

Promising results regarding the reconstructed position, velocity and inclination of several meteoroid trajectories have been obtained. To assess the quality of the reconstruction, a comparison is made with accurate meteoroid trajectories and speeds obtained from optical observations of the CAMS-BeNeLux network (Cameras for All sky Meteor Surveillance - Belgium, The Netherlands and Luxembourg), for which BIRA-IASB provides daily data from 6 cameras. An example of such a reconstruction is shown in Figure 23. The CAMS trajectory is shown in blue. The reconstructed trajectory (in purple) using the time differences only (method 1) is shown on the left. The trajectory obtained thanks to the combination of time differences and interferometric data (method 2) is given on the right. Method 2 is extremely accurate while method 1 provides satisfactory results, at least for the speed measurements and inclination angle.

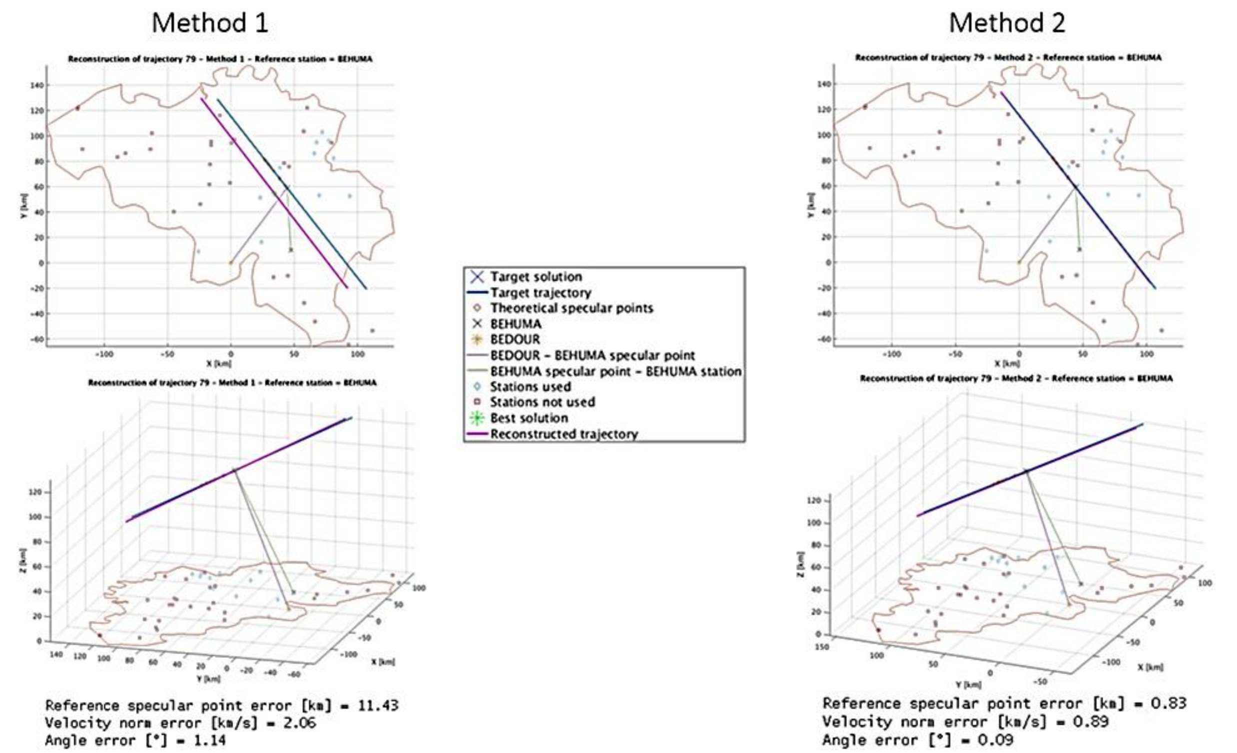

Figure 23: Example of trajectory reconstructions.

Knowing the meteoroid trajectories and speeds is essential for most applications using BRAMS data. They will be used for various scientific purposes such as the classification of meteors in meteor streams, the quantification of the electron line density, the analysis of the mesosphere/lower thermosphere properties (temperature, high-altitude wind speeds), and the characterization of the meteor ablation process. This should allow us to obtain important information about faint and small meteors, which cannot be detected by optical systems.

Radiative transfer tools in support of studies of solar radiation effects on atmospheres

ASIMUT is a radiative transfer and retrieval tool developed at the Royal Belgian Institute for Space Aeronomy (BIRA-IASB). Originally developed for Earth observations from ground and space, it has been expanded for use in planetary science. It is currently being used for Venus and Mars, and many future applications are planned. Support from the STCE was used to add further capabilities to ASIMUT so as to facilitate novel research.

Line-mixing - Line-mixing is a physical effect that changes the absorption cross section of some species at high pressure in the infrared. We found that this effect was largely ignored when retrieving the mixing ratio of methane (CH_4) in the thermal infrared (TIR) region. As part of the ESA supported CH4TIR project, we implemented line-mixing for methane into ASIMUT to investigate whether it had an impact on methane retrievals based on satellite observations from the Infrared Atmospheric Sounder Interferometer (IASI).

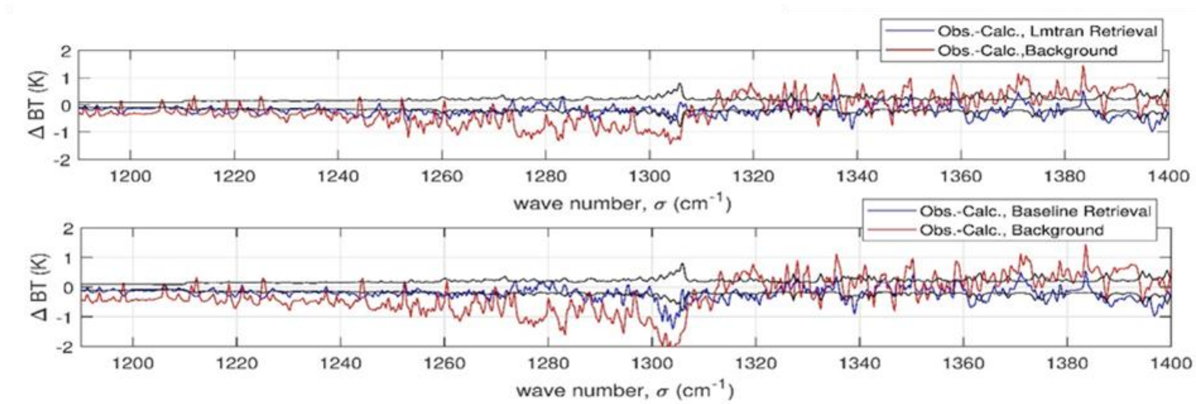

Figure 24: The residuals for an example IASI spectrum with line-mixing (upper panel) and without line-mixing (lower panel). Red lines are the residual before retrieval (a priori) and blue lines are after retrievals (fitting all species).

In Figure 24, the smaller residuals demonstrate that considering line-mixing improves our model fit of the IASI spectrum, especially for the methane Q-branch near the 1300 wavenumber spectral region known to be strongly affected by line-mixing. This means that we can better match observations and increase the accuracy of our knowledge of the global distribution of methane. Since the last laboratory measurements of CH_4 line-mixing were done 20 years ago, we initiated a collaboration with the "Laser and Spectroscopies" (LLS) research unit at the University of Namur to conduct a new campaign of laboratory work. We expect to update the methane line parameters related to line-mixing using modern techniques and theory, and to provide this to the international community.

Lookup Tables - Especially in the infrared region, the computation of the absorption cross-sections takes significant time when retrieving trace gases and temperature. The computational work can be prohibitively intensive for the detailed processing of large datasets. We expanded our radiative transfer retrieval tool so that it now can create and use Lookup Tables (LUTs), which are pre-calculated absorption cross-sections on a large grid of temperature, pressure, and wavelength (Figure 25). By carefully interpolating from the LUTs during individual retrievals, we gain a significant increase in speed (> 1000x) without sacrificing the accuracy and flexibility of using new and innovative line lists and parameters.

Temperature Retrievals - It is possible to infer the temperature at different altitudes in the atmosphere from satellite observations. In the thermal infrared, one can use emission by trace gases (related to the greenhouse effect), and in other regions one can exploit the rotational distribution or line shape of the molecule. We implemented these methods in ASIMUT, adding to its current ability of trace gas, surface temperature, and aerosol retrievals. By first retrieving the temperature structure, we can better model the spectrum, which results in improved trace gas retrievals.

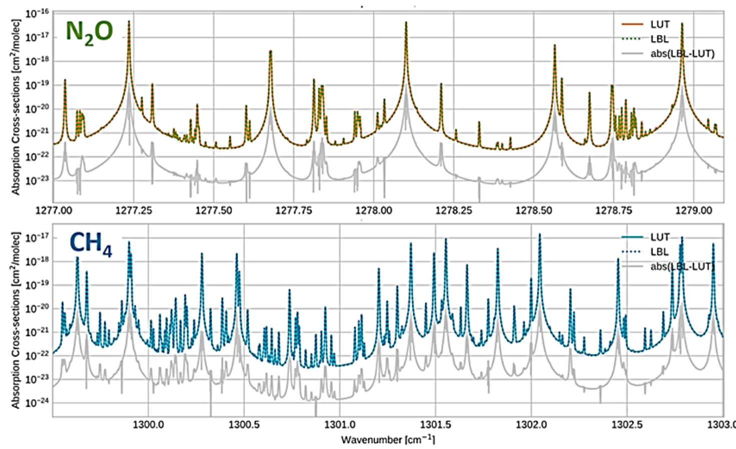

Figure 25: Comparison of absorption cross-sections of N_2O and CH_4 calculated with the line-by-line (LBL, dashed) approach and bi-linear interpolation from a pre-calculated LUT (solid) for a pressure of 2.5 hPa and temperature of 270 K. Also shown is the absolute difference between both approaches (grey).

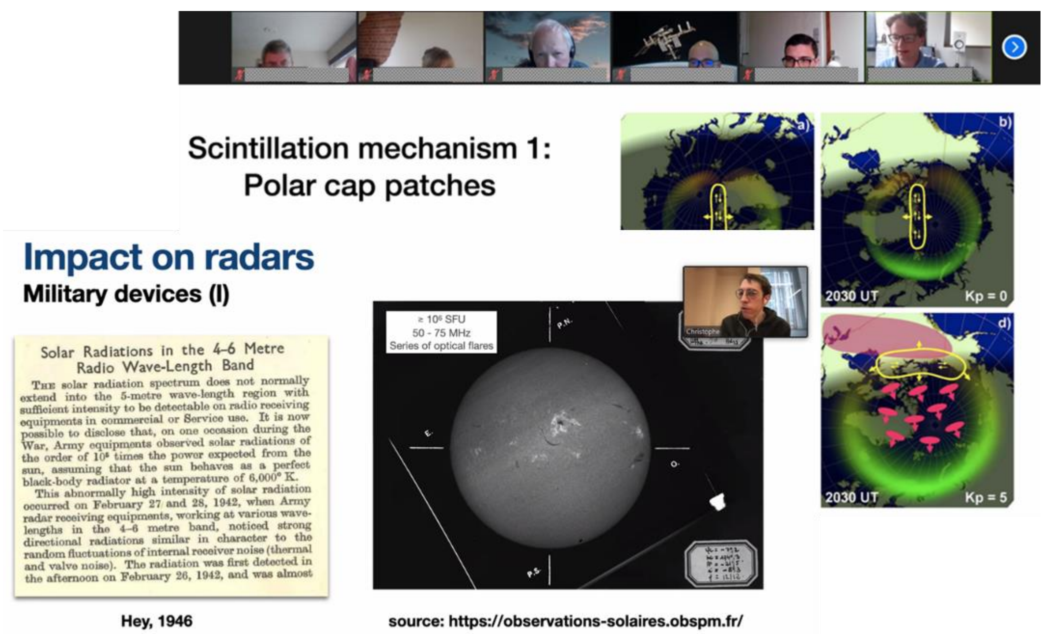

Solar Radiations in the 4–6 Metre Radio Wave-Length Band

The solar radiation spectrum does not normally extend into the 5-metre wave-length region with sufficient intensity to be detectable on radio receiving equipments in commercial or Service use. It is now possible to disclose that, on one occasion during the War, Army equipments observed solar radiations of the order of 10^5 times the power expected from the sun, assuming that the sun behaves as a perfect black-body radiator at a temperature of 6,000° K.

This abnormally high intensity of solar radiation occurred on February 27 and 28, 1942, when Army radar receiving equipments, working at various wave-lengths in the 4–6 metre band, noticed strong directional radiations similar in character to the random fluctuations of internal receiver noise (thermal and valve noise). The radiation was first detected in the afternoon on February 26, 1942, and was almost

The Space Weather Education Center (SWEC) organized no less than 6 SWx Introductory Courses (SWIC) during 2021. These were all given online. SWx knowledge was passed on to the participants through lectures, fancy exercises, and talks from guest speakers such as Dr Christophe Marqué (ROB) on solar radio bursts and Dr Eelco Doornbos (KNMI) on ionospheric scintillations.

Instrumentation and experiments

RMI participates in five-yearly calibration of solar instruments to world standard

In autumn 2021, the RMI participated in a five-yearly field campaign of the World Meteorological Organization (WMO). For three weeks, the solar team compared the Belgian reference solar instruments with the world standard, so that solar and other radiation measurements of the RMI are comparable with measurements made by other meteorological institutes around the world.

Figure 26: Two solar instruments of the RMI, CROM9 and CROM5, mounted on a tracker that tracks the Sun.

Solar instruments or pyrheliometers - The reference instruments we use are so-called pyrheliometers. These can measure direct radiation from the Sun with high precision. To avoid measuring radiation other than the Sun's direct radiation (such as stray light from the atmosphere), the instrument has a very small precision aperture and is pointed at the Sun by means of a tracker. The incident radiation is converted in the radiometer into an electrical signal that can be measured.

The Belgian reference instruments used were built by the RMI. The first instrument is a copy of one used during a Spacelab space mission to measure solar radiation. The second instrument served as a prototype for radiometers (SOLCON and SOVA) used during space missions.

The world standard in Davos (Switzerland) - Every five years, teams from around the world travel together with their solar instruments to Davos in Switzerland. That is where the World Radiometric Reference (WRR) is located. The atmospheric conditions at this location are ideal: high in the Swiss Alps, clear skies, and as little fine dust in the atmosphere as possible guarantee the quality of the measurements.

13th International Pyrheliometer Comparison - During this field campaign, all instruments present at the same time as the WRR will be pointed at the Sun for three weeks. This allows the measurements of the various instruments to be compared with the world standard and calibrated using a correction factor.

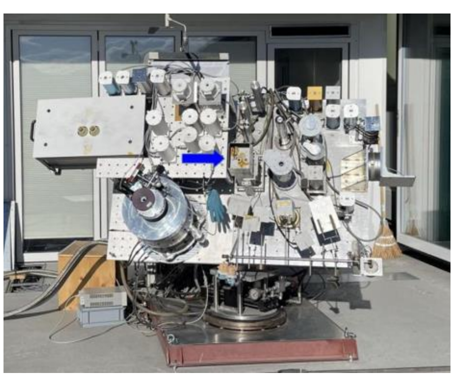

Figure 27: World Radiometric Reference (WRR) including a reference instrument developed and built by the RMI (blue arrow).

Therefore, this exercise also allows us to determine a correction factor for the RMI's solar instruments so that after applying this factor, they measure radiation as accurately as the global standard.

Solar measurements by the RMI - The RMI is historically and currently a regional reference centre for solar radiation measurements. At its site in Uccle, there is a solar tower high enough to protrude above trees and buildings. On the roof of this tower are a number of solar instruments or pyrheliometers that make continuous measurements of direct solar radiation.

There are also so-called pyranometers that measure global solar radiation, which is both direct radiation (from the Sun) and indirect solar radiation (scattered by the atmosphere).

The RMI has about 20 automatic measuring stations spread throughout the country and pyranometers have also been set up there. The two Belgian reference instruments that were calibrated in Davos can now in turn serve to correct the other solar instruments of the RMI's observation network, thus ensuring the quality of our observations.

Figure 28: Pierre Malcorps (technician) at the tracker and night shelter he renovated for the instruments.

Importance of solar radiation measurements - Correctly measuring the Sun's radiation and the radiation scattered by the atmosphere is important both for meteorology (to correctly predict the weather) but also to monitor climate change. It is also important for determining the efficiency of solar energy-based installations, such as solar collectors and photovoltaic panels.

B.RCLab: the Belgian Radiometric Characterization Laboratory

BIRA-IASB has a long-standing involvement in space- and ground-based experiments related to solar irradiance, magnetospheric studies and planetary atmospheres. Contributions are generally provided within consortia, built around an ESA project, supported by BELSPO and including a strong link with industry. In addition to the BIRA-IASB involvement in the scientific part of such a project (PI ship, data processing and dissemination,…), there is a clear demand for experimental tasks. Indeed, any instrumentation needs to be fully characterized and qualified, for example for radiometry and thermal-vacuum behaviour, especially for payloads designed for space missions facing harsh vacuum, thermal and radiative environments, and that is particularly of interest to instruments that use solar irradiance for their measurements. Therefore, it is necessary to have in-house dedicated laboratories to perform such kind of pre-flight characterizations. The year 2021 saw the emergence at BIRA-IASB of the so-called "B.RCLab", which stands for Belgian Radiometric Characterization Laboratory. It is based on the existing laboratories of the "Solar irradiance and radiometry" section of BIRA-IASB.

Figure 29: General view of the B.RCLab at BIRA-IASB.

The objective of radiometry is to perform extensive characterization of opto-mechanical sub-systems (concept validation, space qualification), detectors (photodiodes, array detectors) or entire instruments or even platforms

(CubeSat or small satellites). This requires facilities able to do all types of measurements based on light. At the instrument and detector level, measurement equations and transfer functions are used to convert raw electronic signals into meaningful and useful scientific data. All parameters of such equations are determined during a characterization campaign, including the spectral and thermal dependence of the instrument or detector. For example, for an array detector, it is proposed to explore and characterize the linearity, the QE (Quantum Efficiency) that requires absolute radiometry, latency effects and inter-pixel response variability. Dedicated facilities must then provide a space simulation environment, including thermal cycle and a well-calibrated light flux. Such instrumentation is now available at B.RCLab.

The main facility is composed of a large (0.4 m³) TVAC (Thermal-VACuum chamber), installed in an ISO-5 certified cleanroom and equipped with a cold head offering thermal cycles between 100 K to 400 K. Moreover, optical equipment for VIS - NIR absolute radiometry (monochromatic, calibrated and homogeneous light beam) allows the complete optical characterization of a device installed inside the vacuum chamber. It is worth to mention that this facility can also be used for optically passive devices (such as electronics, mirrors) that must be thermally characterized using cooling cycles. Additional facilities are also available for several radiometric characterizations:

Figure 30: General view of the thermal-vacuum facility.

- A small TVAC (few dm³) equipped with a viewport (for illumination) and a cold plate for temperature range -30 °C to +60 °C.
- Facilities for full radiometric characterization (for angular response, wavelength scale calibration, straylight and linearity assessment, measurement of relative spectral response, filter transmission, …). These facilities can be used for instrumentation designed for solar irradiance measurements, trace species observations (spectroscopy), aurora observations, …
- Absolute radiometric calibration, for spectral irradiance and radiance using secondary standards (calibrated lamps) in the UV-VIS-NIR spectral domain.
- VUV radiometric test bench using a vacuum spectrometer, light sources and a calibrated Silicon detector, for characterizations (relative and absolute spectral response, linearity, transmission of filter) that require the exploration of wavelengths shorter than 200 nm.
- A large (2-meter diameter) integrating sphere for flat field and photometric measurements, will be refurbished soon.

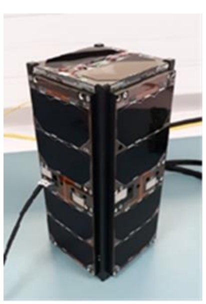

Figure 31: the INSPIRE-SAT 7 satellite.

The team was involved in several projects that required thermal cycle and radiometry. Over the last ten years, the participation in space missions (SOLAR/SOLSPEC, NOMAD, MAJIS/JUICE and ALTIUS) was focused on atmospheric and planetary science and on solar physics. A current project consists in the radiometric characterization and calibration of the 2-Unit French CubeSat INSPIRE-SAT 7 sensors, part of the INternational Satellite Program In Research and Education (INSPIRE) activities. It will contribute to in-orbit studies of the solar irradiance and the Earth's Radiation Budget (ERB).

Future involvements will concern COMPLIMENT on Comet Interceptor, VenSpec-H on ENVISION and the ground-based BIOSPHERE project (EURAMET consortium). Part of the daily work consists in extending the capabilities of the B.RCLab in order to consolidate the experience gained, but also to enhance the operational equipment and to provide new facilities. Precious advice was obtained from the SMD (Federal Services for Metrology - Safety and Metrology Division). One objective is to provide radiometry services to the Space Pole (possibly in collaboration with DeMeLab) and to external partners (industry, other institutes). In the longer term, the plan is to become a designated institute of the SMD for metrology applied to radiometry. A website has been developed and is available at https://brclab.aeronomie.be/

In-flight validation of the SLP instrument on board PICASSO

The Sweeping Langmuir Probe (SLP) instrument on board the Pico-Satellite for Atmospheric and Space Science Observations (PICASSO) has been fully developed at BIRA-IASB with substantial STCE support. PICASSO, an ESA in-orbit demonstrator launched in September 2020, is a triple unit CubeSat orbiting Earth at an altitude of about 540 km with an inclination of 97 degrees. SLP was developed to measure the ambient plasma parameters (electron density and temperature, ion density) as well as the S/C (spacecraft) potential. The measurement principle is based on the conventional Langmuir probe theory: by sweeping the potential of an electric probe with respect to the plasma potential and measuring the collected current, the instrument acquires a current-voltage (I-V) characteristic (see Figure 32) from which the above-mentioned parameters are retrieved.

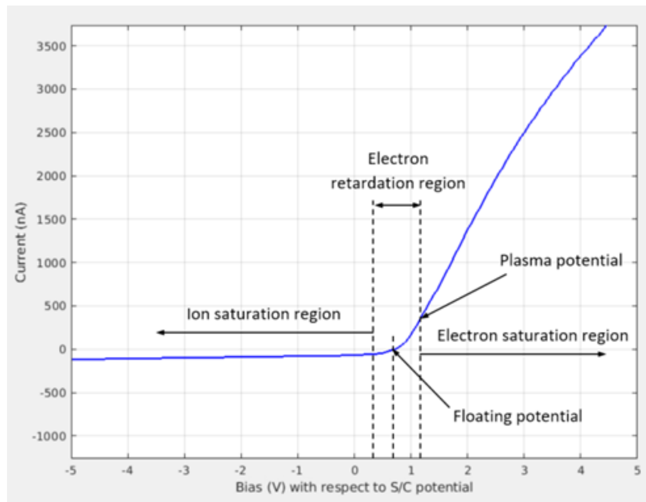

Figure 32: Typical Langmuir probe current-voltage characteristic measured by SLP in the ionosphere on 30.01.2021 at 13:03:47 UTC. The current in the ion saturation region is multiplied by a factor of 3 to better visualize the different parts of the curve.

Because the downlink capabilities of CubeSats are limited, I-V curve data with very fine steps cannot be downloaded in nominal operational mode. To reduce the amount of data to be transmitted while allowing to accurately resolve the I-V curves, the different parts of these curves were sampled with different step sizes: the ion and electron saturation regions are sampled with large steps while the electron retardation region is sampled with finer steps. Because the position of the plasma potential (which separates the electron retardation and saturation regions) varies as a function of the plasma parameters, it has to be computed on board for each sweep. It can be seen from Figure 33 that using the proposed adaptive method, the 60 data point I-V curve can lead to a resolution comparable to the one using 200 data points.

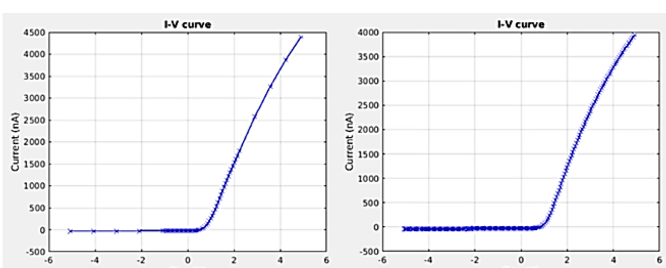

Figure 33: (left) In-flight measured I-V characteristic (linear scale) with 60 data points acquired on 30.01.2021 at 13:03:59 UTC using the adaptive sweep method. (right) In-flight measured I-V characteristic (linear scale) with 200 data points (equidistant steps) acquired on 30.01.2021 at 13:03:49 UTC.

Figure 34 shows the convergence of the plasma potential computed on board by SLP after each sweep for a series of 14 consecutive sweeps with 60 bias steps using the adaptive sweep method. It is seen that the computed values lie within 0.35 V of the target value from the third sweep on.

These results indicate that the adaptive sweep method developed for SLP is functioning nominally in the ionospheric plasma encountered by PICASSO, which was one of the objectives of this in-orbit demonstrator.

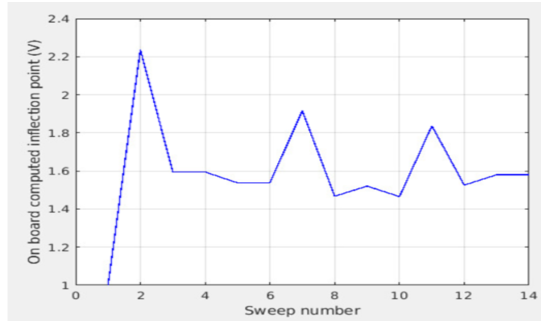

Figure 34: Plasma potential computed from data acquired on 30.01.2021 from 13:03:53 to 13:04:06UTC.

Ozonesonde Measurement Principles and Best Operational Practices

The electrochemical concentration cell (ECC) ozonesonde, versions of which have existed since the 1960s, are expendable, balloon-borne instruments that serve a vital role in global atmospheric ozone monitoring. Always paired with a meteorological radiosonde, the ECC provides continuous, high-quality, in-situ measurements of ozone with high vertical resolution (100-150 m) from the surface to over 30 km altitude, characteristics that no other instrument, remote-sensing or otherwise, can match. The measurement principle of the ECC is based on the wet chemical reaction of ozone in a neutral-buffered potassium iodide (KI) solution, such that approximately two electrons flow in an external circuit in the ECC for each ozone molecule absorbed into the solution. The magnitude of the resulting current is transmitted via the radiosonde to a receiving station and converted into ozone partial pressure. ECC ozonesondes are currently launched at over 50 stations around the globe on a regular base, forming the global ozonesonde network. The data are used for satellite and model evaluation, developing ozone climatologies, pollution and climate studies, and calculating ozone trends. Those different applications have been illustrated using the 50-year time series of Uccle in the paper “Fifty years of balloon-borne ozone profile measurements at Uccle, Belgium: a short history, the scientific relevance, and the achievements in understanding the vertical ozone distribution” by Van Malderen et al. (2021).

As each ozonesonde instrument is unique, the use of e.g. the 50-year Uccle time series for ozone trends assessment is only meaningful if the consistency between the individual instruments can be guaranteed. Therefore, each instrument must be carefully prepared, characterized and calibrated before launch; this introduces some uncertainty into a station time series. Tests in simulation chambers or in the field show a relative bias of about 5% between sondes from two different manufacturers when charged with the same chemical sensing solution. Likewise, a 3%-10% bias results when sondes of the same type are charged with different sensing solutions. These biases must be accounted for in the preparation steps and post-flight data processing corrections, all of which contribute to random and systematic errors in ozonesonde records.

Of course, not only the homogeneity of the time series at one station must be ascertained, an overall consistency of the measurements at the 50 active stations that form the global ozonesonde network should be aimed at. Since 2004, the World Meteorological Organization/Global Atmospheric Watch (WMO-GAW)-sponsored ASOPOS (Assessment of Standard Operating Procedures [SOP] of OzoneSondes) team of experts has periodically evaluated ozone records and the results of field and laboratory experiments that intercompare ECC instruments. In 2021, this panel, including a STCE member (Roeland Van Malderen), published a WMO-GAW report on “Ozonesonde Measurement Principles and Best Operational Practices” that provides an update of the current knowledge of the measurement principles of the instrument based on analyses of reprocessed sonde data since 2015, laboratory tests of ozonesonde components, and the 2017 Jülich OzoneSonde Intercomparison Experiment (JOSIE) in the simulation chamber of the World Calibration Center for Ozonesondes in Jülich. In the report, the uncertainty chain of the parameters affecting the measurement and revised data processing protocols are described in detail. Expanded guidelines on data quality indicators and the rationale for enhanced metadata are given. There are new recommendations on sonde preparation steps, metadata collection as well as traceability to the world standard ozone photometer.

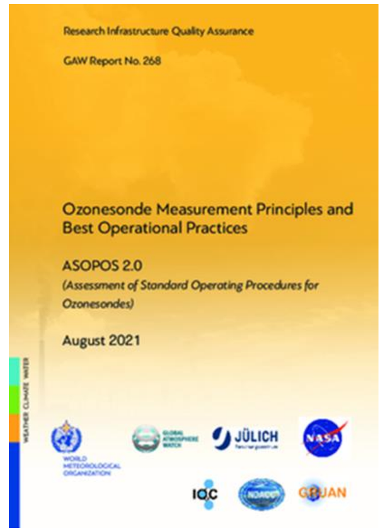

Figure 35: Title page of the new WMO-GAW report on “Ozonesonde Measurement Principles and Best Operational Practices”

The STCE member Roeland Van Malderen was the leading author on the chapter of the “Assessment of the Standard Operating Procedures for Ozonesondes” and for the appendices with practical guidelines to “Determine Ozone Partial Pressure by ECC Sonde, and Its Associated Uncertainty” and to “Homogenize Historical Ozonesonde Records”. Moreover, one of the two in-person meetings of the author team, held in September 2019 in Brussels, was organized and sponsored by the STCE.

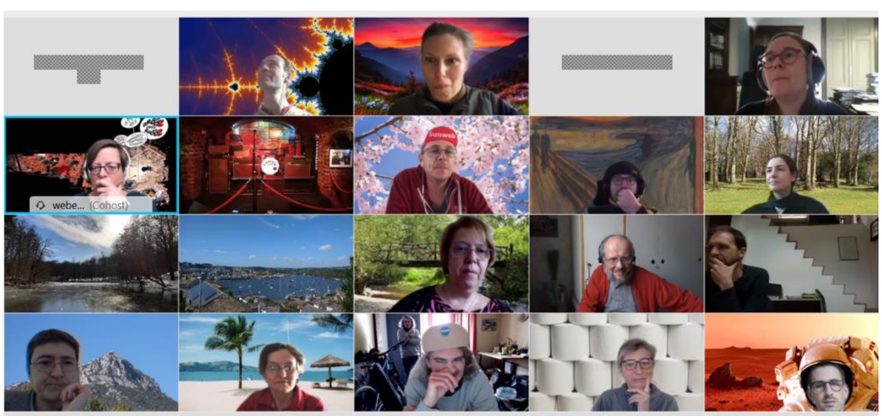

The Monthly Management Meetings of the ROB’s Solar Physics department were still held online in 2021. To keep spirits high, during one meeting, the participants were asked to experiment with their Webex background…

Applications, modeling and services

Solar Virtual Observatory: improving access to solar physics data

At the Royal Observatory of Belgium, we collect, store and distribute data from the Sun obtained with space-based instruments (e.g. SWAP and LYRA on board the PROBA-2 mission or EUI on the Solar Orbiter mission) as well as with ground-based instruments (e.g. using the solar telescopes from USET or through the radio antenna from the Humain Radioastronomy Station). In order to allow for an extensive usage of these different datasets and for a maximum return in terms of new discovery, we are dedicated to making them as easily available as possible to the global solar physics community by developing user-friendly tools to find and access these data.

In recent years there has also been an international drive from academia, industry and funding agencies to make scholarly data more reusable. This has resulted in the creation of guidelines summarized in the "FAIR" Data Principles, where "FAIR" stands for "Findable, Accessible, Interoperable and Reusable". The FAIR guidelines put emphasis on enhancing the ability of machines to automatically "find" and get "access" to the data, as well as the possibility of a smooth transfer from one software to another, e.g. for plotting the data ("interoperability") and of course the ability to "reuse" the data thanks to the adoption of standard data format. In 2021, our team has become increasingly familiarized with the FAIR principles and we have used them to improve our data management at ROB. All these efforts also improved international collaboration and scientific output.

In 2021, one of our major achievements regarding improving data access was to turn the Solar Virtual Observatory (SVO; URL: https://solarnet.oma.be/) into an operational system. A Virtual Observatory is a collection of interoperating data archives and software tools connected through the internet. Our SVO does this specifically for solar data.

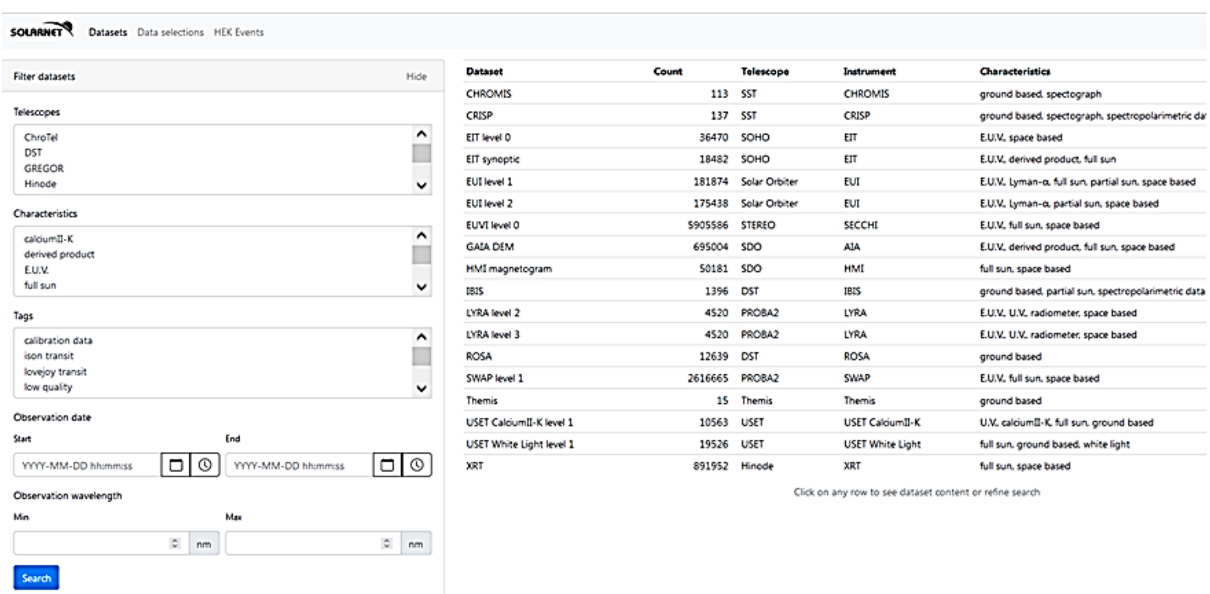

Figure 36: The SVO web interface datasets search tab

Development on the SVO started in the EU FP7 SOLARNET project with a prototype version. Further development continued in the EU H2020 SOLARNET project, where the SVO was turned into an operational system. Additionally, new features are being developed in the framework of the EU H2020 ESCAPE project. We are also continuously expanding the number of datasets that are made available through the SVO.

Via the SVO, users can search and access solar physics data from ROB and other research institutes through a web interface (see Figure 36), software libraries (Python and IDL) and through the REST API (RESTful Application Programming Interface, with REST standing for REpresentational State Transfer). Users can search across multiple datasets which let them quickly see which solar telescopes were taking measurements at a certain time. This is quite useful as the ground-based solar telescopes can obviously only take data during sunny days, and not in a continuous manner as space-based telescopes can. Whenever available, you can also see a quick-look version and metadata description of the data.

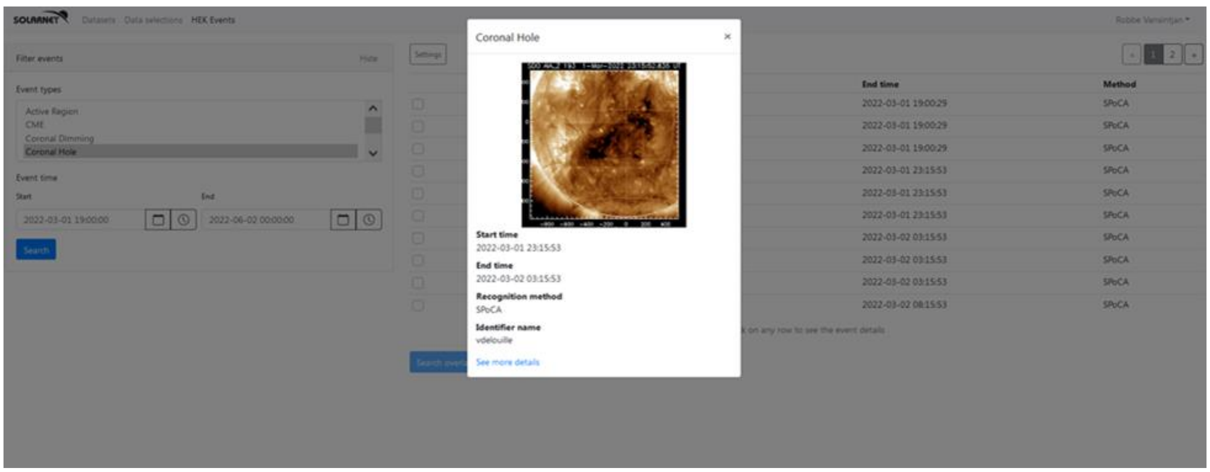

Figure 37: The SVO web interface event search tab showing a quick-look image of a coronal hole.

It is also possible to search on events from the Heliophysics Events Knowledgebase (HEK) database, which allows for quick-look visualization (see Figure 37). One of the new features that we are developing, is to let users search for data with the ROB Solar Event Database as well.

Once a user has made a selection of data, they can easily share this data with collaborators as the SVO gives you an ftp address which you can send around.

We are working on expanding the number of datasets available through the SVO as well as the ways in which our database can be queried by setting up a Table Access Protocol (TAP) service (which follows an international standard for Virtual Observatory) and interfacing the SVO with it.

A final area of development is to interface the SVO with tools like jHelioviewer which lets users visualize and combine different solar datasets like ours.

A novel Belgian K index monitoring geomagnetic disturbances

A novel dual-station geomagnetic K index nowcast system for Belgium (K_{BEL}) was implemented, thanks to the cooperation between the ionospheric and geomagnetic field research groups in Dourbes, and also between the STCE and Magnetic Valley projects. The development was immediately adopted by STCE in the PECASUS project. Key advantages of the novel nowcast: substantially improved index accuracy and service availability, leading to much higher service reliability overall. K_{BEL} is a new, local K index used to monitor the variations in the magnetic field. It is based on data from two independent magnetometers located in the magnetic observatories of Belgium: Dourbes and Manhay (the Intermagnet codes are DOU and MAB respectively).

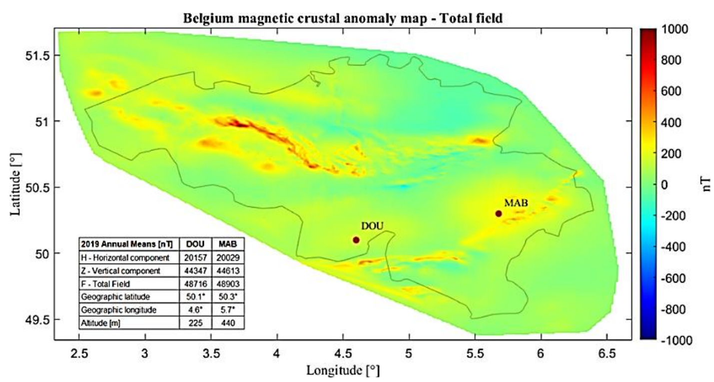

Figure 38: Location of the RMI geomagnetic observatories, shown here on a map of the crustal magnetic anomaly of Belgium (credit: Verhulst et al. 2021).

The need for a local K index - As we increasingly rely on technologies that can be affected by geomagnetic disturbances such as e.g. GNSS systems, not only major geomagnetic storms are worth being monitored, but also the much more frequent lower intensity events. The well-known K_p index is a planetary geomagnetic activity scale, ranging from 0 to 9, based on ground-based magnetic field variations. Aside this global index, a local K index provides a more accurate geomagnetic activity level over a limited area (a few thousands km²). Such a local index can detect smaller disturbances, and can often detect them earlier than a global one. The RMI has been providing in real time a local K index based solely on the observations from Dourbes for about ten years. However, over this period some issues have come to light where the inclusion of data from the Manhay observatory presents some advantages.

Advantages of K_{BEL} in comparison with a local K index based on a single station - Those advantages are directly related to the close proximity of the two observatories: the distance between the two sites (about 80 km) is sufficient to consider local conditions as independent, but remains small enough so that the real variations recorded by the magnetometers must be similar.

The first major advantage is in the quality of the automated real-time data validation process. The validation of geomagnetic data is a challenging issue because magnetic data can significantly change from one second to another, unpredictably, resulting in a difficult process of identifying outliers. For instance, a spike due to a local power-grid issue may significantly influence the index if not removed. The real-time comparison of the two data sets offers a reliable tool to eliminate any outlier. Since both observatories can be assumed to provide independent measurements, any variations caused by technical issues, interference, etc. will only be present in one data set. This provides a cleaner dataset than what can be obtained in real time from a single observatory, thus the K_{BEL} index is more accurate than any single station index.

The second major advantage is to guarantee the operational service availability. A local K index based on one single observatory fails if the related magnetic observatory fails to deliver data, and the combined index K_{BEL} needs data from both observatories to be available. However, in the new operational system, single observatory indices K_{DOU} and K_{MAB} are still calculated for both observatories in parallel with the combined index. Availability of at least one of the three indices is guaranteed 24/7 (more than 99% of time, based on data from the past years) even if one of the two observatories temporarily fails to deliver data.

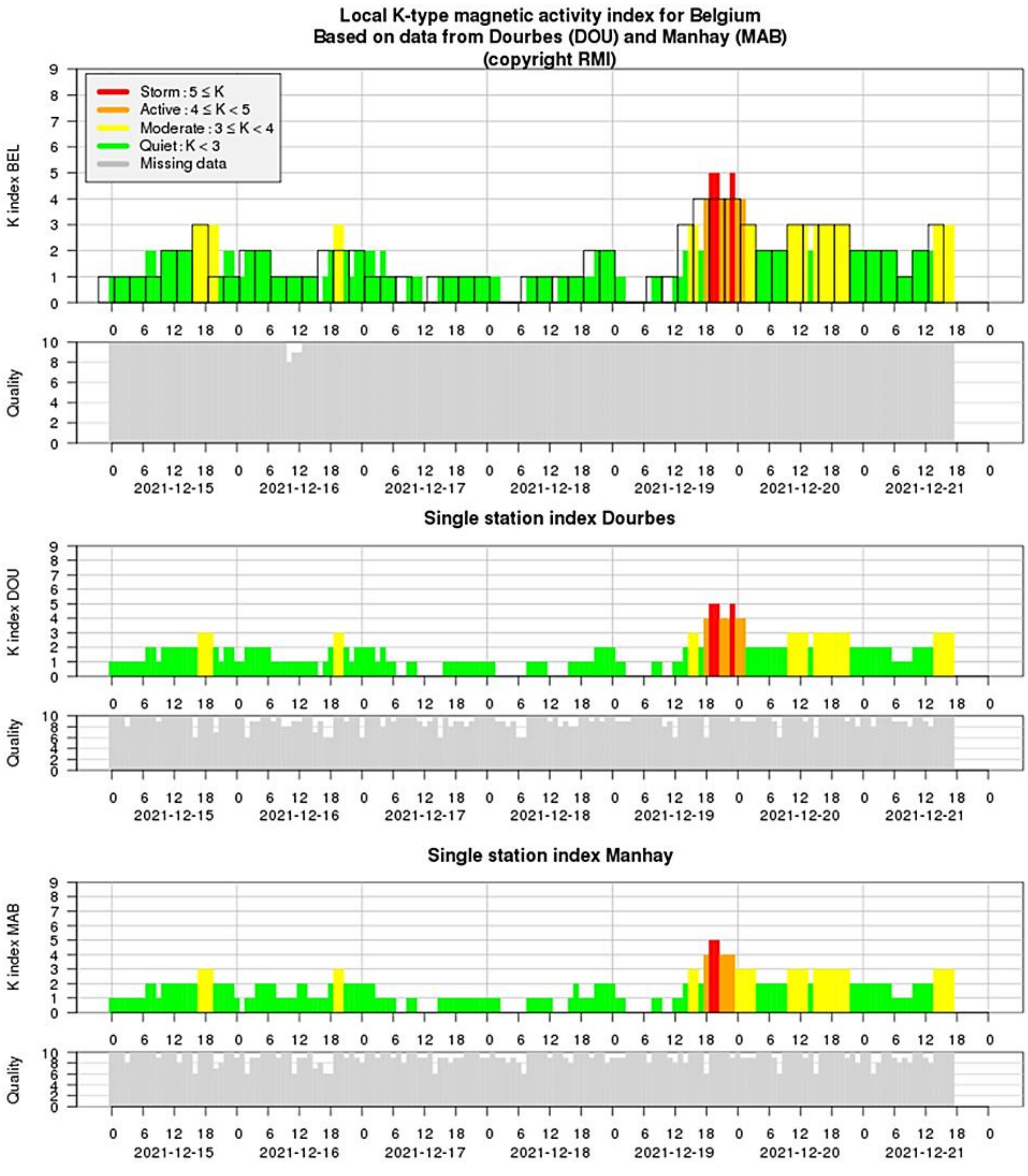

*Figure 39: Screenshot of the K_{BEL} nowcast service (**http://ionosphere.meteo.be/geomagnetism/K_BEL/**)*

Note - More background information and real-time K indices (both the single station indices and K_{BEL}) can be found at http://ionosphere.meteo.be/geomagnetism/, or in the paper describing the operational system: Verhulst et al. (2021).

How can space weather forecasts benefit from machine learning techniques?

The main goal of the ESA project DEeply uNderstanding Space weathER (DENSER) was to investigate how space weather forecasts can benefit from machine learning techniques and provide a guideline for future developments. The project was led by Space Applications Services NV/SA with contributions from the Royal Belgian Institute of Space Aeronomy (BIRA-IASB) and the Finnish Meteorological Institute (FMI). To achieve the goal, an extensive literature study was conducted and two forecast models were developed for time series predictions from two completely different space weather domains, namely the proton flux just outside the magnetosphere due to solar eruptions (ForMaL-SEP) and the ground-based magnetic field north component following geomagnetic disturbances (ForMaL-Xrange). BIRA-IASB was involved in the development of ForMaL-SEP.

Solar flares and coronal mass ejections can accelerate particles like electrons, protons and heavier ions to high energies. The Solar Energetic Particles (SEP) escape into the interplanetary space following the magnetic field embedded in the solar wind. The sudden increases of several orders of magnitude in the particle fluxes observed near Earth can last for several days or even weeks. The Earth's magnetic field deflects most of these particles and those that are able to penetrate are mostly absorbed in the atmosphere. These energetic particles remain a concern for polar regions where particles can penetrate the magnetosphere more easily. They can cause damage to avionics, disturb communications, and result in an increased absorbed radiation dose for aircrew and passengers on polar flight routes. Satellites, spacecraft and astronauts are less protected by Earth's natural shields and extra caution is required when such eruptions are predicted to happen.

BIRA-IASB has coordinated several work packages and activities of the DENSER project, and provided a significant contribution to many aspects of the project. In particular, BIRA-IASB:

- Coordinated the extensive literature review of more than 100 publications describing existing space weather forecast models based on machine learning algorithms, and performed the review covering the solar, heliospheric and space radiation domains;
- Developed processing and cleaning techniques for the solar x-ray and proton flux measurements that serve as input to ForMaL-SEP;

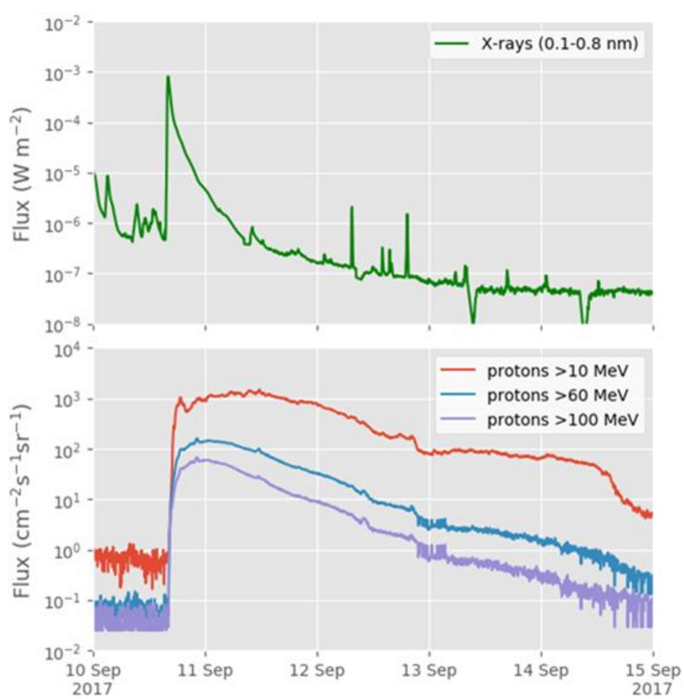

Figure 40: Measurements of solar x-ray (top) and proton (bottom) fluxes during 5 days in September 2017. The strong X8.2 flare that occurred in the afternoon of 10 September was soon followed by a sudden increase in energetic proton fluxes and radiation levels remained elevated for several days.

- Provided scientific support for the ForMaL-SEP model training and performed a validation of the results;
- Coordinated the end user test campaigns and executed the campaign for ForMaL-SEP;
- Coordinated and contributed to the recommendations for future improvements to the developed models, possible machine learning based developments of forecast models within the space weather domain, and infrastructure needs to support such developments.

The outcome of the DENSER project provided many recommendations where machine learning could be applied, as well as how these techniques should be applied. Unfortunately, the ForMaL-SEP prediction model turned out to provide too many false positives. The teams involved are currently exploring possibilities to reduce these false positives by improving the model training as well as including additional input data.

Advancing towards an operational plasmasphere model

The Belgian Space Weather Integrated Forecasting Framework (SWIFF) Plasmasphere Model (BSPM) is a code developed in the Space Physics group at BIRA-IASB since the 2000's to study and predict the time-varying behaviour of the plasmasphere. In 2021, the model has been improved in different ways, including the introduction of plasmaspheric refilling from the ionosphere and accounting for the plasmaspheric wind (Pierrard et al. 2021a). In addition, a new parametrization of the equations to estimate the density outside the plasmasphere, i.e. in the plasmatrough region, has been deduced from Van Allen Probes and ARASE measurements (Botek et al. 2021).

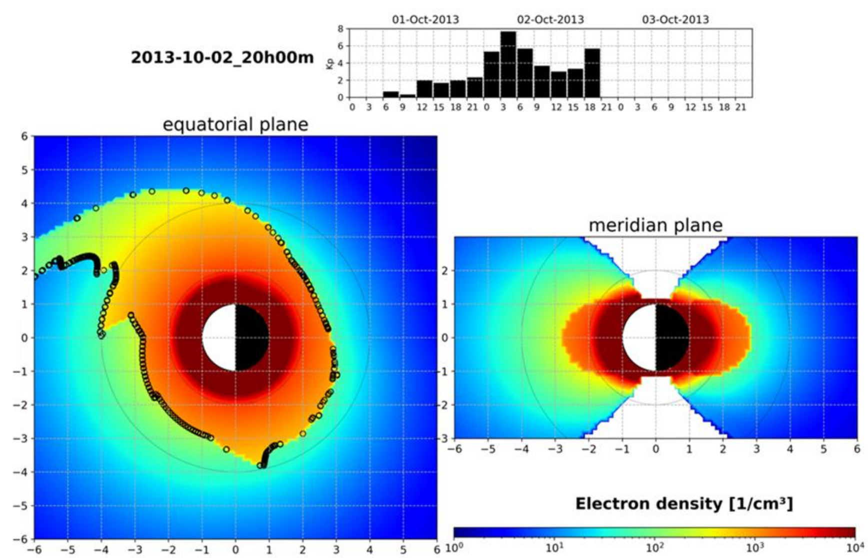

Figure 41: Electron density obtained with the BSPM model for a period of high geomagnetic activity (Pierrard et al. 2021a).

The accompanying figure (Figure 41) illustrates a simulation of the near-Earth cold plasma performed with BSPM. It corresponds to stormy geomagnetic conditions represented by high K_p index values (top panel). The bottom panels display equatorial and meridian cross-sections of the electron density in units of particles/cm^3 surrounding the Earth (sunlight coming from the left). Different regions of cold plasma can be noticed: the more reddish interior region is the ionosphere, the orange-yellow region corresponds to the plasmasphere and the more exterior green-blue region represents the plasmatrough. There is a well-defined limit between the plasmasphere (high electron density) and the plasmatrough (very low electron density) called the plasmapause as indicated by black dots in Figure 41.

A better knowledge of the time-dependent plasmasphere response to external factors, such as strong geomagnetic activity conditions caused by solar storms, is an essential gear to protect our human activities in space. Since electron density in the plasmasphere is closely related to that in the ionosphere, plasmasphere models are especially useful when it comes to electromagnetic signal propagation, i.e. for the impact on telecommunication (aircraft, radio amateurs, …) and global navigation systems.

Since January 2017, the BSPM code provides a daily forecast of the electron density and temperature of the plasmasphere in the ESA Space Weather Service Network (webpage). In 2021 a modified version of the model has been elaborated as part of a chain of different models for the SafeSpace H2020 project, with the goal of improving radiation belts forecasts.

PITHIA-NRF

PITHIA-NRF is short for “Plasmasphere Ionosphere Thermosphere Integrated Research Environment and Access services: a Network of Research Facilities”. It is a new European project (EU-101007599), funded in the Horizon 2020 framework, that started in April 2021 with the RMI and ROB as two of the twenty-three partners. The PITHIA-NRF project aims at building a European distributed network that integrates observing facilities, data processing tools and prediction models dedicated to ionosphere, thermosphere and plasmasphere research. For the first time, PITHIA-NRF integrates on a European scale, and opens up to all European researchers, key national and regional research infrastructures such as EISCAT, LOFAR, Ionosondes and Digisondes, GNSS receivers, Doppler sounding systems, riometers, and VLF receivers, ensuring optimal use and joint development. PITHIA-NRF is designed to provide organized access to experimental facilities, FAIR data, standardized data products, training and innovation services. Furthermore, the project facilitates drastically research advances in the field of upper atmosphere and near-Earth space, through the integration of data collections from satellite missions and results from key prediction models that can be accessed by scientific users for joint exploitation of the data collected by the research infrastructures of the network.

Figure 42: Logo of the PITHIA-NRF project

The members of the K_{BEL} team (S. Stankov, T. Verhulst, F. Humbled, S. Bracke) in front of the Dourbes Magnetic Observatory.

Publications

This overview of publications consists of three lists: the peer-reviewed articles, the presentations and posters at conferences, and the public outreach talks and publications for the general public. It does not include non-refereed articles, press releases, the daily, weekly and monthly bulletins that are part of our public services,… These data are available at the STCE website or upon request.

Authors belonging to the STCE have been highlighted in the list of peer-reviewed articles.

Peer reviewed articles

1. Abunina, M.; Bütikofer, R.; Klein, K.-L.; Kryakunova, O.; Laurenza, M.; Ruffolo, D.; **Sapundjiev, D.**; Steigies, C.T.; Usoskin, I.
NMDB@Home2020 - 1st virtual symposium on cosmic ray studies with neutron detectors
NMDB@Home 2020: Proceedings of the 1st virtual symposium on cosmic ray studies with neutron detectors - Volume 1 (Eds. M. Abunina, R. Bütikofer, K.-L. Klein, O. Kryakunova, M. Laurenza, D. Ruffolo, D. **Sapundjiev**, C.T. Steigies, and I. Usoskin), Universitätsverlag Kiel, Kiel University Publishing, Kiel, 7-12, DOI: 10.38072/2748-3150/p1

2. Andretta, V.; Bemporad, A.; De Leo, Y.; … ; **Mierla, M.**; … ; **Talpeanu, D.-C.**; … ; **Berghmans, D.**; … and 65 co-authors
The first Coronal Mass Ejection observed in both visible-light and UV H I Ly-alpha channels of the Metis Coronagraph on board Solar Orbiter
Astronomy & Astrophysics, 656, L14, 2021, DOI: 10.1051/0004-6361/202142407

3. Aran, A.; Pacheco, D.; Laurenza, M.; … ; **Samara, E**.; … ; **Rodriguez, L.**; … ; **Berghmans, D**.; … ; **Magdalenic, J.**; … ; **Verbeeck, C.**; … ; **Zhukov, A.N.**; and 55 co-authors
Evidence for local particle acceleration in the first recurrent Galactic Cosmic Ray depression observed by Solar Orbiter. The ion event on 19 June 2020.
Astronomy & Astrophysics, 656, L10, 2021, DOI: 10.1051/0004-6361/202140966

4. **Berghmans, D.**; Auchère, F.; Long, D.M.; … ; … ; **Mierla, M.; Zhukov, A.N**.; … ; **Dolla, L.; Verbeeck, C.; Gissot, S.**; … ; **Katsiyannis, A.C.; Rodriguez, L.; Kraaikamp, E**.; … ; **Stegen, K**.; … and 16 co-authors
Extreme-UV quiet Sun brightenings observed by the Solar Orbiter/EUI
Astronomy & Astrophysics, 656, L4, 2021, DOI: 10.1051/0004-6361/202140380

5. Besliu-Ionescu, D.; **Mierla, M.**
Geoeffectiveness prediction of CMEs
Frontiers in Astronomy and Space Sciences, 8 : 672203, 2021, DOI: 10.3389/fspas.2021.672203

6. **Bhattacharya, S.**; Teague, E.T.H.; **Fay, S.; Lefèvre, L.**; Jansen, M.; **Clette, F.**
A Modern Reconstruction of Richard Carrington's Observations (1853-1861)
Solar Physics, 296, 8, 118, 2021, DOI: 10.1007/s11207-021-01864-8

7. Botek, E.; Pierrard, V.; Darrouzet, F.
Assessment of the Earth's cold plasmatrough modeling by using Van Allen Probes/EMFISIS and Arase/PWE electron density data
Journal of Geophysical Research: Space Physics, 126, 12, e29737, 2021, DOI: 10.1029/2021JA029737

8. Chen, Y.; Przybylski, D.; Peter, H.; Tian, H.; Auchère, F.; **Berghmans, D.**
Transient small-scale brightenings in the quiet solar corona: A model for campfires observed with Solar Orbiter
Astronomy & Astrophysics, 656, L7, 2021, DOI: 10.1051/0004-6361/202140638

9. Chitta, L.P.; Solanki, S.K.; Peter, H.; Aznar Cuadrado, R.; Teriaca, L.; Schühle, U.; Auchère, F.; **Berghmans, D.; Kraaikamp, E.; Gissot, S.; Verbeeck, C.**
Capturing transient plasma flows and jets in the solar corona
Astronomy & Astrophysics, 656, L13, 2021, DOI: 10.1051/0004-6361/202141683

10. Clette, F.
Is the $F_{10.7cm}$ - Sunspot Number relation linear and stable?
Journal of Space Weather and Space Climate, 11, 2, 2021, DOI: 10.1051/swsc/2020071

11. Gul, B.; Ayyaz Ameen, M.; **Verhulst, T.G.W.**
Correlation between f_oE_s and zonal winds over Rome, Okinawa and Townsville using Horizontal Wind Model (HWM14) during solar cycle 22
Advances in Space Research, 68, 11, 4658-4664, 2021, DOI: 10.1016/j.asr.2021.08.027

12. Hinrichs, J.; Davies, J.A.; **West, M.J.**; Bothmer, V.; **Bourgoignie, B.**; Eyles, C.J.; Huke, P.; Jiggens, P.; **Nicula, B.**; Tappin, J.
Analysis of signal to noise ratio in coronagraph observations of coronal mass ejections
Journal of Space Weather and Space Climate, 11, 11, 2021, DOI: 10.1051/swsc/2020070

13. Hou, Z.; Tian, H.; **Berghmans, D.**; Chen, H.; Teriaca, L.; Schühle, U.; Gao, Y.; Chen, Y.; He, J.; Wang, L.; Bai, X.
Coronal Microjets in Quiet-Sun Regions Observed with the Extreme Ultraviolet Imager on Board the Solar Orbiter
The Astrophysical Journal Letters, 918, 1, L20, 2021, DOI: 10.3847/2041-8213/ac1f30

14. Inhester, B.; **Mierla, M.; Shestov, S.; Zhukov, A.N.**
Error Estimation of Linear Polarization Data from Coronagraphs - Application to STEREO-A/SECCHI-COR1 Observations
Solar Physics, 296, 4, 72, 2021, DOI: 10.1007/s11207-021-01815-3

15. Janssens, J.
Prediction of the amplitude of solar cycle 25 using polar faculae observations
Journal of Space Weather and Space Climate, 11, 3, 2021, DOI: 10.1051/swsc/2020081

16. **Jebaraj, I.C.**; Kouloumvakos, A.; **Magdalenic, J.**; Rouillard, A.P.; Mann, G.; Krupar, V.; Poedts, S.
Generation of interplanetary type II radio emission
Astronomy & Astrophysics, 654, A64, 2021, DOI: 10.1051/0004-6361/202141695

17. Kauristie, K.; **Andries, J.**; Beck, P.; … ; **Berghmans, D.**; … ; **De Donder, E.; de Patoul, J.; Dierckxsens, M.**; … ; **Maneva, Y.**; … ; **Rodriguez, L.**; … ; **Vanlommel, P.; Verhulst, T.**; … and 24 co-authors
Space weather services for civil aviation - challenges and solutions
Remote Sensing, 13, 18, 3685, 2021, DOI: 10.3390/rs13183685

18. Kirichenko, A.; Kuzin, S.; **Shestov, S.**; … and 26 co-authors
KORTES Mission for Solar Activity Monitoring Onboard International Space Station
Frontiers in Astronomy and Space Sciences, 8, 66, 1-11, 2021, DOI: 10.3389/fspas.2021.646895

19. Kouloumvakos, A.; Rouillard, A.; Warmuth, A.; **Magdalenic, J.; Jebaraj, I.C.**; Mann, G.; Vainio, R.; Monstein, C.
Coronal Conditions for the Occurrence of Type II Radio Bursts
The Astrophysical Journal, 913, 2, 99, 2021, DOI: 10.3847/1538-4357/abf435

20. Lemaire, J.; Katsiyannis, A.
Radial Distributions of Coronal Electron Temperatures: Specificities of the DYN Model
Solar Physics, 296, 4, 64, 2021, DOI: 10.1007/s11207-021-01814-4

21. Li, D.; Ge, M.; **Dominique, M.**; Zhao, H.; Li, G.; Li, X.; Zhang, S.; Lu, F.; Gan, W.; Ning, Z.
Detection of Flare Multiperiodic Pulsations in Mid-ultraviolet Balmer Continuum, Lyα, Hard X-Ray, and Radio Emissions Simultaneously
The Astrophysical Journal, 921, 2, 179, 2021, DOI: 10.3847/1538-4357/ac1c05

22. Lilensten, J.; Dumbovic, M.; Spogli, L.; … ; **Van der Linden, R.**; … ; **Cessateur, G.; De Donder, E.**; … and 12 co-authors
Quo vadis, European Space Weather community?
Journal of Space Weather and Space Climate, 11, 26, 2021, DOI: 10.1051/swsc/2021009

23. Linker, J.A.; Heinemann, S.G.; Temmer, M.; … ; **Delouille, V.**; … ; **Jebaraj, I.C.**; … ; **Samara, E.**; … and 11 co-authors
Coronal Hole Detection and Open Magnetic Flux
The Astrophysical Journal, 918, 1, 21, 2021, DOI: 10.3847/1538-4357/ac090a

24. Maksimovic, M.; Walsh, A.; **Pierrard, V.**; Stverak, S.; Zouganelis, I.
Electron Kappa distributions in the solar wind: cause of the acceleration or consequence of the expansion?
Kappa Distributions, From Observational Evidences via Controversial Predictions to a Consistent Theory of Nonequilibrium Plasmas (Eds. M. Lazar and H. Fichtner), Astrophysics and Space Science Library, Cham: Springer International Publishing, 464, 39-51, 2021, DOI: 10.1007/978-3-030-82623-9_3

25. Mandal, S.; Peter, H.; Chitta, L.P.; Solanki, S.K.; Aznar Cuadrado, R.; Teriaca, L.; Schühle, U.; **Berghmans, D.**; Auchère, F.
Propagating brightenings in small loop-like structures in the quiet-Sun corona: Observations from Solar Orbiter/EUI
Astronomy & Astrophysics, 656, L16, 2021, DOI: 10.1051/0004-6361/202142041

26. Meftah, M.; Snow, M.; Damé, L.; **Bolsée, D.; Pereira, N.; Cessateur, G.**; Bekki, S.; Keckhut, P.; Sarkissian, A.; Hauchecorne, A.
SOLAR-v: A new solar spectral irradiance dataset based on SOLAR/SOLSPEC observations during solar cycle 24
Astronomy & Astrophysics, 645, A2, 2021, DOI: 10.1051/0004-6361/202038422

27. **Micera, A.; Zhukov, A.N.**; López, R.; Boella, E.; Tenerani, A.; Velli, M.; Lapenta, G.; Innocenti, M.E.

On the Role of Solar Wind Expansion as a Source of Whistler Waves: Scattering of Suprathermal Electrons and Heat Flux Regulation in the Inner Heliosphere
The Astrophysical Journal, 919, 1, 42, 2021, DOI: 10.3847/1538-4357/ac1067

28. **Moraux, A.; Dewitte, S.**; Cornelis, B.; Munteanu, A.
A Deep Learning Multimodal Method for Precipitation Estimation
Remote Sensing, 13, 16, 3278, 2021, DOI: 10.3390/rs13163278

29. Morel, L.; Moudnin, O.; Durand, F.; Nicolas, J.; Follin, J.-M.; Durand, S.; **Pottiaux, E.**; Van Baelen, J.; de Oliveira, P.S. Jr
On the relation between GPS tropospheric gradients and the local topography
Advances in Space Research, 68, 4, 1676-1689, 2021, DOI: 10.1016/j.asr.2021.04.008

30. Němeček, Z.; Šafránková, J.; Němec, F.; Ďurovcová, T.; Pitňa, AZ.; Alterman, B.L.; **Voitenko, Y.M.**; Pavlů, J.; Stevens, M.L.
Spectra of Temperature Fluctuations in the Solar Wind
Atmosphere*, 12, 10, 1277, 2021, DOI:10.3390/atmos12101277*

31. Nitta, N.V.; Mulligan, T.; Kilpua, E.K.J.; … ; **Mierla, M.**; … ; **Rodriguez, L.**; … ; **Talpeanu, D.C.**; … ; **Zhukov, A.N.**; and 10 co-authors
Understanding the Origins of Problem Geomagnetic Storms Associated With "Stealth" Coronal Mass Ejections
Space Science Reviews, 217, 8, 82, 2021, DOI: 10.1007/s11214-021-00857-0

32. Palmerio, E.; Nitta, N.; Mulligan, T.; **Mierla, M.**; O'Kane, J.; Richardson, I.; Sinha, S.; Srivastava, N.; Yardley, S.; **Zhukov, A.N.**
Investigating Remote-Sensing Techniques to Reveal Stealth Coronal Mass Ejections
Frontiers in Astronomy and Space Sciences, 8:695966, 2021, DOI: 10.3389/fspas.2021.695966

33. Palmerio, E.; Kilpua, E.; Witasse, O.; … ; **Mierla, M.; Zhukov, A.N.**; … ; **Rodriguez, L.**; … and 12 co-authors
CME Magnetic Structure and IMF Preconditioning Affecting SEP Transport
Space Weather, 19, 4, 2021, DOI: 10.1029/2020SW002654

34. Panesar, N.K.; Tiwari, S.K.; **Berghmans, D.**; Cheung, M.C.M.; Müller, D.; Auchère, F.; **Zhukov, A.N.**
The Magnetic Origin of Solar Campfires
The Astrophysical Journal Letters, 921, 1, L20, 2021, DOI: 10.3847/2041-8213/ac3007

35. Paschalis, P.; Tezari, A.; Mavromichalaki, H.; Karaiskos, P.; **Crosby, N.; Dierckxsens, M.**
Cosmic radiation exposure of aviators for solar cycles 23 and 24
NMDB@Home 2020: Proceedings of the 1st virtual symposium on cosmic ray studies with neutron detectors - Volume 1 (Eds. M. Abunina, R. Bütikofer, K.-L. Klein, O. Kryakunova, M. Laurenza, D. Ruffolo, D. **Sapundjiev**, C.T. Steigies, and I. Usoskin), Universitätsverlag Kiel, Kiel University Publishing, Kiel, 109-113, DOI: 10.38072/2748-3150/p13

36. Patel, R.; Pant, V.; Iyer, P.; Banerjee, D.; **Mierla, M.; West, M.J.**
Automated Detection of Accelerating Solar Eruptions Using Parabolic Hough Transform
Solar Physics, 296, 2, 31, 2021, DOI:10.1007/s11207-021-01770-z

37. Peter, H.; Ballester, E.A.; Andretta, V.; … ; **Berghmans, D.**; … 19 co-authors
Magnetic imaging of the outer solar atmosphere (MImOSA)
Experimental Astronomy, 2021, DOI: 10.1007/s10686-021-09774-0

38. Pierrard, V.; Botek, E.; Darrouzet, F.
Improving Predictions of the 3D Dynamic Model of the Plasmasphere
Frontiers in Astronomy and Space Sciences, 8:681401, 2021, DOI: 10.3389/fspas.2021.681401

39. **Pierrard, V.; Botek, E.**; Ripoll, J.-F.; Thaller, S.A.; Moldwin, M.B.; Ruohoniemi, M.; Reeves, G.
Links of the plasmapause with other boundary layers of the magnetosphere: ionospheric convection, radiation belts boundaries, auroral oval
Frontiers in Astronomy and Space Sciences, 8:728531, 2021, DOI: 10.3389/fspas.2021.728531

40. **Pierrard, V.**; Lazar, M.; Maksimovic, M.
Suprathermal populations and their effects in space plasmas: Kappa vs. Maxwellian
Kappa Distributions, From Observational Evidences via Controversial Predictions to a Consistent Theory of Nonequilibrium Plasmas (Eds: M. Lazar and H. Fichtner), Astrophysics and Space Science Library, Cham: Springer International Publishing, 464, 15-38, 2021, DOI: 10.1007/978-3-030-82623-9_2

41. **Pierrard, V.**; Ripoll, J.-F.; Cunningham, G.; **Botek, E.**; Santolik, O.; Thaller, S.; Kurth, W.; Cosmides, M.
Observations and simulations of dropout events and flux enhancements in October 2013: Comparing MEO equatorial with LEO polar orbit
Journal of Geophysical Research: Space Physics, 126, 6, e28850, 2021, DOI: 10.1029/2020JA028850.

42. Podladchikova, O.; Harra, L.; Barczynski, K.; Mandrini, C.H.; Auchère, F.; **Berghmans, D.**; Buchlin, É.; **Dolla, L.; Mierla, M.**; Parenti, S.; **Rodriguez, L.**
Stereoscopic Measurements of Coronal Doppler Velocities
Astronomy & Astrophysics, 655, A57, 2021, DOI: 10.1051/0004-6361/202140457

43. Reiss, M.A.; Muglach, K.; Moestl, C.; … ; **Delouille, V.**; … ; COSPAR ISWAT Coronal Hole Boundary Working Team; and 14 co-authors
The Observational Uncertainty of Coronal Hole Boundaries in Automated Detection Schemes
The Astrophysical Journal, 913, 1, 28, 2021, DOI: 10.3847/1538-4357/abf2c8

44. Rouillard, A.P.; Viall, N.; Vocks, C.; Wu, Y.; Pinto, R.; Lavarra, M.; Matteini, L.; **Pierrard, V.**; Sanchez-Diaz, E.; Alexandrova, O.; Lavraud, B.
The solar wind
Solar Physics and Solar wind, AGU Monograph (Eds. N.-E. Raouafi, A. Vourlidas, Y. Zhang, L.J. Paxton), Geophysical Monograph Series, American Geophysical Union, Wiley, 258, 2021, DOI: 10.1002/9781119815600.ch1

45. **Samara, E.**; Pinto, R.F.; **Magdalenic, J.**; Wijsen, N.; Jercic, V.; **Scolini, C.; Jebaraj, I.C.; Rodriguez, L.**; Poedts, S.
Implementing the MULTI-VP coronal model in EUHFORIA: Test case results and comparisons with the WSA coronal model
Astronomy & Astrophysics, 648, A35, 2021, DOI: 10.1051/0004-6361/202039325

46. **Schifano, L.**; Smeesters, L.; Berghmans, F.; **Dewitte, S.**
Wide-Field-of-View Longwave Camera for the Characterization of the Earth's Outgoing Longwave Radiation
Sensors, 21, 13, 4444, 2021, DOI: 10.3390/s21134444

47. **Schifano, L.**; Smeesters, L.; Berghmans, F.; **Dewitte, S.**
Towards a next-generation Earth Radiation Budget radiometer by optimization of the cavity geometry and coating
SPIE 2021, International Conference on Space Optics - ICSO 2021, Proceedings Volume 11852, 118520O, 2021, DOI: 10.1117/12.2599171

48. **Schifano, L.**; Smeesters, L.; Berghmans, F.; **Dewitte, S.**
Compact wide field-of-view camera design for remote sensing of the Earth's emitted thermal radiation
SPIE 2021, Remote Sensing of Clouds and the Atmosphere XXVI, Proceedings Volume 11859, 118590C, 2021, DOI: 10.1117/12.2600084

49. **Scolini, C.**; Dasso, S.; **Rodriguez, L.; Zhukov, A.N.**; Poedts, S.
Exploring the radial evolution of Interplanetary Coronal Mass Ejections using EUHFORIA
Astronomy & Astrophysics, 649, A69, 2021, DOI: 10.1051/0004-6361/202040226

50. Shestov, S.V.; Zhukov, A.N.; Inhester, B.; **Dolla, L.; Mierla, M.**
Expected performances of the PROBA-3/ASPIICS solar coronagraph: Simulated data
Astronomy & Astrophysics, 652, A4, 2021, DOI: 10.1051/0004-6361/202140467

51. Srivastava, N.; **Mierla, M.**; Zhang, J.
Editorial: Space Weather Prediction: Challenges and Future prospects
Frontiers in Astronomy and Space Sciences, 8, 230, 2021, DOI: 10.3389/fspas.2021.818878

52. Steinbrecht, W.; Kubistin, D.; Plass-Dülmer, C.; … ; **Van Malderen, R.; Delcloo, A.W.**; … ; and 48 co-authors
COVID-19 Crisis Reduces Free Tropospheric Ozone across the Northern Hemisphere
Geophysical Research Letters, 48, 5, e2020GL091987, 2021, DOI: 10.1029/2020GL091987

53. Sun, H.; Zhao, J.; Liu, W.; **Voitenko, Y.; Pierrard, V.**; Shi, C.; Yao, Y.; Xie, H.; Wu, D.
Electron heat flux instabilities in the inner heliosphere: Radial distribution and implication on the evolution of electron velocity distribution function
The Astrophysical Journal Letters, 916, L4, 2021, DOI: 10.3847/2041-8213/ac0f02

54. Tarasick, D.W.; Smit, H.G.J.; Thompson, A.M.; Morris, G.A.; Witte, J.C.; Davies, J.; Nakano, T.; **Van Malderen, R.;** Stauffer, R.M.; Johnson, B.J.; Stübi, R.; Oltmans, S.J.; Vömel, H.
Improving ECC Ozonesonde Data Quality: Assessment of Current Methods and Outstanding Issues
Earth and Space Science, 8, 3, e2019EA000914, 2021, DOI: 10.1029/2019EA000914

55. Tarrio, C.; Berg, R.; Lucatorto, T.; Eparvier, F.; Jones, A.; Templeman, B.; Woodraska, D.; **Dominique, M.**
Evidence against carbonization of the thin-film filters of the Extreme Ultraviolet Variability Experiment on the Solar Dynamics Observatory
Solar Physics, 296, 3, 55, 2021, DOI: 10.1007/s11207-021-01806-4

56. Thiemann, E.; **Dominique, M.**
PROBA2 LYRA Occultations: Thermospheric Temperature and Composition, Sensitivity to EUV Forcing and Comparisons with Mars
Journal of Geophysical Research - Space Physics, 126, 7, e29262, 2021, DOI: 10.1029/2021JA029262

57. **Van Malderen, R.; De Muer, D.; De Backer, H.; Poyraz, D.; Verstraeten, W.W.; De Bock, V.; Delcloo, A.W.;**

Mangold, A.; Laffineur, Q.; Allaart, M.; Fierens, F.; Thouret, V.
Fifty years of balloon-borne ozone profile measurements at Uccle, Belgium: a short history, the scientific relevance, and the achievements in understanding the vertical ozone distribution
Atmospheric Chemistry and Physics, 21, 16, 12385-12411, 2021, DOI: 10.5194/acp-21-12385-2021

58. Verhulst, T.G.W.; Bracke, S.; Humbled, F.; Stankov, S.M.
Local Magnetic Activity Index Nowcast Based on Concurrent Measurements at Two Observatories in Close Proximity
Space Weather, 19, 8, e2020SW002709, 2021, DOI: 10.1029/2020SW002709

59. Wagner, T.; Beirle, S.; Dörner, S.; Borger, C.; **Van Malderen, R.**
Identification of atmospheric and oceanic teleconnection patterns in a 20-year global data set of the atmospheric water vapour column measured from satellites in the visible spectral range
Atmospheric Chemistry and Physics, 21, 7, 5315-5353, 2021, DOI: 10.5194/acp-21-5315-2021

60. Wijsen, N.; **Samara, E.**; Aran, A.; Lario, D.; Pomoell, J.; Poedts, S.
A self-consistent simulation of proton acceleration and transport near a high-speedsolar wind stream
The Astrophysical Journal Letters, 908, 2, L26, 2021, DOI: 10.3847/2041-8213/abe1cb

61. **Zhukov, A.N.; Mierla, M.**; Auchère, F.; **Gissot, S.; Rodriguez, L.**; … ; **Nicula, B.**; … ; **Verbeeck, C.; Kraaikamp, E.**; … ; **Stegen, K.; Dolla, L.**; … ; **Katsiyannis, A.C.**; … ; **Berghmans, D.;** and 18 co-authors
Stereoscopy of extreme UV quiet Sun brightenings observed by Solar Orbiter/EUI
Astronomy & Astrophysics, 656, A35, 2021, DOI: 10.1051/0004-6361/202141010

Presentations and posters at conference

1. Ancellet, G.; Godin-Beekmann, S.; Bodichon, R.; Pazmino, A.; Smit, H.G.J.; Stauffer, R.M.; Van Malderen, R.
Homogenisation of the Observation de Haute Provence ECC Ozonesonde Data Record: Comparison with Lidar and Satellite Observation
Quadrennial Ozone Symposium, Online, 3-9 October 2021 (poster)

2. Aran, A.; Pacheco, D.; Laurenza, M.; Wijsen, N.; Samara, E.; Lario, D.; Balmaceda, L.; Freiherr von Forstner, J.L.; Benella, S.; Rodriguez, L.; Gómez-Herrero, R.; and the The low-energy ion event on 2020 June 19 study Team
The Low-Energy Ion Event on 19 June 2020 Measured by Solar Orbiter
EGU General Assembly 2021, Online, 19-30 April 2021 (poster)

3. Auchère, F.; Dalmasso, K.; Berghmans, D.; … and 14 others
Solar Orbiter/EUI very wide field observations of the EUV corona
ESPM-16, Online, 6-10 September 2021

4. Bechet, S.
Non-radial intensity variation correction on full-disk images
SPRING Progress meeting, Online, 18-19 February 2021

5. Bergeot, N.; Pierrard, V.; Darrouzet, F.; Chevalier, J.-M.
Comparison between empirical and physical models of the topside ionospheric-plasmaspheric electron content above Antarctica
URSI GASS XXXIV, Rome (Italy) and online, 28 August-4 September 2021

6. Berghmans, D.; Auchère, F.; Long, D.M.; … and 25 others
Extreme UV quiet Sun brightenings observed by Solar Orbiter/EUI
ESPM-16, Online, 6-10 September 2021 (poster)

7. Berghmans, D.; Harra, L.K.; Zhukov, A.N.; Auchère, F.; Long, D.; Schuehle, U.; Rochus, P.
The Extreme ultraviolet imager onboard Solar Orbiter
43rd COSPAR Scientific Assembly, Sydney (Australia) and online, 28 January-4 February 2021

8. Berghmans, D.; Auchère, F.; Zhukov, A.N.; Mierla, M.; Chen, Y.; Peter, H.; Panesar, N.K.; Chitta, L.P.; Antolin, P.; Anzar Cuadrado, R.; Tian, H.; Zhenyong, H.; Podladchikova, O.
Campfires observed by EUI: What have we learned so far?
AGU Fall Meeting, New Orleans (Louisiana, USA) and online, 13-17 December 2021

9. Berghmans, D.; Auchère, F.; Harra, L.; Schuehle, U.; Long, D.; Rochus, P.; and the EUI Team
First Results from Solar Orbiter
MPPC Annual Meeting, Online, 19-22 and 25-26 January 2021 (invited talk)

10. Bhattacharya, S.; Jansen, M.; Lefèvre, L.; Clette, F.
Quality Assessment of Sunspot data using various catalogs
Applications of Statistical Methods and Machine Learning in the Space Sciences, Online, 17-21 May 2021 (poster)

11. Botek, E.; Pierrard, V.; Darrouzet, F.
Using the Van Allen Probes/EMFISIS and Arase/PWE electron density data to improve the inner magnetosphere modeling
ESWW17, Glasgow (Scotland, UK) and online, 25-29 October 2021

12. Chang, K.-L.; Cooper, O.R.; Gaudel, A.; and 12 others
Impact of the COVID-19 economic downturn on tropospheric ozone trends: an uncertainty weighted data synthesis for quantifying regional anomalies above western North America and Europe
AGU Fall Meeting, New Orleans (Louisiana, USA) and online, 13-17 December 2021

13. Chen, Y.; Przybylski, D.; Peter, H.; Tian, H.; Auchère, F.; Berghmans, D.
Transient small-scale brightenings in the quiet solar corona: a model for campfires observed with Solar Orbiter
ESPM-16, Online, 6-10 September 2021 (poster)

14. Cisneros, M. and the MAJIS project
Characterization facility for VIS-NIR detectors
NYRIA Workshop 2021, Online, 21-29 October 2021 (poster)

15. Cunningham, G.; Khoo, L.; Munn, J.C.; Malaspina, D.; Botek, E.; Pierrard, V.
Predicting the effect of the NWC transmitter on relativistic electrons using DREAM3D
AGU Fall Meeting, New Orleans (Louisiana, USA) and online, 13-17 December 2021

16. Da Deppo, V.; Nisticò, G.; Giordano, S.; Battams, K.; Gallagher, B.; Chioetto, P.; and the Metis "Comets and other Solar System Bodies" Topical Team
Observing comets with the Metis coronagraph on-board the Solar Orbiter mission
Europlanet Science Congress 2021, Online, 13-24 September 2021 (poster)

17. Daglis, I.A.; Bourdarie, S.; Cueto Rodriguez, J.; Darrouzet, F.; Lavraud, B.; Poedts, S.; Sandberg, I.; Santolik, O.; and the SafeSpace Team
Safespace: designing radiation belt environmental indicators for the safety of space assets
43rd COSPAR Scientific Assembly, Sydney (Australia) and online, 28 January-4 February 2021

18. Daglis, I.A.; Bourdarie, S.; Cueto Rodriguez, J.; Darrouzet, F.; Lavraud, B.; Poedts, S.; Sandberg, I.; Santolik, O.; and the SafeSpace Team
Improving nowcasting and forecasting of the Sun-to-Belts space weather chain through the H2020 Safespace project
EGU General Assembly 2021, Online, 19-30 April 2021

19. Dahmen, N.; Sicard, A.; Santolik, O.; Pierrard, V.; Brunet, A.; Darrouzet, F.
Fast computation of wave-particle interaction diffusion coefficients for electron radiation belt modelling with a dynamic diffusion frame
AGU Fall Meeting, New Orleans (Louisiana, USA) and online, 13-17 December 2021

20. Darrouzet, F.; Botek, E.; Pierrard, V.
New equations for the plasmatrough and redefinition of the plasmapause transition region in the BIRA-IASB plasmasphere model
SafeSpace 2021: Sun-to-Belts Workshop, Milos, Greece, 21-23 July 2021

21. Dasso, S.; Rodriguez, L.; Demoulin, P.; Masias-Meza, J.; Janvier, M.; Lanabere, V.
Magnetic twist distribution inside interplanetary flux ropes
43rd COSPAR Scientific Assembly, Sydney (Australia) and online, 28 January-4 February 2021

22. De Backer, H.; Van Malderen, R.; De Muer, D.; Poyraz, D.; Verstraeten, W.W.; De Bock, V.; Delcloo, A.; Mangold, A.; Laffineur, Q.; Allaart, M.; Fierens, F.; Thouret, V.
50 Years of Balloon-Borne Ozone Profile Measurements at Uccle, Belgium
Quadrennial Ozone Symposium, Online, 3-9 October 2021 (poster)

23. De Donder, E.
Radiation modelling and effects on electronic devices with SPENVIS
Joint SEE Symposium and MAPLD Workshop, Online, 31 August-2 September 2021

24. De Donder, E.
Tutorial: The SPace ENVironment Information System (SPENVIS) - A New Framework
ASEC 2021, Online, 1-5 November 2021

25. De Donder, E.; Messios, N.; Calders, S.; Calegaro, A.; Mezhoud, S.; Heynderickx, D.; Akandouch, M.; Clucas, S; Evans, H.
The SPaceENVironment Information System (SPENVIS): a new framework
ESWW17, Glasgow (Scotland, UK) and online, 25-29 October 2021 (poster)

26. Delouille, V.; Mampaey, B.; Vansintjan, R.
Be FAIR with the Solar Virtual Observatory
AGU Fall Meeting, New Orleans (Louisiana, USA) and online, 13-17 December 2021 (poster)

27. Delouille, V.; Mampaey, B.; Verstringe, F.
Catalog of Coronal Hole detection in TAP service
Provenance in Practice - ASOV meeting, Online, 14-15 December 2021

28. Delouille, V.; Mampaey, B.; Verstringe, F.
Catalog of Coronal Hole detection in TAP service
ESCAPE European Data Provider Forum and Training Event, Online, 23-25 November 2021

29. Delouille, V.; Mampaey, B.; Verstringe, F.
USET Sunspot group data, ROB SPoCA-CH data
VESPA Implementation workshop, Online, 29 November-2 December 2021

30. D'Huys, E.; Long, D.; Berghmans, D.; Barczynski, K.; Warmuth, A.; Vourlidas, A.; Krucker, S.; Veronig, A.; Mierla, M.; Rodriguez, L.
The first eruptions imaged by Solar Orbiter
ESPM-16, Online, 6-10 September 2021 (poster)

31. Dierckxsens, M.; Vasalos, G.; Papaioannou, A.; Anastasiadis, A.; Jiggens, P.
Validating the ASPECS Tool
ESWW17, Glasgow (Scotland, UK) and online, 25-29 October 2021 (poster)

32. Dierckxsens, M.; Calders, S.; Melcot, M.
The DENSER ForMaL-SEP Forecast Model
ESWW17, Glasgow (Scotland, UK) and online, 25-29 October 2021 (poster)

33. Dominique, M.; Gissot, S.
LYRA Science and the future with SOSPIM
SoSpIM Science Meeting, Online, 21 October 2021 (invited talk)

34. Dominique, M.; Dolla, L.; Zhukov, A.N.; … and 12 others
How Can Solar-C/SOSPIM Contribute to the Understanding of Quasi-Periodic Pulsations in Solar Flares?
AGU Fall Meeting, New Orleans (Louisiana, USA) and online, 13-17 December 2021 (poster)

35. Dominique, M.; Zhukov, A.N.; Dolla, L.; Wauters, L.
Comparison of QPPs characteristics in Lyman-α and SXR solar measurements
ESPM-16, Online, 6-10 September 2021 (poster)

36. Gissot, S.; Auchère, F.; Berghmans, D.; … and 18 others
Performance of the Extreme Ultraviolet Imager (EUI) High-Resolution Imager (HRI-EUV) telescope: from ground calibration to first in-flight images, and future EUV space solar instruments
317.PTB Seminar "VUV and EUV Metrology", Berlin (Germany) and online, 19-20 October 2021 (invited talk)

37. Hubert, D.; Azouz, N.; Godin-Beekmann, S.; … and 22 others
LOTUS : Global Trends in Stratospheric Ozone Between 2000 and 2020
ATMOS-2021, Online, 22-26 November 2021

38. Janssens, J.; Berghmans, D.; Niembro Hernandez, T.; … and 14 others
Double prominence eruption observed by Solar Orbiter and PSP
ESPM-16, Online, 6-10 September 2021 (poster)

39. Jebaraj, I.C.; Kouloumvakos, A.; Magdalenic, J.; Rouillard, A.; Warmuth, A.; Mann, G.; Krupar, V.; Poedts, S.; Vainio, R.
Evolution of shock waves and associated type II radio emission in the low corona and interplanetary space
AGU Fall Meeting, New Orleans (Louisiana, USA) and online, 13-17 December 2021

40. Jebaraj, I.C.
Tracking Heliospheric shock waves by radio triangulation and modelling
Thesis, Public PhD Defense, Heverlee (Belgium) and online, 10 December 2021

41. Jebaraj, I.C.; Kouloumvakos, A.; Magdalenic, J.; Rouillard, A.; Mann, G.; Krupar, V.; Poedts, S.
Source regions of type II radio emission on the surface of an interplanetary shock wave
ESPM-16, Online, 6-10 September 2021

42. Jebaraj, I.C.; Kouloumvakos, A.; Magdalenic, J.; Rouillard, A.; Krupar, V.; Poedts, S.
Conditions needed for generation of type II radio emission in the interplanetary space
EGU General Assembly 2021, Online, 19-30 April 2021

43. Jebaraj, I.C.; Poedts, S.; Krupar, V.; Kilpua, E.; Magdalenic, J.; Podladchikova, T.; Pomoell, J.; Dissauer, K.; Veronig, A.; Scolini, C.
Diagnosing CME/Shock wave association using the radio triangulation technique
43rd COSPAR Scientific Assembly, Sydney (Australia) and online, 28 January-4 February 2021

44. Jebaraj, I.C.; Poedts, S.; Krupar, V.; Magdalenic, J.
Fine structures of interplanetary radio bursts
43rd COSPAR Scientific Assembly, Sydney (Australia) and online, 28 January-4 February 2021

45. Keppens, A.; Hubert, D.; Lambert, J.-C.; Heue, K.-P.; Loyola, D.; Coheur, P.-F.; Wespes, C.; Van Malderen, R.
Vertical Harmonization of Satellite Ozone Data Records for the IGAC Tropospheric Ozone Assessment Report (TOAR-II)
ATMOS-2021, Online, 22-26 November 2021 (poster)

46. Kivi, R.; Heikkinen, P.; Nilsen, K.; Van Malderen, R.; Poyraz, D.; Stauffer, R.M.; Smit, H.G.J.
Long Term Ozonesonde Observations at Sodankylä
Quadrennial Ozone Symposium, Online, 3-9 October 2021 (poster)

47. Kollonige, D.E.; Thompson, A.M.; Smit, H.G.J.; Stauffer, R.M.; Tarasick, D.W.; Johnson, B.J.; Van Malderen, R.; Vömel, H.; Von der Gathen, P.; Morris, G.; Querel, R.
ASOPOS (Assessment of Standard Operating Procedures (SOPs) for OzoneSondes) 2.0: Ozonesonde Measurement Principles and Best Operational Practices
Quadrennial Ozone Symposium, Online, 3-9 October 2021 (poster)

48. Kollonige, D.E.; Thompson, A.M.; Smit, H.G.J.; Stauffer, R.M.; Tarasick, D.W.; Johnson, B.J.; Van Malderen, R.; Vömel, H.; Von der Gathen, P.; Morris, G.; Querel, R.
ASOPOS (Assessment of Standard Operating Procedures (SOPs) for OzoneSondes) 2.0: Ozonesonde Measurement Principles and Best Operational Practices
AGU Fall Meeting, New Orleans (Louisiana, USA) and online, 13-17 December 2021 (poster)

49. Koukras, A.; Keppens, R.; Dolla, L.
Estimating uncertainties in the back mapping of the fast solar wind
ESPM-16, Online, 6-10 September 2021 (poster)

50. Maget, V.; Bourdarie, S.; Ferlin, A.; … and 14 others
A new Earth Radiation Belt Forecast And Nowcast (RB-FAN) Framework based on the Salammbô data assimilation codes
ESWW17, Glasgow (Scotland, UK) and online, 25-29 October 2021 (poster)

51. Maggiolo, R.; Gunell, H.; Cessateur, G.; De Keyser, J.; Pierrard, V.; Vandaele, A.C.; Darrouzet, F.; Hamrin, M.
Semi-empirical modelling of the effect of planetary magnetization on atmospheric escape for various solar wind pressure levels
MACH workshop, Online, 15-17 June 2021

52. Maharana, A.; Poedts, S.; Scolini, C.; Isavnin, A.; Wijsen, N.; Rodriguez, L.; Mierla, M.; Magdalenic, J.
Employing advanced FRi3D CME model coupled with EUHFORIA in predictions of CME geo-effectiveness

AGU Fall Meeting, New Orleans (Louisiana, USA) and online, 13-17 December 2021

53. Maharana, A.; Poedts, S.; Scolini, C.; Isavnin, A.; Rodriguez, L.; Mierla, M.; Magdalenic, J.
Observations-based CME modelling with FRi3D model in EUHFORIA
ESWW17, Glasgow (Scotland, UK) and online, 25-29 October 2021

54. Marqué, C.
Observatory Report: Radio astronomy station of Humain
CRAF Annual Meeting, Online, 30 November 2021

55. Micera, A.; Zhukov, A.N.; López, R.A.; Innocenti, M.E.; Lazar, M.; Boella, E.; Lapenta, G.
Particle-In-Cell simulations of resonant interactions between whistler waves and electrons in the near-Sun solar wind: scattering of the strahl into the halo and heat flux regulation
EGU General Assembly 2021, Online, 19-30 April 2021

56. Micera, A.; Innocenti, M.E.; Zhukov, A.N.; López, R.; Boella, E.; Tenerani, A.; Velli, M.; Lapenta, G.
On the role of solar wind expansion as source of whistler waves: scattering of suprathermal electrons and heat flux regulation in the inner hemisphere
Parker Solar Probe Annual Conference 1, Online, 14-18 June 2021 (poster)

57. Micera, A.
Observations and Modeling of the Solar wind Kinetics
Thesis, Public PhD Defense, Online, 22 October 2021

58. Mierla, M.; Rodriguez, L.; Zhukov, A.N.; … and 51 others
Three Eruptions Observed by EUI Onboard Solar Orbiter on 21 February and 21-22 March 2021
ESPM-16, Online, 6-10 September 2021 (poster)

59. Moeller, G.; Ao, C.; Adavi, Z. ; … and 14 others
Tomographic fusion strategies for the reconstruction of atmospheric water vapor
IAG Scientific Assembly 2021, Beijing (China) and online, 28 June-2 July 2021

60. Niemela, A.; Wijsen, N.; Rodriguez, L.; Magdalenic, J.; Poedts, S.
The Solar Energetic Particle Event of March 15 2013 - Characterization of the interplanetary medium conditions
EGU General Assembly 2021, Online, 19-30 April 2021 (poster)

61. Niemela, A.; Wijsen, N.; Rodriguez, L.; Magdalenic, J.; Aran, A.; Poedts, S.
Modeling the SEP Event of 15 March 2013 with EUHFORIA and PARADISE
ESWW17, Glasgow (Scotland, UK) and online, 25-29 October 2021 (poster)

62. Pacione, R.; Santos, M.; Dick, G.; Jones, J.; Pottiaux, E.; Rinke, A.; Van Malderen, R.; Elgered, G.
Ground-based GNSS for climate research: review and perspectives
ICCC Workshop 1, Online, 29-31 March 2021 (invited talk)

63. Pacione, R.; Santos, M.; Dick, G.; Jones, J.; Pottiaux, E.; Rinke, A.; Van Malderen, R.; Elgered, G.
Ground-based GNSS for climate research: review and perspectives
EGU General Assembly 2021, Online, 19-30 April 2021 (talk and poster)

64. Petrova, E.; Magyar, N.; Van Doorsselaere, T.; Berghmans, David
High-frequency oscillations in EUI observations
Hinode-14 / IRIS-11 Joint Science Meeting, Online, 25-28 October 2021 (poster)

65. Pierrard, V.
Turbulence in the solar wind
Workshop **"**Growth of Small Scales in the Corona and Solar Wind 2021**"**, Online, 14-18 June 2021 (invited talk)

66. Pierrard, V.; Botek, E.; Darrouzet, F.; Santolik, O.
Improvement to the plasmasphere and its influence on the radiation belts
SafeSpace 2021: Sun-to-Belts Workshop, Milos, Greece, 21-23 July 2021

67. Pierrard, V.
Space weather models for the solar wind and the plasmasphere
URSI GASS XXXIV, Rome (Italy) and online, 28 August-4 September 2021

68. Pierrard, V.; Verscharen, D.
Kinetic models of solar wind
ISSI: Heliospheric Energy Budget: From Kinetic Scales to Global Solar Wind Dynamics, Bern, Switzerland, 22-26 November 2021

69. Pierrard, V.; Botek, E.; Ripoll, J.-F.
Loss mechanisms in the radiation belts: comparing dropouts and flux decays simulated and observed by PROBA-V/EPT and Van Allen Probes/MagEIS
AGU Fall Meeting, New Orleans (Louisiana, USA) and online, 13-17 December 2021

70. Podladchikova, O.; Harra, L.; Barczynski, K.; Mandrini, C.; Auchère, F.; Berghmans, D.; Buchlin, E.; Dolla, L.; Mierla, M.; Parenti, S.; Rodriguez, L.
Full Vector Velocity Reconstruction Using Solar Orbiter Doppler Map Observations

AGU Fall Meeting, New Orleans (Louisiana, USA) and online, 13-17 December 2021 (poster)

71. Podladchikova, O.; Harra, L.; Mandrini, C.; Rodriguez, L.; Parenti, S.; Dolla, L.; Buchlin, E.; Auchère, F.; Mierla, M.; Barczynski, K.
Stereoscopic Measurements of Coronal Doppler Velocities aboard Solar Orbiter
43rd COSPAR Scientific Assembly, Sydney (Australia) and online, 28 January-4 February 2021 (poster)

72. Podladchikova, O.; Harra, L.; Berghmans, D.; … and 29 others
Energy Distribution Heating Events Observed by HRIEUV During the May 2020 Solar Orbiter Perihelion
ESPM-16, Online, 6-10 September 2021 (poster)

73. Poedts, S.; Rodriguez, L.; Mierla, M.; Magdalenic, J.; Samara, E.; and the EUHFORIA Team
EUropean Heliospheric FORecasting Information Asset 2.0
ESWW17, Glasgow (Scotland, UK) and online, 25-29 October 2021 (poster)

74. Pottiaux, E.
GNSS for Meteorology and Climate: Review and Perspectives
BNCGG 2021, Online, 21 January 2021 (invited talk)

75. Poyraz, D., Smit, H.G.J.; Van Malderen, R.; Nakano, T.; Stuebi, R.
The Cell Temperature of ECC Ozonesondes in Relation to the Measured Pump Temperature: Impact of Freezing and Boiling Effects Observed during JOSIE
Quadrennial Ozone Symposium, Online, 3-9 October 2021 (poster)

76. Querel, R.; Shiona, H.; Geddes, A.; Poyraz, D.; Van Malderen, R.
Update on Lauder Ozonesonde Homogenisation
Quadrennial Ozone Symposium, Online, 3-9 October 2021 (poster)

77. Rodriguez, L.; Magdalenic, J. ; Niemela, A.; Samara, E.; Maharana, A.; Shukhobodskaia, D.; Verbeke, C.; Mierla, M.; Vansintjan, R.; Sarkar, R.; Kilpua, E.; Asvestari, E.; Poedts, S.
Initial results in the validation of EUHFORIA for CME runs
ESWW17, Glasgow (Scotland, UK) and online, 25-29 October 2021 (poster)

78. Rodriguez, L.; Mierla, M.; Berghmans, D.; … and 22 others
The eruption of 22 April 2021 as observed by Solar Orbiter, STEREO and Earth bound instruments
ESPM-16, Online, 6-10 September 2021 (poster)

79. Samara, E.; Magdalenic, J.; Heinemann, S.; Asvestari, E.; Rodriguez, L.; Hofmeister, S.; Poedts, S.
Correlating coronal hole characteristics with the insitu fast solar wind speed: Comparison between ob-served and modeled values with EUHFORIA
43rd COSPAR Scientific Assembly, Sydney (Australia) and online, 28 January-4 February 2021 (poster)

80. Samara, E.; Laperre, B.; Kieokaew, R.; Temmer, M.; Verbeke, C.; Rodriguez, L.; Magdalenic, J.; Poedts, S.
The Dynamic Time Warping as a means to assess solar wind time series
EGU General Assembly 2021, Online, 19-30 April 2021 (poster)

81. Samara, E.; Pinto, R.; Verbeke, C.; Rodriguez, L.; Magdalenic, J.; Poedts, S.
Modeling CMEs with EUHFORIA using different coronal models: evaluation of results with old and new metrics
ESWW17, Glasgow (Scotland, UK) and online, 25-29 October 2021 (poster)

82. Samara, E.; Heinemann, S.; Magdalenic, J.; Rodriguez, L.; Poedts, S.
How the shape of coronal holes influences the high-speed stream peak velocity at Earth
ESPM-16, Online, 6-10 September 2021 (poster)

83. Samara, E.; Laperre, B.; Kieokaew, R.; Temmer, M.; Verbeke, C.; Rodriguez, L.; Magdalenic, J.; Poedts, S.
The Dynamic Time Warping as a means to assess solar wind time series
AGU Fall Meeting, New Orleans (Louisiana, USA) and online, 13-17 December 2021 (poster)

84. Sapundjiev, D.; Stankov, S.M.
Space Weather Event Signatures From Ionosonde Observations
CPAESS Space Weather Workshop, Online, 20-22 April 2021

85. Sarkar, R.; Pomoell, J.; Asvestari, E.; Kilpua, E.; Mierla, M.; Rodriguez, L.; Poedts, S.
On the prediction of magnetic field vectors of ICME using data constrained simulation with EUHFORIA
EGU General Assembly 2021, Online, 19-30 April 2021 (poster)

86. Sarkar, R.; Pomoell, J.; Kilpua, E.; Asvestari, E.; Wijsen, N.; Maharana, A.; Poedts, S.; Rodriguez, L.; Marilena, M.
Implementing new techniques to constrain the spheromak model in EUHFORIA and assessing the model results
ESPM-16, Online, 6-10 September 2021

87. Schifano, L.
ASTERIX: a CubeSat to measure the Total Solar Irradiance and Earth's radiation budget for climate monitoring
IPC-XIII, Davos, Switzerland, 27 September-25 October 2021

88. Schifano, L.
Space-based wide-field-of-view cameras to improve climate change monitoring
BePOM 2021, Brussels (Belgium) and online, 23-24 September 2021

89. Scolini, C.; Pomoell, J.; Chané, E.; Poedts, S.; Rodriguez, L.; Kilpua, E.; Temmer, M.; Verbeke, C.; Dissauer, K.; Veronig, A.; Palmerio, E.; Dumbović, M.
Observation-based modelling of magnetised CMEs in the inner heliosphere with EUHFORIA
43rd COSPAR Scientific Assembly, Sydney (Australia) and online, 28 January-4 February 2021 (invited talk)

90. Smit, H.G.J.; Poyraz, D.; Van Malderen, R.; Tarasick, D.W.; Voemel, H.; Johnson, B.J.; Davies, J.; Stuebi, R.; Stauffer, R.M.; Thompson, A.M.; Allaart, M.; Morris, G.; Nakano, T.
New Insights from the Jülich Ozone-Sonde Intercomparison Experiments: Calibration Functions Traceable to One Ozone Reference Instrument
Quadrennial Ozone Symposium, Online, 3-9 October 2021 (poster)

91. Smit, H.G.J.; Thompson, A.M.; Johnson, B.J.; … and the JOSIE-ASOPOS-O3SDQA teams
The 25th Anniversary of the Juelich Ozone Sonde Intercomparison Experiment (JOSIE): 25 Years of Ozonesonde QA/QC and Data Quality Improvements
Quadrennial Ozone Symposium, Online, 3-9 October 2021

92. Stankov, S.M.; Verhulst, T.G.W.; Sapundjiev, D.
On the quality of automatic scaling of digital ionograms: DPS-4D/ARTIST-5 performance at a mid-latitude location
URSI GASS XXXIV, Rome (Italy) and online, 28 August-4 September 2021

93. Stauffer, R.M.; Thompson, A.M.; Kollonige, D.E.; … and 11 others
A Post-2013 Drop-off in Total Ozone at a Third of Global Ozonesonde Stations: ECC Instrument Artifacts?
101st AMS Annual Meeting, Online, 10-15 January 2021

94. Stauffer, R.M.; Thompson, A.M.; Kollonige, D.E.; Tarasick, D.W.; Vömel, H.; Morris, G.A.; Van Malderen, R.; Johnson, B.J.; Cullis, P.D.; Stübi, R.; Smit, H.G.J.
An Updated Examination of the Post-2013 Ozonesonde Total Column Ozone Dropoff
Quadrennial Ozone Symposium, Online, 3-9 October 2021

95. Stauffer, R.M.; Thompson, A.M.; Kollonige, D.E.; Tarasick, D.W.; Vömel, H.; Morris, G.A.; Van Malderen, R.; Johnson, B.J.; Cullis, P.D.; Stübi, R.; Smit, H.G.J.
An Updated Examination of the Post-2013 Ozonesonde Total Column Ozone Dropoff
AGU Fall Meeting, New Orleans (Louisiana, USA) and online, 13-17 December 2021 (invited talk)

96. Steinbrecht, W.; Kubistin, D.; Plass-Dülmer, C.; … and 53 others
COVID-19 crisis reduces free tropospheric ozone across the Northern Hemisphere
Quadrennial GAW Symposium 2021, Online, 28 June-2 July 2021

97. Steinbrecht, W.; Kubistin, D.; Plass-Dülmer, C.; … and 53 others
Free Tropospheric Ozone Reductions due to Reduced Emissions in the COVID-19 Pandemic
Quadrennial Ozone Symposium, Online, 3-9 October 2021

98. Steinbrecht, W.; Van Malderen, R.; Poyraz, D.; … and 30 others
Ozone Trends in the Lower Stratosphere from Ozone Sondes
Quadrennial Ozone Symposium, Online, 3-9 October 2021 (poster)

99. Talpeanu, D.-C.; Poedts, S.; D'Huys, E.; Mierla, M.
Propagation, in-situ signatures and geoeffectiveness of consecutive solar eruptions simulated in different solar wind conditions
ESPM-16, Online, 6-10 September 2021 (poster)

100. Talpeanu, D.-C.; Poedts, S.; D'Huys, E.; Mierla, M.; Richardson, I.G.
Study of the propagation and geoeffectiveness of simulated consecutive CMEs and interaction with the solar wind
ESWW17, Glasgow (Scotland, UK) and online, 25-29 October 2021

101. Talpeanu, D.-C.; Chané, E.; Poedts, S.; D'Huys, E.; Mierla, M.; Roussev, I.
Numerical Modelling of Consecutive Solar Eruptions Inserted in Different Solar Wind Speeds and Comparison of In-situ Signatures at 1AU and their Geoeffectiveness
43rd COSPAR Scientific Assembly, Sydney (Australia) and online, 28 January-4 February 2021

102. Tarasick, D.W.; Smit, H.G.J.; Thompson, A.M.; Morris, G.A.; Witte, J.C.; Davies, J.; Nakano, T.; Van Malderen, R.; Stauffer, R.M.; Johnson, B.J.; Stübi, R.; Oltmans, S.J.; Vömel, H.
Evaluating Long-Term Changes in Atmospheric Ozone
Quadrennial Ozone Symposium, Online, 3-9 October 2021 (poster)

103. Thiemann, E.; Dominique, M.; Bougher, S.; Yiğit, E.; Gasperini, F.; Payne, C.
Comparing the Variability of the of Earth and Mars Thermospheres during Solar Cycle 24 using Solar Occultation
WHPI Workshop, Online, 13-17 September 2021 (poster)

104. Thiemann, E.; Dominique, M.
EUV Solar Occultations of the Thermosphere Reveal Unexpectedly Cool Temperatures at the Evening Terminator
IAGA-IASPEI 2021, Online, 21-27 August 2021

105. Tiburzi, C.; Shaifullah, G.M.; Zucca, P.; Bondonneau, L.; Capuano, G.; Griessmeier, J.-M.; Guglielmino, S.; Jebaraj, I.; Magdalenic, J.; Pellizzoni, A.; Samara, E.; Theureau, G.
Low-frequency observations of pulsars sample the Heliosphere
URSI GASS XXXIV, Rome (Italy) and online, 28 August-4 September 2021

106. Tiwari, S.; Hansteen, V.; De Pontieu, B.; Panesar, N.K.; Berghmans, D.
SOLO/EUI Observations and Bifrost MHD Simulations of Prevalent Fine-scale Bright Dots in Emerging Flux Regions
Hinode-14 / IRIS-11 Joint Science Meeting, Online, 25-28 October 2021 (poster)

107. Van Malderen, R.; Smit, H.G.J.; Blot, R.; … and the WG members
Harmonization and Evaluation of Ground-based Instruments for Free-Tropospheric Ozone Measurements by TOAR-II Focus Working Group "HEGIFTOM"
16th IGAC Scientific Conference, Online, 12-20 September 2021 (poster)

108. Van Malderen, R.; Poyraz, D.; Smit, H.G.J.; … and 29 others
Update of the Homogenization of the Long-Term Global Ozonesonde Records
Quadrennial Ozone Symposium, Online, 3-9 October 2021

109. Vansintjan, R.; Mampaey, B.; Delouille, V.
The SOLARNET project and the Solar Virtual Observatory (SVO)
ESPM-16, Online, 6-10 September 2021 (poster)

110. Vansintjan, R.
BE-WISSDOM: The SDO and SVO datacenters
3rd SOLARNET Forum for Telescopes & Databases, Online, 15 November 2021 (invited talk)

111. Vansintjan, R.
VSWMC validation activities
ESWW17, Glasgow (Scotland, UK) and online, 25-29 October 2021 (invited talk)

112. Verbeke, C.; Schmieder, B.; Rodriguez, L.; Poedts, S.; Magdalenic, J.; Pomoell, J.; Temmer, M.; Asvestari, E.; Scolini, C.; Heinemann, S.; Hinterreiter, J.; Samara, E.
Modeling Coronal Mass Ejections with EUHFORIA
43rd COSPAR Scientific Assembly, Sydney (Australia) and online, 28 January-4 February 2021 (invited talk)

113. Vömel, H.; Smit, H.G.J.; Tarasick, D.; Johnson, B.; Oltmans, S.; Selkirk, H.; Thompson, A.M.; Stauffer, R.M.; Witte, J.C.; Davies, J.; Van Malderen, R.; Morris, G.; Nakano, T.; Stübi, R.
A New Method for Correcting the ECC Ozone Sonde Time Response and Its Implications for “Background Current” and Pump Efficiency
101st AMS Annual Meeting, Online, 10-15 January 2021

114. Vömel, H.; Smit, H.G.J.; Tarasick, D.; Johnson, B.; Oltmans, S.; Selkirk, H.; Thompson, A.M.; Stauffer, R.M.; Witte, J.C.; Davies, J.; Van Malderen, R.; Morris, G.; Nakano, T.; Stübi, R.
The Importance of Correcting the Time Response of the Electrochemical Concentration Cell (ECC) Ozonesonde
Quadrennial Ozone Symposium, Online, 3-9 October 2021

115. West, M.J.; Seaton, D.B.; D'Huys, E.; Berghmans, D.; Mierla, M.; Rachmeler, L.
SWAP and the Middle Corona
AGU Fall Meeting, New Orleans (Louisiana, USA) and online, 13-17 December 2021 (poster)

116. Yuan, P.; Van Malderen, R.; Yin, X.; Vogelmann, H.; Awange, J.; Kutterer, H.
Assessments of integrated water vapor from atmospheric reanalyses against ground-based GPS over Europe
IAG Scientific Assembly 2021, Beijing (China) and online, 28 June-2 July 2021

117. Yuan, P.; Blewitt, G.; Kreemer, C.; Hammond, W.C.; Argus, D.; Yin, X.; Van Malderen, R.; Mayer, M.; Jiang, W.; Awange, J.; Kutterer, H.
A high temporal resolution integrated water vapor dataset from more than 10,000 global ground-based GPS stations in 2020
AGU Fall Meeting, New Orleans (Louisiana, USA) and online, 13-17 December 2021 (poster)

118. Zhukov, A.N.; Mierla, M.; Auchère, F.; … and 26 others
Stereoscopy of extreme UV quiet Sun brightenings observed by Solar Orbiter/EUI
ESPM-16, Online, 6-10 September 2021 (poster)

119. Zhukov, A.N.; Mierla, M.; Gissot, S.; ... and others
Stereoscopy of extreme UV quiet Sun brightenings observed by Solar Orbiter/EUI
AGU Fall Meeting, New Orleans (Louisiana, USA) and online, 13-17 December 2021

Public Outreach: talks and publications for the general public

1. Bolsée, D.; Vanlaeken, L.; and the MAJIS project
La contribution fédérale belge pour la mission JUICE de l'ESA
Science Connection 65, August-September 2021

2. Bolsée, D.; and the MAJIS project
Objectif Jupiter à Uccle
Daily Science, 2 June 2021

3. Cisneros, M.; and the MAJIS project
LabVIEW y a siguiente missión a Júpiter
University of Mexico (Online), YouTube, 22 June 2021

4. Clery, D.; Matthews, S.; Klimchuk, J.; Berghmans, D.; Mueller, D.; Chen, Y.; Peter, H.; Surajit Mondal, D.
Solar 'campfires' may heat the Sun's atmosphere to scorching temperatures
Science Magazine, 27 April 2021

5. D'Huys, E.
P2SC news items
PROBA2 Science Centre, 10 items, 2021

6. D'Huys, E.
De Zon en Ruimteweer
VVS Zonnekijkdag, Online, 3 July 2021

7. Harra, L.; Alberti, A.; Berghmans, D.; ... and 12 others
A Spectral Solar Irradiance Monitor (SoSpIM) on the JAXA Solar-C Space Mission
SCOSTEP/PRESTO NEWSLETTER, April 2021, 27, 1-2

8. Janssens, Jan
Zon en ruimteweer
Lecture for Astronomy Course at MIRA Public Observatory, Belgium, 22 September 2021

9. Noël, J.; Marqué, C.; Honet, V.
Radioastronomie et forage font désormais bon ménage à Humain
L'Avenir, 8 February 2021

10. *SWIC - Space Weather Introductory Course*
D'Huys, E; Janssens, J.; Vanlommel, P.; STCE collaborators and international partners
Lectures, Exercises, Visits, Quiz
- SWIC4USAF on 8-9-11-12 February 2021
- SWIC 2021/1 on 22-23-25 February 2021
- SWIC 2021/2 on 22-23-25 March 2021
- SWIC 2021/3 on 17-18-20-21 May 2021
- SWIC 2021/4 on 11-12-14-15 October 2021
- SWIC 2021/5 on 22-23-25-26 November 2021

11. Vanlommel, P.; D'Huys, E.; Janssens, J.
STCE Newsletter
Weekly newsletter, 52 issues, 2021

12. Vanlommel, P.; Berghmans, D.
Kampvuren op de Zon
Science Connection 64, April-May-June 2021

13. Verbeeck, C.
De gedeeltelijke zonsverduistering van 10 juni 2021
6th year primary school "Kinderpad", Bevel, Belgium, 10 June 2021

14. West, M.J.; D'Huys, E.
The Sun in 2020
ESA Communication, 7 January 2021

15. Zychova, L.
The bubbling galaxy
Astronomy seminars at Urania Public Observatory, Belgium, 21 September 2021

16. Zychova, L.
Universe, will you kill us?
Pint of Science, Online, 17 May 2021 (oral presentation, virtual event)

With the end of the COVID-19 crisis in sight…- Credits: [El Arroyo]

List of abbreviations

~	About, proportional to
Δ	Delta (difference)
//	Parallel
⊥	Perpendicular
1D, 2D, 3D,…	One, two, three,… dimensional
Å	Ångstrom (0.1 nm)
A	Article
AAS	American Astronomical Society
ACE	Advanced Composition Explorer
AFFECTS	Advanced Forecast For Ensuring Communications Through Space
AGU	American Geophysical Union
AIA	Atmospheric Imaging Assembly (SDO)
ALTIUS	Atmospheric Limb Tracker for Investigation of the Upcoming Stratosphere
AM	Amplitude Modulation
AMS	American Meteorological Society
AOGS	Asia Oceania Geosciences Society
API	Application Programming Interface
APS	(1) American Physical Society ; (2) Active Pixel System (PROBA2)
AR	(1) Active Region ; (2) Annual Report
ARASE	Nickname of the ERG satellite (JAXA)
ARCAS	Augmented Resolution Callisto Spectrometer
ARTIST	Automatic Real-Time Ionogram Scaler with True height (software)
ASEC	Applied Space Environments Conference
ASGARD	An educational space programme for schools (no acronym)
ASIMUT	Radiative transfer and retrieval tool developed at BIRA-IASB (no acronym)
ASL	Above Sea Level
ASOPOS	Assessment of Standard Operating Procedures for OzoneSondes
ASOV	Action Spécifique Observatoire Virtuel
ASPECS	Advanced Solar Particle Event Casting System
ASPIICS	Association of Spacecraft for Polarimetric and Imaging Investigation of the Corona of the Sun (PROBA-3)
ASTERIX	Absolute Solar-TErrestrial Radiation Imbalance eXplorer
ATMOS	Atmospheric Science Conference (ESA)
AU, au	Astronomical Unit; about 150 million km
B	Magnetic field (strength)
B_0	Heliographic latitude of the central point of the solar disk (The range of B_0 is $\pm$7.23°)
BE	Belgium
BE-WISSDOM	Belgian Web Incessant Screening for SDO Mission
BELSPO	Belgian Science Policy Office
BeNELux	Belgium, The Netherlands, and Luxembourg
BEPOM	Belgian Photonics Online Meetup
Bifrost	Code for simulating stellar atmospheres (no acronym)
BIOSPHERE	Metrology for Earth Biosphere: Cosmic rays, ultraviolet radiation and fragility of ozone shield Metrology for Earth Biosphere: Cosmic rays, ultraviolet radiation and fragility of ozone shield (EURAMET)
BIRA	Koninklijk Belgisch Instituut voor Ruimte-Aëronomie
BIRA-IASB	Royal Belgian Institute for Space Aeronomy
BISA	Royal Belgian Institute for Space Aeronomy
BNCGG	Belgian National Committee for Geodesy and Geophysics
BRAIN-be	Belgian Research Action through Interdisciplinary Networks (BELSPO)

BRAMS	Belgian RAdio Meteor Stations
B.RCLab	Belgian Radiometric Characterization Laboratory
BRITEC	Bringing Research into ThE Classroom
BSPM	Belgian SWIFF Plasmasphere Model
BUKS	Belgium, UK, and Spain
B.USOC	Belgian User Support and Operation Centre
Bz	Component of the IMF perpendicular to the ecliptic ("north-south" component)
°C	Degrees Celsius
C1, C2, C3	Coronagraphs of LASCO (SoHO)
C-class flare	Common x-ray flare
C/N_0	Carrier-to-Noise
CA	COST Action (COST)
Ca II H	A blue line in the solar spectrum at 396.85 nm
Ca II K	A blue line in the solar spectrum at 393.37 nm
CACTus	Computer Aided CME Tracking software
CALLISTO	Compound Astronomical Low frequency Low-cost Instrument for Spectroscopy and Transportable Observatory
CAMS	Cameras for All sky Meteor Surveillance
CCMC	Community Coordinated Modeling Center
CESRA	Community of European Solar Radio Astronomers
CH	Coronal Hole
CH_4	Methane
CH_4TIR	CH4 Thermal InfraRed
CIR	Co-rotating Interaction Region
Cluster	ESA/NASA mission to study the Earth's magnetosphere (no acronym)
cm, cm^2, cm^3	centimeter, square centimeter, cubic centimeter
CME	Coronal Mass Ejection
CMOS	Complementary Metal-Oxide-Semiconductor
CNES	Centre national d'études spatiales (France)
CNRS	Centre national de la recherche scientifique (France)
Co.	Cooperation
CO_2	Carbon Dioxide
COMESEP	COronal Mass Ejections and Solar Energetic Particles
COMPLIMENT	COMetary Plasma Light InstruMENT (Comet Interceptor ; ESA)
COPUOS	COmmittee on the Peaceful Uses of Outer Space (UN)
COR (1/2)	Coronagraph (Inner/Outer) onboard STEREO
CORS	Continuously Operating Reference Stations (GNSS)
COSPAR	COmmittee on SPAce Research
COST	(European) COoperation in Science & Technology
COTS	Commercial off-the-shelf
COVID-19	Coronavirus disease 2019
CPAESS	Cooperative Programs for the Advancement of Earth System Science
CR	Carrington Rotation
CRAF	Committee on Radio Astronomy Frequencies
CROM	A type of pyrheliometer developed by D. Crommelynck (RMI)
CSL	Centre Spatial de Liège
CubeSat	A small satellite measuring 10cm x 10cm x 10cm
CUSUM	Cumulative sum
dB-Hz	decibel-Hertz (bandwidth relative to 1 Hz)
DeMeLab	Detector Measurements Laboratory (aka STCL)
DENSER	DEeply uNderstanding Space weather (ESA)
Digisonde	Digitally Integrating Goniometric IonoSONDE
DLR	German Aerospace Center
dm, dm^2, dm^3	decimeter, square decimeter, cubic decimeter
DOI	Digital Object Identifier
DOU	Dourbes (Intermagnet)
DoY	Day of Year

DPS	(1) Division for Planetary Sciences (EPSC) ; (2) Digital Portable Sounder
Dr.	Doctor
DRBS	Dourbes (Belgium, NMDB)
DREAM.3D	A Digital Representation Environment for the Analysis of Microstructure in 3D
DSCOVR	Deep Space Climate Observatory
Dst	Disturbance Storm Time index (geomagnetic)
E	East
E, E_- , E_+	Energy, Ingoing energy, Outgoing energy
e.g.	exempli gratia (example given)
e-Callisto	extended Compact Astronomical Low-cost Low-frequency Instrument for Spectroscopy and Transportable Observatory
E-GVAP	EUMETNET GNSS water Vapour Programme
EC	European Commission
ECC	Electrochemical Concentration Cell
ed.	Edition
Eds.	Editors
EGNOS	European Geostationary Navigation Overlay Service
EGNSS	European GNSS
EGU	European Geosciences Union
EHF	Electron Heat Flux event
EISCAT	European Incoherent SCATter scientific association
EIT	Extreme ultraviolet Imaging Telescope (SOHO)
EM	(1) Electromagnetic (2) Engineering Model
EMFISIS	Electric and Magnetic Field Instrument Suite and Integrated Science (Van Allen Probes)
EnVision	ESA mission to Venus (no acronym)
EPN	EUREF Permanent Network
E-PROFILE	EUMETNET Profiling Programme
EPS	European Physical Society
EPSC	European Planetary Science Congress
EPT	Energetic Particle Telescope (PROBA-V)
erg	10^{-7} Joule
ERG	Exploration of energization and Radiation in Geospace (now called ARASE ; JAXA)
Es	Sporadic E-layer (ionosphere)
ES	Earth System (Science and Environmental Management (COST)
ESA	European Space Agency
ESAC	European Space Astronomy Centre
ESC	Expert Service Centre (SSCC)
ESD	ElectroStatic Discharge
ESCAPE	(1) European SpaceCraft for the study of Atmospheric Particle Escape (2) European Science Cluster of Astronomy & Particle physics ESFRI research infrastructures
ESERO	European Space Education Resource Office
ESFRI	European Strategy Forum on Research Infrastructures
ESOC	European Space Operations Centre
ESPD	European Solar Physics Division (EPS)
ESPM	European Solar Physics Meeting
ESTEC	European Space Research and Technology Centre
ESWW	European Space Weather Week
et al.	et alii (and other)
etc.	et cetera (and so forth)
EU	European Union
EUHFORIA	European Heliospheric Forecasting Information Asset
EUI	Extreme-Ultraviolet Imager (Solar Orbiter)
EUMETNET	Network of European Meteorological Services
EUMETSAT	European Organisation for the Exploitation of Meteorological Satellites
EURAMET	The European Association of National Metrology Institutes
EUREF	EUropean Reference Frame
EUV	Extreme Ultraviolet

EUVI	Extreme Ultraviolet Imager (STEREO/SECCHI; LGRRS)
eV	electron volt (1 eV = 1.602 × 10^{-19} joules)
EVE	Extreme ultraviolet Variability Experiment (SDO)
ExoMars	Exobiology on Mars (ESA, Roscosmos)
$F_{10.7}$, $F_{10.7\ cm}$	Solar radio flux at 10.7 cm wavelength
F_2	Main ionospheric layer
FAIR	Findable, Accessible, Interoperable, and Re-usable
Fe IX-X	8 respectively 9 times ionized iron
FITS	Flexible Image Transport System
FM	(1) Flight Model (2) Frequency Modulation
FMI	Finnish Meteorological Institute
FNRS	Fonds National de la Recherche Scientifique
foEs	Sporadic E critical frequency
foF2	Critical frequency F2-layer
ForMaL-SEP	Prediction tool for the expected maximum proton flux levels for ≥10 MeV (DENSER)
ForMaL-Xrange	Tool for the forecast of the hourly range of the ground-based magnetic field north component (DENSER)
FOV	Field-Of-View
FP7	Framework Programme 7 (EU)
FPA	Focal Plane Assembly
Fri3D	Flux Rope in 3D
FRS	Fonds de la Recherche Scientifique
FSI	Full Sun Imager (Solar Orbiter / EUI)
FSMT	Fort Smith (Canada, NMDB)
FTE	Full-Time Equivalent
ftp	file transfer protocol
FUV	Far Ultraviolet
G, GB	Gigabyte (10^9 bytes)
Galileo	European GNSS
GASS	General Assembly and Scientific Symposium
GAW	Global Atmospheric Watch (WMO)
GBO	Ground-Based Observatory
GCR	Galactic Cosmic Rays
GEANT-4	GEometry ANd Tracking (simulation platform)
GeV	Giga electronvolt (10^9 . 1.6 . 10^{-19} Joule)
GFZ	Deutsches GeoForschungsZentrum (German Research Centre for Geosciences)
GHz	Gigahertz (10^9 Hz)
GLE	Ground Level Enhancement
GLONASS	GLObal NAvigation Satellite System (Russia)
GNSS	Global Navigation Satellite System
GOES	Geostationary Operational Environmental Satellite
GONG	Global Oscillation Network Group
GPS	Global Positioning System (USA)
GRAPE	GNSS Research and Application for Polar Environment
GSFC	Goddard Space Flight Center
h	(1) hour ; (2) Planck's constant (6.62607004 × 10^{-34} m^2 kg / s)
H	(1) Hydrogen ; (2) Heat flux
H-alpha (Hα)	A red visible spectral line at 656.28 nm created by Hydrogen
H2020	Horizon 2020 (EU)
He, He II	Helium, ionized Helium
HEGIFTOM	Harmonization and Evaluation of Ground-based Instruments for Free Tropospheric Ozone Measurements
HEK	Heliophysics Events Knowledgebase
HF	High Frequency (3-30 MHz)
HI	(1) Neutral atomic Hydrogen ; (2) Heliospheric Imager (STEREO)
h_mF_2	peak density height of F_2-layer
HMI	Heliospheric and Magnetic Imager (SDO)
hPa	hectopascal (atmospheric pressure)
HRI	High Resolution Imager (Solar Orbiter / EUI)

HRIEUV	High Resolution Imager in the EUV (Solar Orbiter / EUI)
HSRS	Humain Solar Radio Spectrograph
HSS	High Speed Stream
HuRAS	Humain Radio Astronomy Station
HWM	Horizontal Wind Model
HXR	Hard x-rays
Hz	Hertz (per second)
i	The index in a counter or series
I	Current
I-V	Current-Voltage
IAG	International Association of Geodesy
IAGA	International Association of Geomagnetism and Aeronomy
IAS	Institut d'Astrophysique Spatiale (France)
IASB	Institut royal d'Aéronomie Spatiale de Belgique
IASC	International Arctic Science Committee
IASI	Infrared Atmospheric Sounder Interferometer
IASPEI	International Association of Seismology and Physics of the Earth's Interior
IAU	International Astronomical Union
ICAO	International Civil Aviation Organization
ICCC	Inter-Commission Committee on "Geodesy for Climate Research"
ICME	Interplanetary CME
ICSO	International Conference on Space Optics
ICT	Information and Communication Technologies
IDL	Interactive Data Language
i.e.	"id est" (that is)
IEEE	Institute of Electrical and Electronics Engineers
IGAC	International Global Atmospheric Chemistry project
IGS	International GNSS Service
IMC	International Meteor Conference
IMF	Interplanetary Magnetic Field
IMO	International Meteor Organization
INGV	Istituto nazionale di geofisica e vulcanologia (Italy)
INSPIRE	(1) International Satellite Program in Research and Education (2) Infrastructure for Spatial Information in the European Community (EU)
IOP	Institute of Physics
IPAG	Institut de Planétologie et d'Astrophysique de Grenoble
IPC	International Pyrheliometer Comparison
IQR	InterQuartile Range
IR	Infrared
IRAP	Institut de Recherche en Astrophysique et Planétologie (France)
IRI	International Reference Ionosphere
IRIS	Interface Region Imaging Spectrograph (NASA)
IRM	Institut Royal Météorologique
ISAS	Institute of Space and Astronautical Science
ISC	(1) International Science Council; (2) International Steering Committee
ISN	International Sunspot Number
ISO	International Organization for Standardization
ISS	International Space Station
ISSI	International Space Science Institute
ISSS	(1) International School of Space Science; (2) International School/Symposium for Space Simulations
ISWAT	International Space Weather Action Teams (COSPAR)
IT	Information Technology
IUGG	International Union of Geodesy and Geophysics
IVOA	International Virtual Observatory Alliance
IWV	Integrated Water Vapour
JAXA	Japan Aerospace Exploration Agency
JGR	Journal of Geophysical Research

jHV	jHelioViewer
JOSIE	Jülich Ozone Sonde Intercomparison Experiment
JPEG	Joint Photographic Experts Group
JSON	JavaScript Object Notation
JSWSC	Journal of Space Weather and Space Climate
JUICE	JUpiter ICy moons Explorer
k	wave number
K	(1) Local K index: A 3-hour geomagnetic index, ranging from 0 (quiet) to 9 (extremely severe storm); (2) degrees Kelvin
K*	Local 1-minute resolution K index
Ka-band	"Kürz above": Radio frequency band from 27-40 GHz
KAW	Kinetic Alfvén Waves
KBEL	Local K index for Belgium
keV	kilo electronvolt ($10^3 . 1.6 . 10^{-19}$ Joule)
kHz	kilo Hertz (10^3 /second)
KI	Potassium iodide
km, km^2	kilometer, square kilometer
km/s	kilometers per second
KMI	Koninklijk Meteorologisch Instituut
KNMI	Koninklijk Nederlands Meteorologisch Instituut
KORTES	KOronal X-Ray TElescope and Spectrometer (Russia ; ISS)
K_p	"planetarische Kennziffer", a geomagnetic index, ranging from 0 (quiet) to 9 (extremely severe storm)
KSO	Kanzelhöhe Solar Observatory
KSB	Koninklijke Sterrenwacht van België
KUL, KULeuven	Katholieke Universiteit Leuven
kV	kiloVolt (10^3 Volt)
λ	wavelength
λ_e	electron inertial length
l/m^2	Liter per square meter
L-class	Large class satellite (ESA)
L	Letter (manuscript)
L*	Set of Earth's magnetic field lines which cross the Earth's magnetic equator at * earth radii from the centre of the Earth (e.g. L = 2)
L_0	Heliographic longitude of the central point of the solar disk
L1, … , L5	First, … , fifth Lagrangian point
L1, L2	GPS frequencies: L1 = 1575.42 MHz, L2 = 1227.60 MHz
LASCO	Large Angle Spectrometric Coronagraph (SOHO); small (C2) and wide (C3) field of view
Lat	Latitude
LATMOS	Laboratoire ATmosphères, Milieux, Observations Spatiales (France)
LBL	line-by-line
LDE	Long Duration Event
LEO	Low Earth Orbit (below 2000 km ASL)
LIDAR	LIght Detection And Radar
LIEDR	Local Ionospheric Electron Density profile Reconstruction
LLS	Research Unit "Lasers and Spectroscopies" at the Université de Namur (Belgium)
LMSAL	Lockheed Martin Solar and Astrophysics Laboratory
LOC	Local Organising Committee
LOFAR	Low-Frequency Array
Lon	Longitude
LOTUS	Long-term Ozone Trends and Uncertainties in the Stratosphere
Ls	Solar longitude
LT	Local Time
LUT	LookUp tables
Ly-α	Lyman-alpha, a spectral line in the VUV at 121.6 nm
LYA	Ly-α
LYRA	Large Yield Radiometer, formerly called Lyman Alpha Radiometer (PROBA2)
LWS	Living With a Star
μm	micrometer (10^{-6} meter)
M-class	Medium class satellite (ESA)
M-class flare	Medium x-ray flare
m, m^2, m^3	Meter, square meter, cubic meter
MAB	Manhay (Intermagnet)

MACH	Magnetic fields, Atmospheres, and the Connection to Habitability
MagEIS	MAGnetic Electron Ion Spectrometer (Van Allen probes)
MAJIS	Moons And Jupiter Imaging Spectrometer (JUICE)
MAPLD	Military and Aerospace Programmable Logic Devices
MB	Megabyte (10^6 bytes)
mbar	millibar
MEO	Medium Earth Orbit (between 2000 and 35,786 km ASL
METIS	Multi Element Telescope for Imaging and Spectroscopy (SolO)
MeV	Mega electronvolt ($10^6 . 1.6 . 10^{-19}$ Joule)
MHD	Magnetohydrodynamics
MHz	Megahertz (10^6/s)
MImOSA	Magnetic imaging of the outer solar atmosphere
MIT	Massachusetts Institute of Technology
MJD	Modified Julian Day
ML	Maximum Likelihood
MLH	mixing layer height
MLT	Magnetic Local Time
mm	millimeter (10^{-3} meter)
Mm	Megameter (10^6 meter)
mm/s	millimeter per second
MOMA	Multi-wavelength Observations and Modelling of Aurora
MoMo	Model of Mars Ionosphere
MOMSTER	MObile Meteor STation for Education & outreach
MPPC	Max Planck-Princeton Center
MPS	Max Planck Institute for Solar System Research
ms	millisecond (10^{-3} second)
MULTI-VP	multiple-1D solar wind model (not an acronym)
MUV	Mid Ultraviolet
ν	Frequency
N	North
N-S	North-South
N_2	Nitrogen
N_2O	Nitrous oxide ("laughing gas")
nA	nano Ampère (10^{-9} meter)
NASA	National Aeronautics and Space Administration
NASU	National Academy of Sciences of Ukraine
NATO	North Atlantic Treaty Organization
Nc, Ns, Ng	the number of spots Ns, the number of groups Ng, and the composite Nc = Ns + 10Ng
NeQuick	Electron density Quick calculation model (ionospheric model)
Net-TIDE	Pilot Network for Identification of Travelling Ionospheric Disturbances in Europe
NIR	Near IR
NL	The Netherlands
NM	Neutron Monitor
nm	nanometer (10^{-9} meter)
NMDB	Neutron Monitor DataBase
N_mF_2	peak density of F_2-layer
No.	Number of
NO_2	Nitrogen dioxide
NOAA	National Oceanic and Atmospheric Administration
NOMAD	Nadir and Occultation for MArs Discovery (ExoMars)
NP	Non-parametric test
NRT	Near Real Time
ns	nanosecond (10^{-9} second)
NSO	National Solar Observatory
nT	nano-Tesla (10^{-9} Tesla)
NUV	Near Ultraviolet
NV/SA	Naamloze Vennootschap / Société Anonyme
NWC	Northwest Cape of Australia
NWP	Numerical Weather Prediction
NYRIA	Network of Young Researchers in Instrumentation for Astronomy
Ω_{ce} , Ω_{cp}	electron-cyclotron frequencies, proton-cyclotron frequencies
O	Oxygen
O_3	Ozone
O3S	Ozone Sonde
O3S-DQA	O3S Data Quality Assessment
ODC	On Duty Center (PECASUS)
ORB	Observatoire Royal de Belgique

ORFEES	Observation Radio Fréquences pour l'Etude des Eruptions Solaires
P	The position angle between the geocentric north pole and the solar rotational north pole measured eastward from geocentric north. The range in P is ±26.3°
P2SC	PROBA2 Science Center
PARADISE	Particle Radiation Asset Directed at Interplanetary Space Exploration
PB	Petabyte (10^{15} bytes)
PBC	Primary Backup-Center (PECASUS)
PC	Personal Computer
PDF	Probability Density Functions
PECASUS	Partnership for Excellence in Civil Aviation Space weather User Services (ICAO) *(original: Pan-European Consortium for Aviation Space weather User Services)*
PFSS	Potential Field Source Surface
pfu	particle (proton) flux unit: the number of particles registered per second, per square cm, and per steradian
PhD	Doctor of Philosophy
PHI	Polarimetric and Helioseismic Imager (Solar Orbiter)
PI	Principal Investigator
PICASSO	PICo-satellite for Atmospheric and Space Science Observations
PITHIA-NRF	Plasmasphere Ionosphere Thermosphere Integrated Research Environment and Access services: a Network of Research Facilities (EU)
PRESTO	(1) Fast warning message for important SWx events (2) PREdictability of the Solar-Terrestrial Coupling (SCOSTEP)
PROBA	PRoject for OnBoard Autonomy
PROBA-V	PROBA-Vegetation
ps	picosecond (10^{-12} second)
PSP	Parker Solar Probe
PTB	Physikalish-Technische Bundesanstalt (Germany)
PWE	Plasma Wave Experiment (ARASE)
px	pixel
Python	Programming language (no acronym)
Q&A	Questions and Answers
QA	Quality Assurance
QC	Quality Control
QE	Quantum Efficiency
QPP	Quasi-periodic pulsation
ρ_T	gyroradius
R	Resistor
R&D	Research and Development
R-ESC	Space Radiation ESC (SSCC)
RAS	Royal Astronomical Society
RB-FAN	Radiation Belt Forecast And Nowcast
REST	REpresentational State Transfer
RF	Radio Frequency
RHESSI	Reuven Ramaty High Energy Solar Spectroscopic Imager
RMI(B)	Royal Meteorological Institute (of Belgium)
RMS	Root Mean Square
ROADMAP	ROle and impAct of Dust and clouds in the Martian AtmosPhere
ROB	Royal Observatory of Belgium
Roscosmos	Russian Space Agency
RSSB	Royal Statistical Society of Belgium
R_{sun}	Solar radius (~ 696,000 km)
RWC	Regional Warning Center
Rx	Receiver
σ	sigma (confidence level)
s	second
S	South
S-band	Radio frequency band from 2-4 GHz
S/C	Spacecraft
S-class	Small class satellite (ESA)
SAA	South Atlantic Anomaly
SAFIRE	SolAr Flux monItoRing Equipment
SANSA	South African National Space Agency
SAR	(1) Superactive region; (2) Synthetic Aperture Radar
SBC	Secondary Backup-Center (PECASUS)
SC24, SC25	Solar Cycle 24, Solar Cycle 25

SCAR	Scientific Committee on Antarctic Research
SCK-CEN	Studiecentrum voor Kernenergie - Centre d'Etude de l'Energie Nucléaire
SCOPE	Solar Coronagraph for OPErations
SCOSTEP	Scientific Committee on Solar Terrestrial Physics
SDO	Solar Dynamics Observatory
SDR	Software Defined Radio
SECCHI	Sun Earth Connection Coronal and Heliospheric Investigation (STEREO)
SEE	Single Event Effects
SEP	Solar Energetic Particle
SEPEM	Solar Energetic Particle Environment Modelling
SEU	Single Event Upset
SFU, sfu	Solar Flux Unit (10^{-22} W m^{-2} Hz^{-1})
SHINE	Solar Heliospheric & Interplanetary Environment
SIDC	Solar Influences Data analysis Center
SILSO	Sunspot Index and Long-term Solar Observations (ROB)
SIMBA	Sun-earth IMBAlance
SKA	Square Kilometre Array
SLP	Sweeping / Segmented / Single/ Split / Spherical Langmuir Probe
SLT	Solar Local Time
SM	Spare Model
SMD	Safety and Metrology Division (Federal Services for Metrology)
SMILE	Solar wind-Magnetosphere-Ionosphere Link Explorer (ESA)
sms	short message service
S_N , SN	(1) Sunspot Number ; (2) Space weather and Near-earth objects ; (3) Standard normal homogenization tests
SOC	Science Operations Centre
SOHO	SOlar & Heliospheric Observatory
SOL-ACES	SOLar Auto-Calibrating Extreme ultraviolet and ultraviolet Spectrometers (ISS-SOLAR)
SOLAR	ESA project onboard ISS (Columbus Laboratory), controlled by B.USOC, and having 3 main instruments: SOVIM, SOLSPEC and SOL-ACES
Solar-C	Next Generation Solar physics Mission (JAXA)
SOLAR-v	A solar spectral irradiance dataset based on SOLAR/SOLSPEC observations during SC24 (relative variability)
SOLARNET	European network of solar physics researchers and facilities (H2020)
SOLCON	SOLar CONstant radiometer
SOLIS	Synoptic Optical Long-term Investigations of the Sun (NSO)
SolO	Solar Orbiter
SOLSPEC	SOLar SPECtral irradiance measurements (ISS-SOLAR)
SOP	Standard Operating Procedures
SOPB	South Pole Bares (Antarctica, NMDB)
SOPO	South Pole (Antarctica, NMDB)
SoSpIM	Spectral Solar Irradiance Monitor (Solar-C)
SOVA	SOlar constant and VAriability
SOVIM	Solar Variations and Irradiance Monitor (ISS-SOLAR)
SPADE	Small Phased Array DEmonstrator
SPD	Solar Physics Division (AAS)
SPENVIS (-NG)	SPace ENVironment Information System (- Next Generation)
SPICE	Spectral Imaging of the Coronal Environment (SolO)
SPIE	Society of Photo-optical Instrumentation Engineers
SPOCA	Spatial Possibilistic Clustering Algorithm
SPRING	Solar Physics Research Integrated Network Group (SOLARNET)
SPS	Science for Peace and Security (NATO)

sr	steradian
SRB	Solar Radio Burst
SREM	Standard Radiation Environment Monitor (Integral, Rosetta)
SSA	(1) Space Situational Awareness ; (2) singular spectrum analysis
SSCC	SSA Space Weather Coordination Centre (ESA)
SSI	Solar Spectral Irradiance
SSN	SunSpot Number
STAFF	Solar Timelines viewer for AFFECTS
STCE	Solar-Terrestrial Centre of Excellence
STCL	Space Technology & Calibration Laboratories
STEM	Science, Technology, Engineering, Mathematics
STEAM	Science, Technology, Engineering, Arts, Mathematics
STEREO	Solar-TErrestrial RElations Observatory
STM	Structural Model
SunPy	software library for solar physics based on Python
SUVI	Solar Ultraviolet Imager (GOES)
SVO	Solar Virtual Observatory
SW	Space Weather (journal)
SWAP	Sun Watcher using APS detector and image Processing (PROBA2)
SWAVES	STEREO WAVES
SWE	Space Weather
SWEC	Space Weather Education Center
SWEK	Space Weather Event Knowledgebase
SWIC	Space Weather Introductory Course
SWIFF	Space Weather Integrated Forecasting Framework
SWPC	Space Weather Prediction Center (USA)
SWT	Science Working Team
SWx	Space weather
SXR	Soft x-rays
SZA	Solar Zenith Angle
τ, t	Time
T, TB	Terabyte (10^{12} bytes)
TAP	Table Access Protocol
TEC	Total Electron Content
Tech-TIDE	Warning and Mitigation Technologies for TIDs Effects
TECu	TEC unit ($10^{16}e{\cdot}m^{-2}$)
THEMIS	Time History of Events and Macroscale Interactions during Substorms (NASA mission)
TID	Travelling Ionospheric Disturbance
TIR	Thermal InfraRed
TOAR	Tropospheric Ozone Assessment Report
TSI	Total Solar Irradiance
TVAC	Thermal-VACuum chamber
Tx	Transmitter
UCAR	University Corporation for Atmospheric Research
UCL, UCLouvain	Université Catholique de Louvain
UHF	Ultra High Frequency (0.3 - 3 GHz)
UK	United Kingdom
ULB	Université libre de Bruxelles
UNCOPUOS	United Nations Committee on the Peaceful Use of Outer Space
URAN	Ukrainian Radio Interferometer of NASU
URL	Uniform Resource Locator
URSI	International Union of Radio Science - Union Radio-Scientifique Internationale
US(A)	United States (of America)
USAF	United States Air Force
USET	Uccle Solar Equatorial Table
UT(C)	(Coordinated) Universal Time
UV	Ultraviolet
v	Velocity (speed)
V	Volt, voltage
V1, 2, …	Version 1, 2, …
VarSITI	Variability of the Sun and Its Terrestrial Impact
VenSpec-H	Venus Spectrometer with High resolution (EnVision ; ESA)
VESPA	Virtual European Solar and Planetary Access
VHF	Very High Frequency (30-300 MHz)
VIP	Very Important Person

VIRGO	Variability of solar IRradiance and Gravity Oscillations (SoHO)
VIS	Visible
VKI	Von Karman Institute
VLF	Very Low Frequency (3-30 kHz)
Vol.	Volume
VSWMC	Virtual Space Weather Modelling Centre
VTEC	Vertical TEC
VUB	Vrije Universiteit Brussel
VUV	Vacuum Ultraviolet
VVS	Vereniging Voor Sterrenkunde (Belgian Astronomical Association)
W	(1) Watt; (2) West
W/m^2	Watt per square meter
WAVES	Radio and plasma wave investigation (WIND, STEREO)
WDC	World Data Center
WFOV	Wide Field Of View
WG	Working Group
WHPI	Whole Heliosphere and Planetary Interactions
WMO	World Meteorological Organization
WP	Work Package
WRC	World Radiation Center
WRR	World Radiometric Reference
WS	Workshop
WSA	Wang-Sheeley-Arge (model for solar wind)
X-band	Radio frequency band from 8-12 GHz
X-class flare	Extreme x-ray flare
XRT	X-Ray Telescope (Hinode)
ZTD	Zenith Total Delay